Final Report

Federal Agency and Organization: DOE EERE – Geothermal Technologies Program

Recipient Organization: GE Global Research
DUNS Number: 086188401
Recipient Address: One Research Circle, Niskayuna, NY, USA 12309-1027

Award Number: DE-EE0002752
Project Title: High-Temperature-High-Volume Lifting for Enhanced Geothermal Systems
Project Period: April 01, 2010 – December 30, 2013

Principal Investigator: Norman Turnquist
Principal Engineer
turnquist@ge.com
518-387-5978

Date of Report Submission: December 20, 2013
Reporting Period: April 01, 2010 to December 30, 2013

Project Partners: None

DOE Project Team: DOE Contracting Officer – Melissa Jacobi
DOE Project Officer – William A. Vandermeer

Acknowledgement

This report is based upon work supported by the Department of Energy under Award Number DE-EE0002752.

Disclaimer

Authors

Norman Turnquist
Xuele Qi
Tsarafidy Raminosoa
Ken Salas
Omprakash Samudrala
Manoj Shah
Jeremy Van Dam
Weijun Yin
Jalal Zia

Contents

Lists of Tables

List of Figures

1. Introduction

Geothermal energy is the only baseload renewable source of power. Every other source of renewable energy is cyclic and/or relies on weather, tidal, or seasonal phenomena.

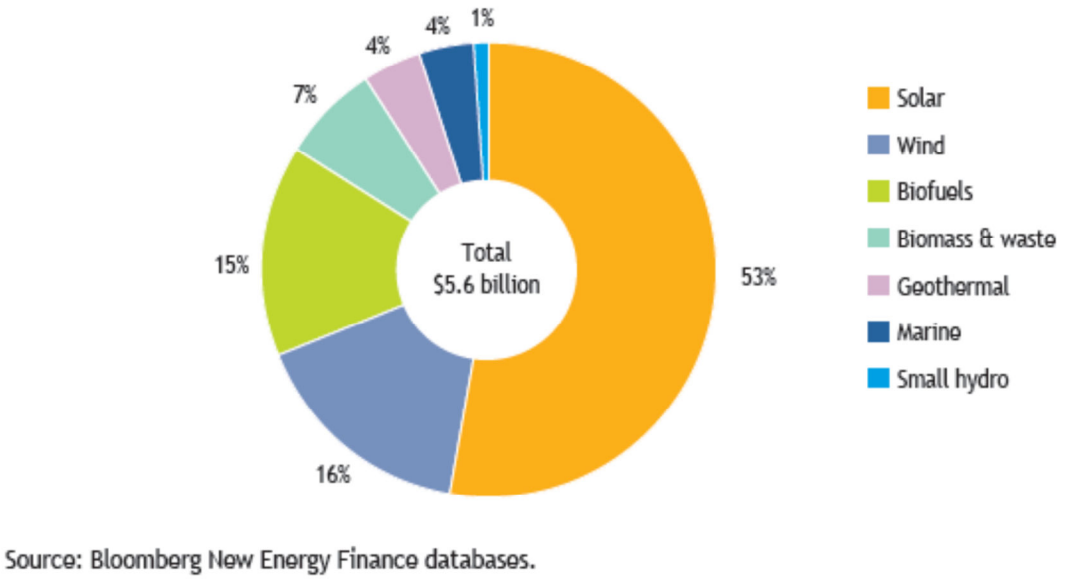

Figure 1.1: 2009 Global spending on renewable energy technologies

Figure 1.1 shows the global spending on research and development in renewable energy technologies. The leading beneficiary of funding is solar power, followed by wind, biofuels, biomass/waste heat, geothermal, small marine and hydro. Despite receiving less than one tenth of the R&D funding support, geothermal sources produced more than twice the electricity of solar sources in 2010.[1]

One of the biggest drawbacks of geothermal energy has traditionally been the limited accessible geographical locations of hydrothermal resources. These are often found in geologically "hot" areas where underground heat coincides with naturally occurring aquifers. Drilling is done to intersect such aquifers, thus raising the risk of a "missed well" and the cost of unsuccessful drilling.

A new technology, called enhanced geothermal systems (EGS), promises to dramatically reduce this risk. It does so by drilling a well and creating a network of passages in the hot rock underground. A unique approach to EGS has been developed by AltaRock Energy. The process is called hydroshearing. Once the formation has been hydrosheared, a low permeability biodegradable polymer is pumped into the formation and the passages are blocked. This allows the next formation to be hydrosheared in the same well. The process is repeated until several hydrosheared zones are created. These zones are then intersected by drilling one or more producer wells. Water is pumped into one well from above ground; it then gathers enthalpy from the underground "heat exchanger" and it flows out of the other well. A surface-based

power plant recovers this enthalpy and generates useful power. The technology to create this underground network of passages has recently been validated by Altarock Inc. at their Newberry, OR site.[2]

Enhanced geothermal energy holds tremendous potential in the USA because it is largely free of the requirement of locating an underground aquifer. All that is needed is an underground temperature gradient. Work by google.org (www.google.org/egs) has shown that economically attractive temperature gradients are ubiquitous in the USA, particularly west of the continental divide. According to a report by the National Renewable Energy Laboratory (NREL),[3] the potential nameplate capacity for enhanced geothermal systems (EGS) in the USA is >3900 GW with a potential annual production of over 31 million GW-hours. These numbers are compared and contrasted with other renewables in Figure 1.2.

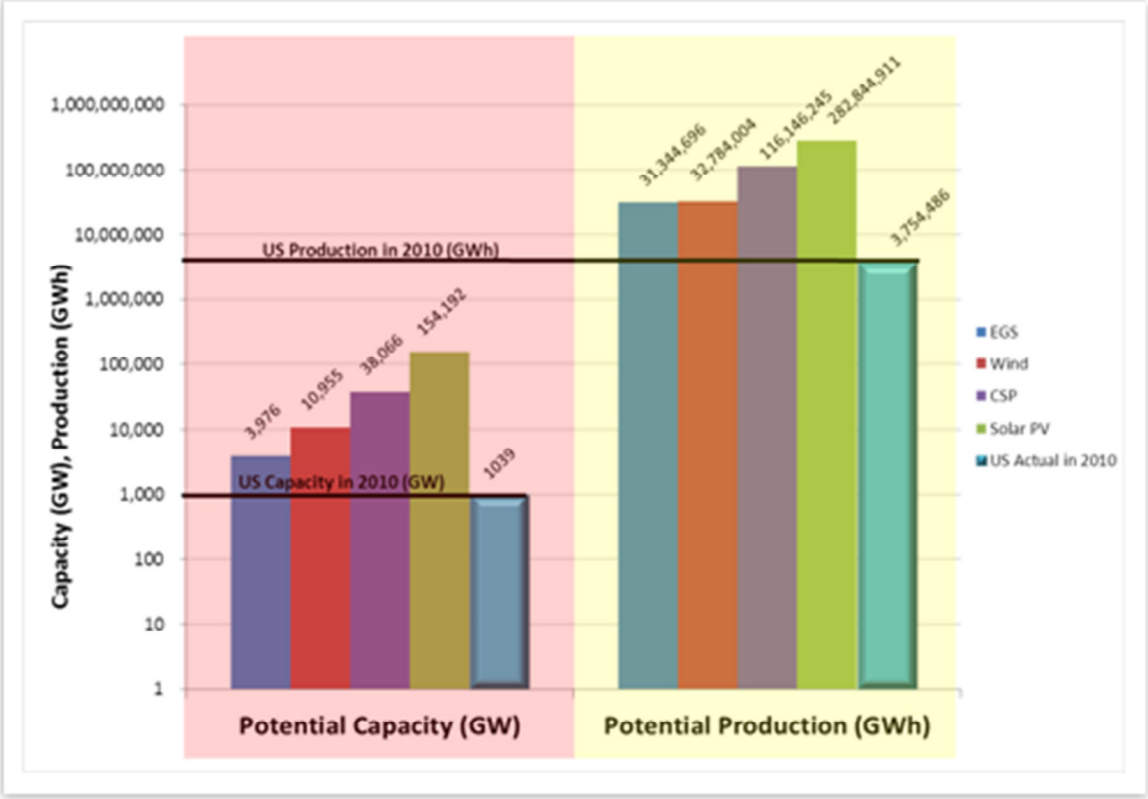

Figure 1.2: Total Potential Capacity (GW) and Potential Annual Production (GWh) for some renewable power sources

A technical barrier to the widespread feasibility of EGS in the United States is the need for a high-temperature, high-volume lifting system to boost the heated water from the production well to the surface. This is a difficult challenge, since high temperature hot rocks tend to be 3–6 km deep on the West Coast and 6–10 km deep on the East Coast. Simply pressurizing the injection wells is not viable, due to the risk of damaging the underground "heat exchanger" formation. What is needed is a lifting system that can provide high flow rates from these depths and operate reliably at temperatures far above the capability of existing lifting systems.

The overall objective of this program is to advance the technology for well fluids lifting systems to meet the foreseeable pressure, temperature, and longevity needs of the Enhanced Geothermal Systems (EGS) industry for the coming ten years. This includes identifying the requirements of an EGS lifting system, evaluating potential lifting methodologies, downselecting the most viable methodology, identifying the technical obstacles to its use in EGS, addressing the technical barriers via component-level development, and designing/fabricating a subscale system and test facility to demonstrate the technology.

2. Lifting System Requirements and Methodologies

2.1 SYSTEM REQUIREMENTS FOR EGS

In EGS production wells, the reservoir pressure is usually insufficient to lift the geothermal fluid all the way up the production tubing to the surface. Raising the reservoir pressure by increasing it at the injection wellhead is not feasible due to the risk of formation damage and possible thermal breakthrough. Higher injection pressure also leads to significant loss of geothermal fluid. Many EGS wells are several kilometers deep, leading to significant losses due to wall friction and pore pressure drop; this results in inadequate production rates. To enhance production, artificial lift techniques must be employed to provide additional boost for lifting the geothermal fluid all the way to the surface.

Historically, geothermal wells have used either line-shaft pumps or electric submersible pumps for lifting geothermal fluids, with the latter being increasingly used for deep wells. Irrespective of the technology employed for lifting, there are a certain set of criteria that must be met for a commercially successful installation of the lifting system in an EGS production well. The following table summarizes the requirements that must be met for a lifting system installed in an EGS production well. Additional explanation on each of these requirements is provided subsequently.

Table 2.1 EGS Lifting system requirements

Criterion	Specification
Mass Flow Rate	> 80 kg/s
Well Inner Bore Size/Drift Inner Diameter	12.348”/12.191”
Bore size variation	9.675” to 16”
Bore Straightness	4 to 6 degrees over 1 km length
Pressure Boost Required	> 300 bar
Target Well Depth	> 6 km
Lifting System Depth	~ 2 km
Geothermal Fluid Temp - Maximum	Up to 350^{o}C
Geothermal Fluid Temp – Operating Range	250-300^{o}C (continuous)
Pump Suction Pressure	Sat Pressure + NPSH + 50 psia

Well head discharge pressure	Suction Pr + Pump Boost - Losses
Water Chemistry – Salinity	2500 to 5000 PPM Total Dissolved Solids
Deposits/Scaling	Site Specific
Water Chemistry – pH level	~ 6.5 (slightly acidic)
Corrosive contaminants	Possible CO2, H2S (Site Specific)
Particulates – concentration, size	Negligible after Equilibrium
Gas fraction	2% or less
Power supply	Higher Voltage to Minimize Losses
Nominal RPM	3500
Variable speed drive	Yes
Reliability	3 yr. MTBF
Availability	> 95%
Service Life	3 years
Maintenance Interval	None
CAPEX	Pump Cost * 1.33 (for spare capacity)
OPEX	Cost of Electricity to Operate Pump
Overall Efficiency	> 70%
Pump support	Tubing String, Polished Bore Receptacle, Y-tool

The required mass flow rate through the lifting system must be at least 80 kg/s. EGS wells are expensive to drill, and a certain minimum production rate per well must be met for the application to be commercially viable. DOE's Geothermal Technologies Program has set this requirement to be at least 80 kg/s based on discussions with experts in the EGS industry. AltaRock Energy, a US-based EGS company, also confirmed this production flow requirement. A Kalina-based plant near Munich, Germany, operates a lifting pump capable of flow rates up to 150 kg/s, albeit at much lower temperatures than what is expected of an EGS application.

Geothermal wells generally have a larger bore size compared to the standard sizes used in the oil & gas industry. A modern geothermal plant near Reno, Nevada has its lifting pumps installed in a bore of 9.875" diameter. The aforementioned Kalina-based plant in Germany employs well bores of 16", 13.375" and 9.875" in its production wells. AltaRock Energy confirmed that the well bore diameter in an EGS well is likely to be 13.375", and that the casing inner diameter around the lifting pump is likely to be 12.348". Expected drift inner diameter is 12.191", meaning that although a bore size of 12.348" is available for water flow, any equipment installed within the well must not exceed a diameter of 12.191" to account for well out-of-roundness and/or non-straightness.

EGS wells are drilled stepping down in bore size and as vertical as possible all the way to the EGS reservoir. Inclinations of up to 7 to 8 degrees have been reported for 12" bores of several thousand feet in length. The lifting system is likely to be installed in a small section that is relatively straight; however it must accommodate this overall bore inclination. Lifting pumps for EGS applications can be more than 100 meters long and hence they cannot handle large bore inclinations.

Modern geothermal plants (specifically EGS) operate in a closed loop with the geothermal fluid under pressure, so it never flashes to vapor. The pressure boost requirement of a lifting pump depends on the depth setting, pressure loss through the production tubing and the plant equipment (heat exchangers, valves etc) until it reaches the injection pump where a further pressure boost is provided to the geothermal fluid. In the Kalina-based plant in Germany referenced above, no injection pumps are present, and the lifting pump is required to provide enough pressure boost to circulate the geothermal fluid through the entire injection/production loop. The pressure boost requirement is very site-specific, and 300 bar provides an industry-accepted requirement for the lifting pump (*Source*: AltaRock Energy).

Target well depth is site-specific depending on the geothermal gradient and the desired fluid temperature. EGS wells are likely to be 4 to 8 km deep to access the hot dry rock at 200 to 400^{o}C. Well depth does not affect the pump design directly and an average number of 6 km is assumed (*Source:* AltaRock Energy).

Pump setting depth is a critical parameter that depends on the actual well bottom pressure and the desired well head pressure. It is also important that the geothermal fluid does not flash at any point in its circulation loop. The lowest pressure point prior to the pressure boost delivered by the lifting pump is at the pump suction. The setting depth must be chosen to ensure that the lowest pressure point at pump suction (impeller leading edge vane at suction) is above the vapor pressure of the geothermal liquid. Note that the pump usually produces a draw down on the well bottom pressure and hence the net positive suction head curve of the pump must also be taken into account. The well bottom pressure dictates the pump setting depth and the well head pressure drives the pressure boost requirement for the pump. As such, pump setting depth is very site-specific. As per industry experts, EGS wells would require large setting depths of the order of approximately 2 km (*Source:* AltaRock Energy).

Geothermal fluid temperature directly correlates with the reservoir rock temperature. Depending on the local geothermal gradient and the depth of the EGS reservoir, geothermal fluid temperature

can be as high as 300 to 350^{o}C. Currently there are no geothermal plants that operate with fluids at such high temperature, but the expectation of the EGS industry is that with improved drilling methods, such temperatures are likely to become standard in the future. A higher geothermal fluid temperature results in greater enthalpy exchange and increased power production. An additional constraint on the allowable maximum temperature of the geothermal fluid is the lifting system itself, where system components need to able to operate reliably at that temperature. Based on the DOE Geothermal Technologies Program requirements and in consultation with AltaRock Energy, Inc., a geothermal fluid temperature range from 250 to 350^{o}C is expected.

As mentioned previously, the pump suction pressure must be higher than the saturation pressure of the geothermal fluid to avoid flashing. To account for pump draw down, add to it the maximum required net positive suction head (NPSH) and provide a buffer of 3 to 4 bar. The saturation pressure depends on the geothermal fluid temperature. The maximum required NPSH depends on the pump design and its operating range. For a 300^{o}C fluid, the suction pressure will be in excess of 1200 psia.

The required wellhead discharge pressure is entirely dependent on the site and the power plant. The required well head discharge pressure must be equal to the suction pressure at the injection pump plus the losses through the piping between the production and injection wells as well as through the power plant equipment (heat exchangers, valves etc.). In addition, the well head discharge pressure must be sufficient to ensure the fluid remains in the liquid state throughout the conduit between the production well and the injection well. The actual wellhead discharge pressure achieved equals the suction pressure at the lifting pump + pressure boost provided by the lifting pump – head loss through the tubing string. The pressure boost provided by the lifting pump must be sufficient to meet the required wellhead discharge pressure.

It is generally expected that the constantly recirculated geothermal fluid quickly reaches equilibrium with respect to accumulation of dissolved salts. Typical dissolved solid content is expected to be in the range of 2500 to 5000 ppm. However this can change from site to site and also over time; the dissolved solid content is likely to be highest during the initial phases of production. Hence scale and deposit formation on the pipes, pumps and plant equipment is a significant concern during the initial phases but is expected to ease fairly quickly. Until equilibrium is reached, scale formation must be monitored and remedial treatments may need to be applied.

Geothermal fluid is likely to be slightly acidic with a pH level around 6.5 or so, due to the presence of dissolved CO2. This also poses a slight corrosion risk and the extent of the risk depends entirely on conditions specific to the EGS site (*Source:* AltaRock Energy).

Particulates such as sand can result in erosion and abrasion of the piping and the lifting system components. During initial phases of operation, some sand particles are expected; however once equilibrium is established, particulate content is likely to be negligible (*Source:* AltaRock Energy).

Power to the lifting pump is provided directly from that produced by the power plant. Higher voltages may be used to minimize transmission losses. At the aforementioned geothermal plant

in Nevada, a 4170V feeder bus is used to power the production Electric Submersible Pumps (ESPs).

Nominal operating speed of the lifting pump depends on the pump type, though 3500 RPM is a standard operating speed of ESPs. In addition, a variable speed drive is commonly used to start up and shut down the production gradually.

The traditional industry standard for operating life is 4 years for a line-shaft pump and 3 years for an electric submersible pump. At the end of the operating life, the pump is typically replaced by a new one. The lifting system is expected to be available 95% of the time and must be maintenance-free (*Source:* AltaRock Energy).

2.2 LIFTING METHODOLOGIES AND DOWN-SELECTION

2.2.1 Categories of Lifting Systems

Lifting pumps play a critical role in enabling commercially viable production rates from EGS production wells (unless the EGS energy conversion system uses flash-steam technologies). Most EGS plants under operation, and those being planned, operate on a binary cycle (ORC, Kalina, etc.) where the geothermal fluid circulates in a closed loop and is always kept under pressure to prevent flashing. In addition, each EGS well is designed for operation at the maximum flow possible for the temperature and well construction, usually around 100 kg/s or greater. Hence there is a critical need for a reliable and cost-effective high temperature and high volume lifting pump for EGS applications.

Lifting Pumps currently used in the Geothermal Industry are usually one of the following three types:

(1) Line Shaft Pumps
  – Downhole pump with a surface electric drive
(2) Electric Submersible Pumps
  – Downhole pump with a downhole electric drive
(3) Turbo Pumps
  – Downhole pump with a downhole hydraulic drive

Each of these pump types will be evaluated for their suitability to meet the target EGS specification (as laid out in the previous section).

Geothermal power generation from EGS wells is a relatively new industry and as we will see later, there exist significant technological gaps that need to be filled before a traditional geothermal lifting pump can be used for high depth / high temperature / high volume EGS production wells. As such, other lifting methods are considered, primarily drawn from artificial lift applications in the oil and gas industry, to broaden the search for an appropriate lifting method for EGS well production. Combining all these lifting methods, a more general method can be employed to

classify them based on the type of power source. The following lifting methods are grouped according to their power source:

(1) Mechanical drive
    a. Reciprocating rod pumps
(2) Pneumatic drive
    a. Gas lift
(3) Hydraulic drive
    a. Turbo pumps
    b. Diaphragm/Piston pumps
    c. Jet pumps
(4) Electric drive
    a. Line shaft pumps
    b. Electric submersible pumps
    c. Progressing cavity pumps

In this section, each candidate lifting system is described briefly and a qualitative assessment is made of its suitability for EGS lifting applications. Then the target EGS lifting system specification is laid out and a rough quantitative analysis is performed to estimate some key performance metrics for each lifting system. Finally a detailed comparison is made of the different lifting methods for EGS applications and a recommendation is made of the most preferred method for lifting geothermal fluid from an EGS well.

2.2.2 Line Shaft Pumps

The most commonly used lifting method for geothermal well production is the line shaft pump. An electric motor, mounted on the surface, drives a long shaft connected to a downhole pump. The downhole pump can be a multi-stage roto-dynamic pump (e.g., centrifugal pump) or a positive displacement pump (e.g., screw pump), though roto-dynamic pumps are used almost exclusively. Fig 2.1 shows a 350 HP line shaft pump installed at the Soultz EGS plant in France. It is capable of pumping up to 40 liters/sec of geothermal fluid at ~ 150^{o}C.

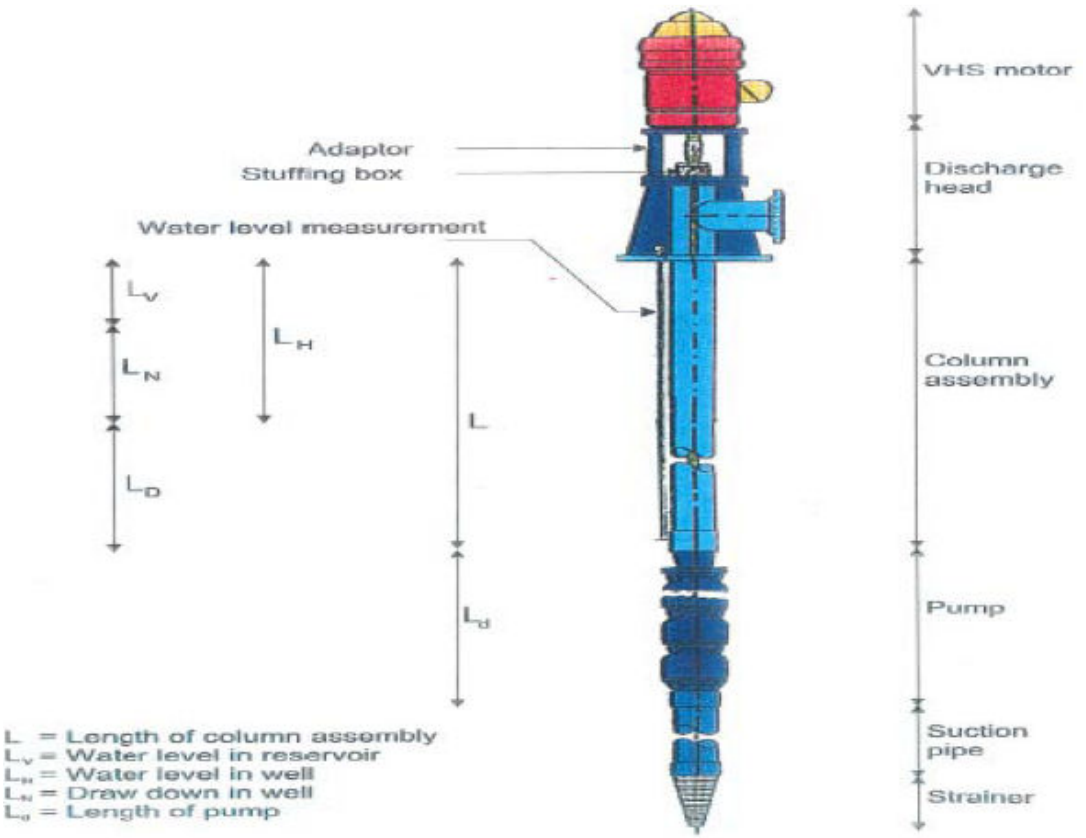

Figure 2.1 - IGE (Icelandic Geothermal Engineering Ltd.) Line Shaft Pump at Soultz EGS Plant, France

Line shaft pumps are not particularly suited for high depth / high volume EGS applications. A key constraint is the pump setting depth, which is currently limited to around 600 m. Line shaft pumps cannot be set at greater depths because the long line shaft flexes too much causing vibration, stress on the bearings, and excessive wear of the pump impellers. An additional limitation arises from the shaft power transmission requirement (usually in the MW range for EGS), which may require an unacceptably large shaft diameter. Large shaft diameters reduce the amount of fluid that can be produced. Also, line shaft pumps require nearly vertical bores, which may not be possible for large setting depths.

Commercially available line shaft pumps can handle production fluid temperatures up to 150^{o}C, though higher operating temperatures are feasible with the right materials and coatings. Line shaft pumps also require constant lubrication of the rotating drive shaft. This can result in lubricant leaking into the production fluid, posing long term environmental risk in addition to near term risk of clogging/fouling of heat exchangers in binary plants. For this purpose, warm demineralized water was used for shaft lubrication at the Soultz EGS plant.

Overall efficiency of line shaft pumps varies from ~65% and 80% and they have a mean operating life of 4 years. Usually the pump is replaced at the end of its life. Apart from the initial cost of the pump, the operating cost involves the parasitic load on the geothermal plant as well as the cost of the lubricant (~ $4/gallon with dosage rates of approximately 2 ppm).

Key advantages to employing a line shaft pump for high volume / high temperature / high depth EGS applications are:

- Line shaft pumps are a mature technology and have been used in the geothermal industry for decades.
- They can handle higher temperatures much more easily than an ESP as there is no downhole motor to cool.

Key disadvantages associated with line shaft pumps are:

- They are limited to a setting depth of ~600 m, whereas EGS wells are likely to require setting depths of several km.
- They require a constant supply of shaft lubricant with the associated cost, fouling risk and environmental risk.
- Line shaft pumps need nearly vertical bores to accommodate the long, straight rotating shaft.
- Line shaft pumps have a significant mechanical risk associated with possible failure of the long shaft.
- High volume line shaft pumps (> 100 liter/sec) are not available commercially.

2.2.3 Electric Submersible Pumps

An electric submersible pump (ESP) is a multi-stage, centrifugal downhole pump driven by a downhole electric motor. The pump and the motor are coupled through a common shaft with a seal section (motor protector) and fluid intake in between. ESPs are typically suspended on a tubing string hung from the wellhead and are submerged in the production fluid. Electricity is supplied from the surface through a special heavy-duty armored cable attached to the tubing, which plugs into the top of the motor. A variable-speed drive mounted at the surface controls the motor and pump operation. Before the geothermal fluid enters the pump, it must flow around the motor, which aids in cooling it and thus keeps the motor internals from overheating. Each stage (impeller/diffuser combination) of the pump adds pressure to the fluid at a given rate. The fluid builds up enough pressure as it reaches the top of the pump to be lifted to the surface and circulated through the power plant loop. Fig 2.2 shows a typical ESP as well as the cross sections of the pump, motor, and seal sections.

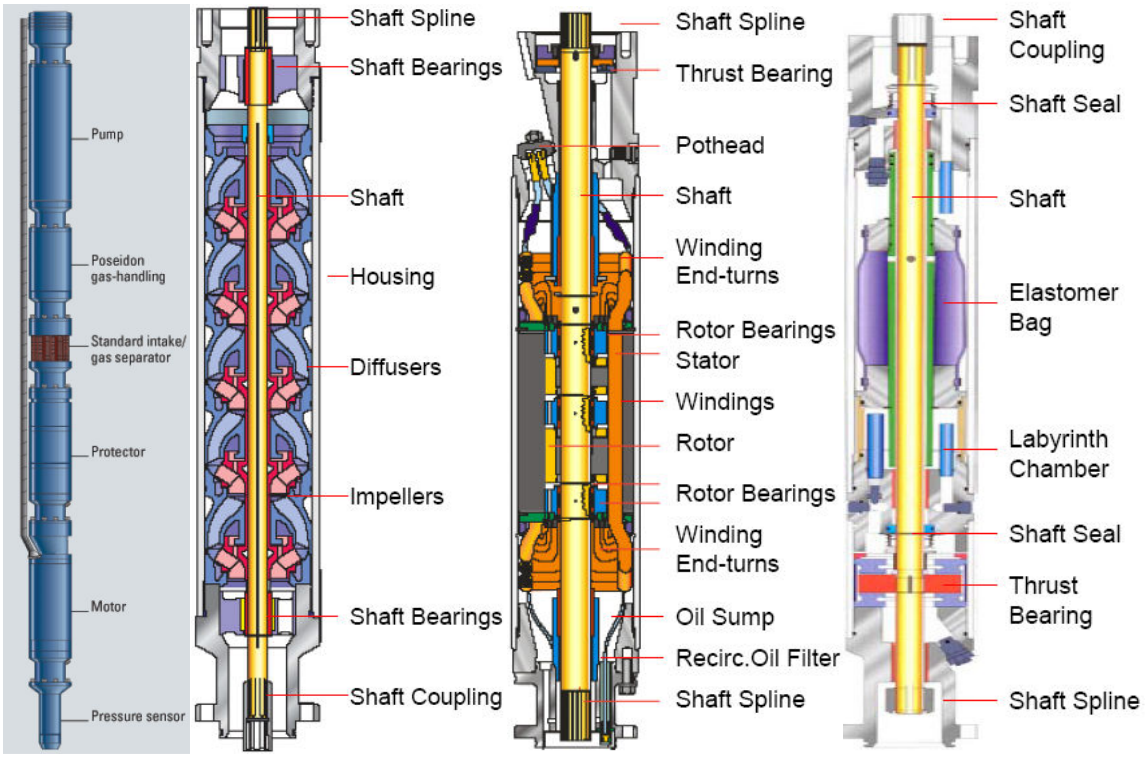

Figure 2.2 - Typical configuration of an electric submersible pump showing (a) Assembly (b) Multi-stage centrifugal pump (c) Motor (d) Protector (*Courtesy* : Schlumberger Reda)

Electric submersible pumps can operate at much greater depths compared to line shaft pumps. In addition, they can deliver much larger volumes – Siemens' EGS plant in Germany has a 150 liter/s ESP currently in operation. ESPs are particularly well-suited for EGS applications because the likely setting depths and flow rates will exceed those possible with the line-shaft pumps. Electric submersible pumps can be installed in wells with large bore inclinations/deviations as long as a small straight section is available at the pump setting depth (ESPs for EGS can be as much as 100 meters long). Because they can be set at great depths, they can produce more fluid from each well since more drawdown can be accommodated. ESPs have a great range of operating flexibility due to a variable speed drive that is capable of accommodating large swings in production volumes.

ESPs depend on movement of produced fluids to transfer heat away from the motor. This places a limit on the operating temperature of the ESP internals, which is currently around 288°C (the current temperature limit on produced fluid is around 218°C). Most pump usage in the geothermal industry has occurred at resources where the fluid temperatures are <175°C. Industry has been working to increase the upper temperature limits on these pumps to 350°C and beyond. Also, close to half of the pump breakdowns experienced in the geothermal industry are due to electrical problems caused by water infiltration. To meet EGS needs associated with long-term, high-temperature, deep-well operation, technical advancements in high temperature dielectric fluids, enhanced thermal management, advanced materials, and seals are required. Electric submersible pumps with 1000-3000 horsepower motors must survive ~3 years at ≥ 300ºC to be viable for EGS needs.

Electric submersible pumps are relatively compact—the bore area taken up by the power supply lines is the smallest by far of various lifting methods being considered here. They are proven at extreme depths and pressures in tough working environments in oil and gas applications. Any wasted energy (converted to heat) only increases the enthalpy of the geothermal flow. However they have some sizeable shortcomings for EGS applications, particularly with respect to motor temperature and power density as well as connectors, seals, and bearings.

Key advantages to employing an electric submersible pump for high volume / high temperature / high depth EGS applications are:

- ESPs can be installed downhole at great depths.
- They have high efficiency at large flow rates.
- Minimal or no maintenance is required.
- There are no operating costs apart from the parasitic load on the plant.
- They have minimal surface equipment requirements.
- ESPs have high resistance to corrosive downhole environments.
- They can be used in deviated wells and bores with large inclinations.
- The system is easy to adapt to automation and can pump intermittently or continuously.

Key disadvantages to employing an ESP for EGS applications are:

- High temperature of the produced fluid can result in overheating of the motor.
- There is electrical risk due to water infiltration / ion migration / insulation failure.
- Possible scale deposits /corrosion can interfere with the operation of the pump.
- ESPs are not easily serviceable – the entire system must be pulled for servicing.
- ESPs generally have poor solids handling capability.

2.2.4 Turbo Pumps

A Turbo pump consists of a down-hole multi-stage centrifugal pump driven by a down-hole hydraulic turbine coupled to it through a common drive shaft. The hydraulic turbine (usually axial flow) itself is driven by pressurized geothermal water supplied to it from a surface pump through a dedicated conduit. Typical installation involves the down-hole pump/turbine assembly attached to the end of a tubing string, which is run into the well. Power fluid is directed down an inner tubing string, which drives the turbine. The power fluid is returned to the surface along with the production fluid through the annulus by the centrifugal pump. Figure 2.3 shows a particular configuration of the turbo pump assembly.

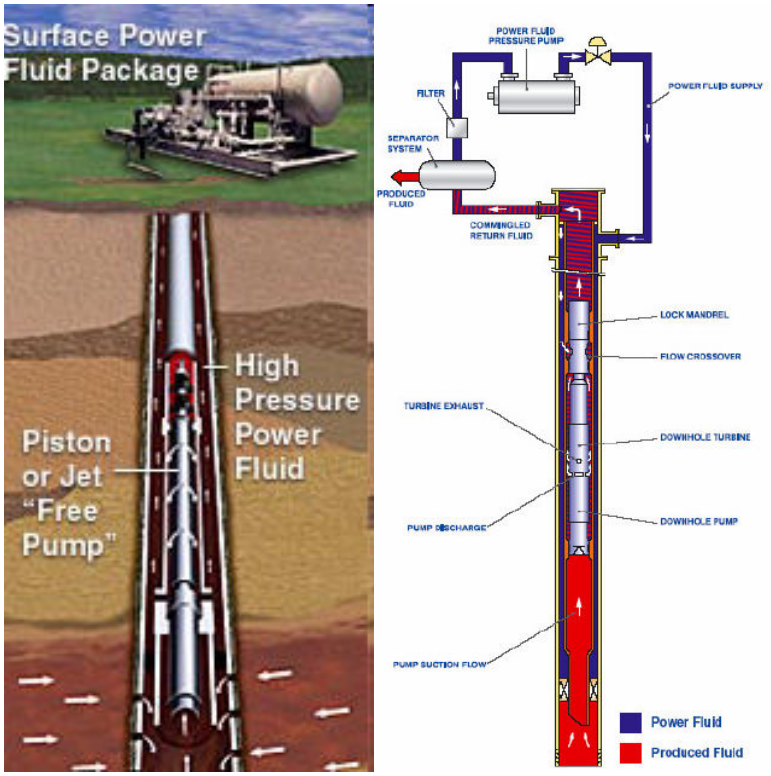

Figure 2.3 - Turbo Pump Operation (Courtesy: World Oil, July 2006)

Turbo pumps offer key advantages for EGS applications:

- They can handle the high temperature of the production fluid expected in EGS applications, as none of the down-hole components need to be cooled.
- Turbo pumps do not require drive shaft lubrication (like in line shaft pumps) and do not require any maintenance of down-hole components.
- Turbo pumps usually are shorter in length than ESPs (for the same application) and hence can tolerate a higher degree of bore inclination.
- They have good operational flexibility. Valves on the well head control the supply of power fluid to the down-hole turbine, thereby controlling the rate of production.
- Turbo pumps can handle very high rates of production up to 200 kg/s.
- They can handle sand content better than ESPs or line shaft pumps.

Turbo pumps also suffer from major disadvantages:

- They have low energy efficiency compared to ESPs or line shaft pumps. Significant losses occur during the conversion process from electric energy (drawn from the plant) to potential energy (hydraulic pressure) and then from potential energy to kinetic energy in the hydraulic turbine.
- Turbo pumps require more topside components than line shaft pumps or ESPs – surface pumps, valves, conduits, storage etc.

- Turbo pumps result in enthalpy dilution due to the mixing of low temperature power fluid with the high temperature production fluid.
- They are only economical where there are a number of wells connected together to a central surface pumping facility.

2.2.5 Diaphragm/Piston Pumps

Hydraulic diaphragm / piston pumps are a variant on the hydraulic turbo pumps, where the power fluid is used to drive a positive displacement diaphragm pump or a piston pump instead of a hydraulic turbine. They offer the same advantages / disadvantages as hydraulic turbo pumps with some key differences which makes them particularly unsuitable for high temperature / high volume EGS lifting applications. Fig 2.4 shows a hydraulic diaphragm pump used for artificial lift applications in Oil & Gas industry.

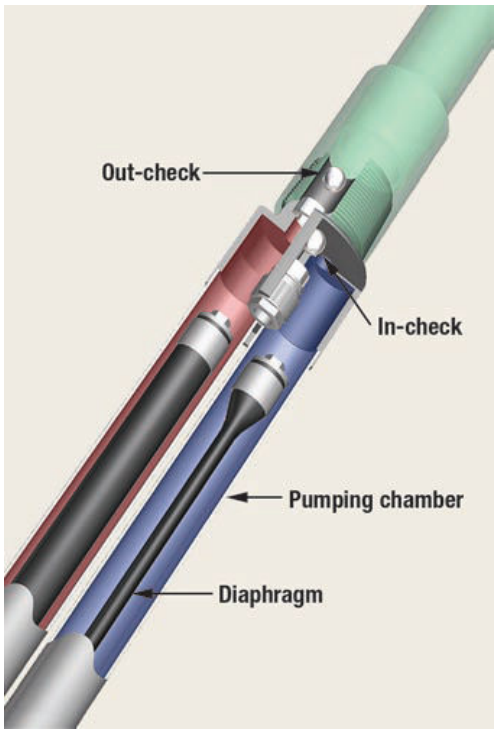

Figure 2.4 - Hydraulic diaphragm pump from Smith Lift (Courtesy: World Oil, July 2006)

Hydraulic diaphragm / piston pumps cannot lift high volumes of geothermal fluids required for EGS applications. In addition, the high temperature poses a particular challenge for diaphragm pumps (it is difficult to maintain stiffness of the diaphragm due to possible creep issues). Piston pumps handle high temperatures better but are prone to mechanical problems. Hydraulic diaphragm / piston pumps are not suitable for EGS applications due to the high temperatures and the low flow rates they can support. Axial flow turbo pumps are much more suitable when employing a hydraulic drive for lifting purposes.

2.2.6 Jet Pumps

Jet pumps are a special class of hydraulic downhole pump sometimes used in place of turbo pumps or reciprocating pumps. Hydraulic jet pumps operate by pumping high-pressure power fluid (water) through a motive nozzle where it is converted to high velocity and low pressure. This in turn entrains the production fluid from the EGS well. Momentum is transferred from the motive fluid to the suction fluid by shear interaction. The two streams are combined in a mixing tube resulting in a single high velocity, low-pressure stream. The combined stream then passes through a diffuser that converts the fluids back to low velocity and high pressure. Fig 2.5 shows a typical jet pump configuration.

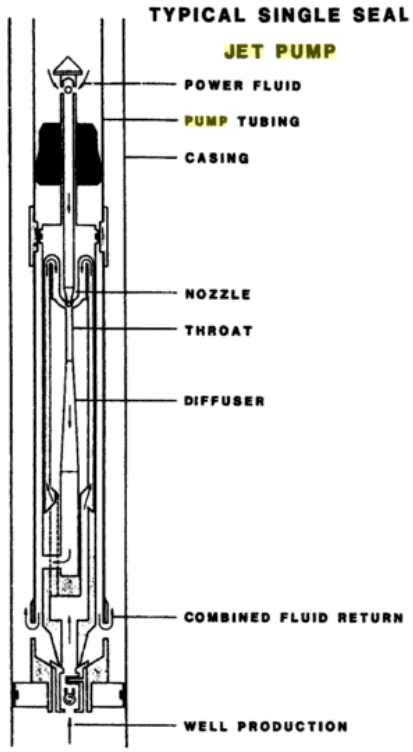

Figure 2.5 - Jet pump configuration

Because hydraulic jet pumps have no moving parts, they require little pump maintenance and have long service lives. Jet pumps can be installed deep (up to 6 km) and can handle flow rates of up to 100 kg/s relatively easily. Production rate depends on the power fluid pressure and flow rates and hence jet pumps have good operational flexibility.

Some common advantages of jet pumps are:

- Jet pumps have no moving parts and have high mechanical reliability.
- Little or no maintenance is required during operation.
- They can handle high temperature production fluids from EGS wells.
- They can be installed at any depth.

- Jet pumps have high volume capability.
- They have good corrosion resistance.
- They have good solids-handling capability.

Disadvantages include:

- Poor efficiency due to high mixing losses.
- They cannot handle wide fluctuations in production rate from the design point.

2.2.7 Reciprocating Rod Pumps

Rod pumps consist of a surface drive connected to a reciprocating piston (sucker rod) located down-hole. The reciprocating action generated by the surface drive unit causes the traveling piston of the downhole pump to move geothermal fluid to the surface. Reciprocating rod pumps are commonly used for artificial lift applications in the oil and gas industry, but are not particularly suited for geothermal applications. The working of a reciprocating rod pump is shown in Figure 2.6.

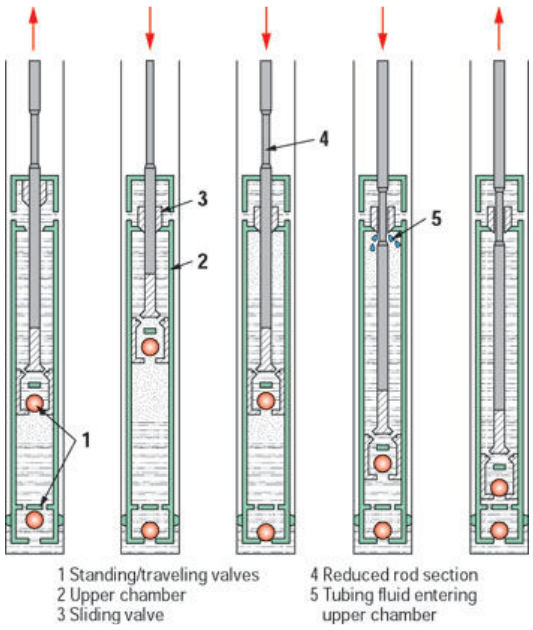

Figure 2.6 - Working of a reciprocating rod pump (Source: World Oil, April 2003)

Key advantages of reciprocating rod pumps are:

- High system efficiency.
- Excellent operational flexibility - production can be adjusted through stroke length and speed.
- They have good solids handling ability.
- They are economical to repair and service.

They also have a host of disadvantages making them particularly unsuitable for EGS applications:

- Reciprocating rod pumps are particularly suitable for pumping highly viscous oils but not low viscosity, high temperature geothermal fluids, where they have a high volumetric efficiency loss.
- Power transmission and setting depth are limited by the weight and strength of the mechanical members and are not in line with EGS requirements.
- They are not suited for high volume flow rates required in EGS production wells.
- They cannot be used in deviated wells.
- They generate large amounts of ambient noise.

2.2.8 Gas Lift

Gas lift involves injecting compressed gas into the geothermal fluid column through gas lift valves attached to mandrels mounted on the production string. The compressed gas is typically air or nitrogen and is supplied from the surface through a dedicated conduit attached to the production string. By displacing the denser liquid, the weight of the fluid column is decreased, increasing the pressure differential between the reservoir and the well bore thus increasing flow. Essentially, the geothermal fluids are lightened by the gas, which allows the reservoir pressure to force the fluids to surface. Gas lift requires extensive surface equipment including a compression unit, separation unit, gas storage facilities, etc. Figure 2.7 shows a gas lift facility.

Gas lift is suitable for oil and gas applications where the objective is mass recovery. Moreover, natural gas is readily available as a by-product during oil extraction, allowing it to be profitably employed in gas lift. For geothermal applications, however, it is likely that air would need to be supplied for gas lift; air is almost twice as dense as natural gas. Energy expenditure for compressing the gas would be prohibitively high, in addition to facilities needed for handling and separating the gas from the production stream. This cost can be offset somewhat if the gas can be supplied to multiple wells by a central compression facility.

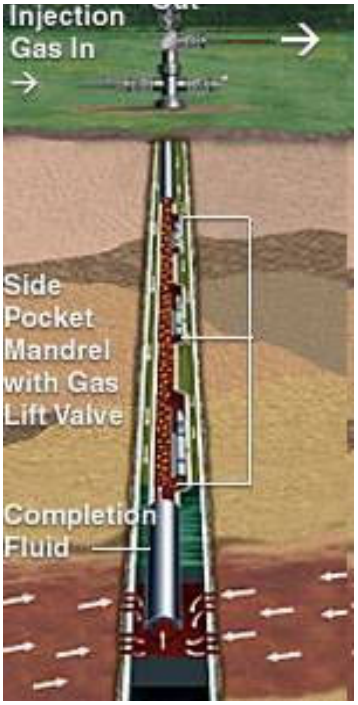

Figure 2.7 - Typical gas lift configuration

Gas lift advantages include:

- High temperature of production fluid is not a concern at all.
- Gas lift provides excellent flexibility in controlling production rate by changing gas injection rate.
- Gas lift has excellent sand and solids handling capability.

Gas lift disadvantages include:

- It is not feasible if no source of gas is present.
- There is high initial capital purchase cost.
- Gas lift is maintenance-intensive.
- It is relatively difficult to operate.
- Compression cost may be high and compressor hardware must be reliable.
- Operating efficiency is fair overall, but poor for intermittent gas lift.

2.2.9 Progressing Cavity Pumps

Progressing Cavity Pumping (PCP) Systems are positive displacement pumps coupled with a downhole electric drive or a surface electric drive. In the case of a surface electric drive, a long drive shaft is used to transfer mechanical power to the pump. The pump consists of a single helical rotor turning inside a double helix stator. The stator is attached to the production tubing string and the rotor is connected to the drive shaft. As the rotor turns, driven by a topside or downhole motor, an advancing series of cavities are formed between the rotor and stator, which

progress from the inlet to the discharge end of the pump. The production fluid is trapped in these cavities and is displaced through the pump and up the tubing. This results in a non-pulsating positive displacement flow with a discharge rate proportional to the size of the cavity, rotational speed of the rotor and the differential pressure across the pump. Fig 2.8 shows a progressing cavity pump configuration as well as a close up view of the rotor & stator.

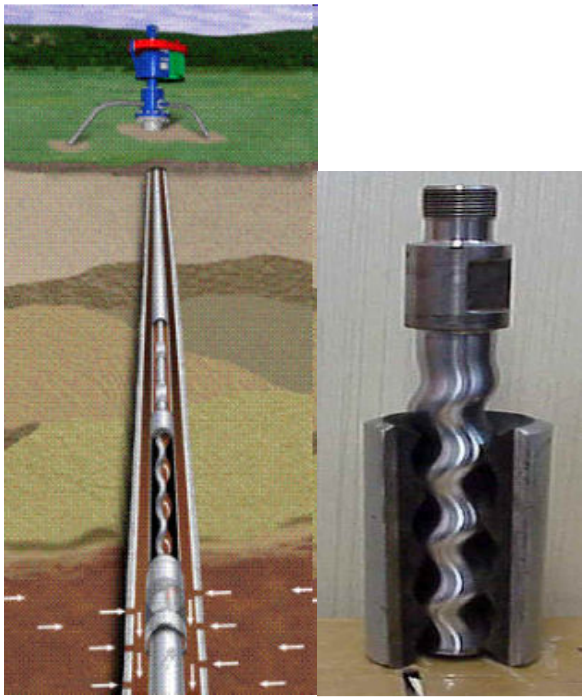

Figure 2.8 - Progressing cavity pump configuration; close up of rotor / stator. (courtesy: World Oil, July 2006)

As they are positive displacement pumps, PCPs have a high volumetric efficiency, but some of this benefit is lost for EGS production, where the fluid temperature is high and viscosity low. PCPs are inexpensive compared to ESPs, but are limited to low production volumes and, in the case of surface drive, to low setting depths.

Some advantages of progressing cavity pumps with respect to EGS applications are:

- Low capital investment (with surface drive).
- High system efficiency.
- Good solids handling ability.
- No maintenance required with a downhole drive.

Key disadvantages of progressing cavity pumps are as follows:

- PCPs cannot be set at large depths required for EGS (with surface drive).
- They cannot handle EGS temperatures without a significant drop in volumetric efficiency.
- They are limited to low production rates – cannot meet EGS requirements.

- High pressure boost is difficult to obtain.

2.2.10 Comparison of Various Lifting Methods

A qualitative assessment of the various lifting options meeting the EGS target specification is shown in Table 2.2.

	Reciprocating Rod Pump	Gas Lift	Turbo Pump	Diaphragm Pump	Jet Pump	Line Shaft Pump	Electrical Submersible Pump	Progressing Cavity Pump
Flow Rates > 80 Kg/s	No	Yes	No	No	Yes	No	Yes	No
Fluid Temp ~ 300 C	No	Yes	Yes	No	Yes	No	No	No
Pressure Boost ~ 300 bar	Yes	No	Yes	Yes	No	Yes	Yes	Yes
Setting Depth ~ 2-3 km	No	Yes	Yes	Yes	Yes	No	Yes	No
Bore Inclination ~ 6 degrees	No	Yes	Yes	Yes	Yes	No	Yes	No
Solids Handling	Good	Bad	Bad	Good	Good	Bad	Bad	Good
Corrosion / scaling Risk	High	Low	Low	High	Low	Low	Low	High
Overall Efficiency	45% to 60%	10% to 30%	30% to 40%	40% to 50%	10% to 30%	65% to 80%	65% to 80%	65% to 80%
Maintenance	Lubrication / Valves	Valves	None	None	None	Lubrication	None	None

Table 2.2 Lifting system assessment

2.2.11 Target Specification for the Lifting System

In a previous section, the design specifications for a lifting pump operating in an EGS production well were laid out. The key items in the target specification can be summarized as follows:

a. Geothermal Fluid (brine) Temperature = 300^{o}C
b. Desired Well Production Rate = 80 kg/s
c. Desired Pressure Boost = 300 bar
d. Bore Size = 13.375”
e. Max. Pump Setting Depth = 3 km

Each of the lifting systems discussed here will be evaluated against its ability to meet the target specification. Quantitative analysis is carried out wherever possible, and is duly supplemented with qualitative discussion. The lifting methods are ranked on five key performance metrics:

(1) Power consumption
(2) Capital cost
(3) Operating cost
(4) Reliability
(5) Contaminant tolerance

Based on the ranking, a recommendation is made on the preferred lifting system for EGS applications. The technology gaps to be filled to achieve a robust design are also identified.

2.2.12 Electric Submersible Pump Performance

The power consumed by an electric submersible pump designed to meet the target specification laid out above can be calculated as follows:

$$P_W = \frac{\dot{Q}_m}{\rho(p_s, T)} \Delta p \, \eta_{mot} \eta_{mech} \eta_{hyd} \eta_{vol}$$

where

$\dot{Q}_m$ = Desired mass flow rate = 80 kg/s

$\rho(p_s, T)$ = Flow density at stage pressure and temperature

Δp = Pressure rise across the pump

Net power is calculated by summing the power consumed by each stage of the pump until the desired pressure rise is obtained. Based on commercial data, it is assumed that the motor efficiency is about 90%, pump mechanical efficiency about 85%, hydraulic efficiency is around 92% and pump volumetric efficiency is around 92%.

Pressure rise per stage is estimated based on the maximum impeller diameter possible (~ 10 in) to determine the number of stages required to yield the desired pressure boost of 300 bar.

$$\Delta p = \frac{1}{2}\left(\frac{\pi DN}{60}\right)^2 \eta_{hyd}\rho(p_s, T)$$

Minimum setting depth required for the pump is also estimated based on the consideration that pump suction pressure cannot fall below the saturation vapor pressure at the fluid temperature.

$$d_{\min} = \frac{P_{sat}(T) + NPSH_{req}}{\rho(P_{sat}, T)g}\frac{1}{1-\beta}$$

where 5 bar is assumed for NPSH requirement and 0.1 as the safety factor β.

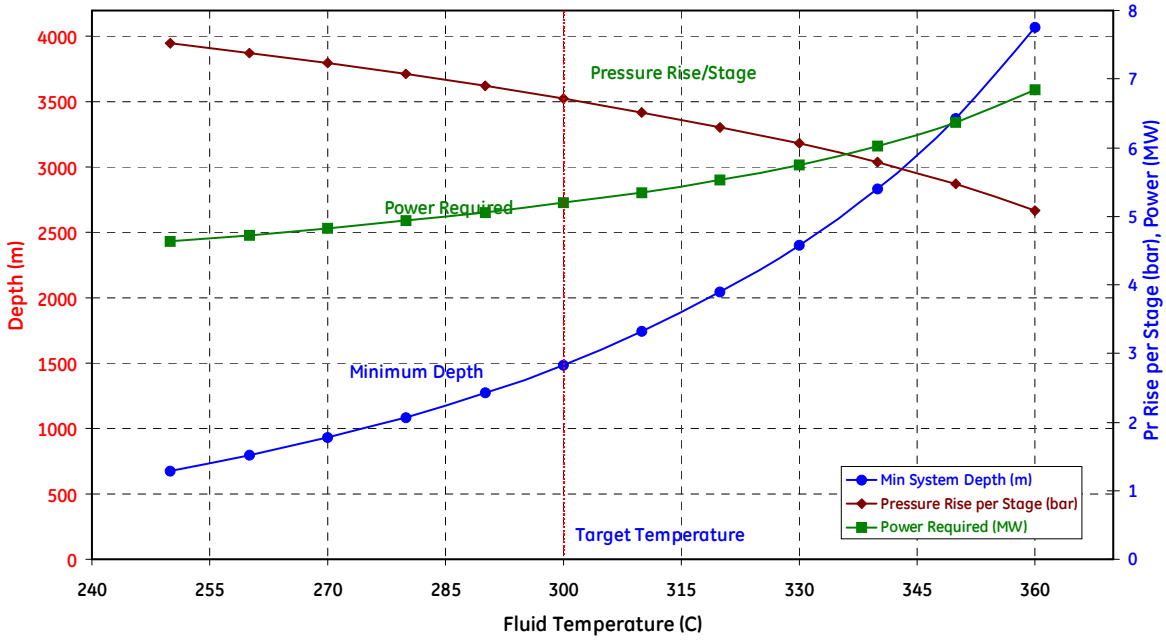

Figure 2.9 - Expected performance of an ESP that meets the target specification

The power consumed by an ESP that meets the target specification is on the order of 5 MW (shown in Figure 2.9). The minimum setting depth exceeds 3 km for fluid temperatures above 340ºC. Hence an ESP set at 3 km depth cannot pump water hotter than 340ºC. Pressure rise per stage is about 6.8 bar at the target specification, which means that about 45 stages are needed to produce the target pressure boost.

2.2.13 Line Shaft Pump Performance

The downhole multistage line shaft centrifugal pump can be assumed to be identical in both electrical submersible pumps and line shaft pumps. The key difference is the length of the drive shaft connecting the motor to the pump though which power transmission occurs. The bearings are likely to be stiffer and number of bearings higher, resulting in increased mechanical losses. Assuming that the mechanical efficiency drops by 10 points due to these increased losses, the

power required to pump 80 kg/s of hot geothermal fluid through a DP of 300 bar will increase to 5.9 MW. Fig. 2.10 shows the variation in the power required as a function of geothermal fluid temperature.

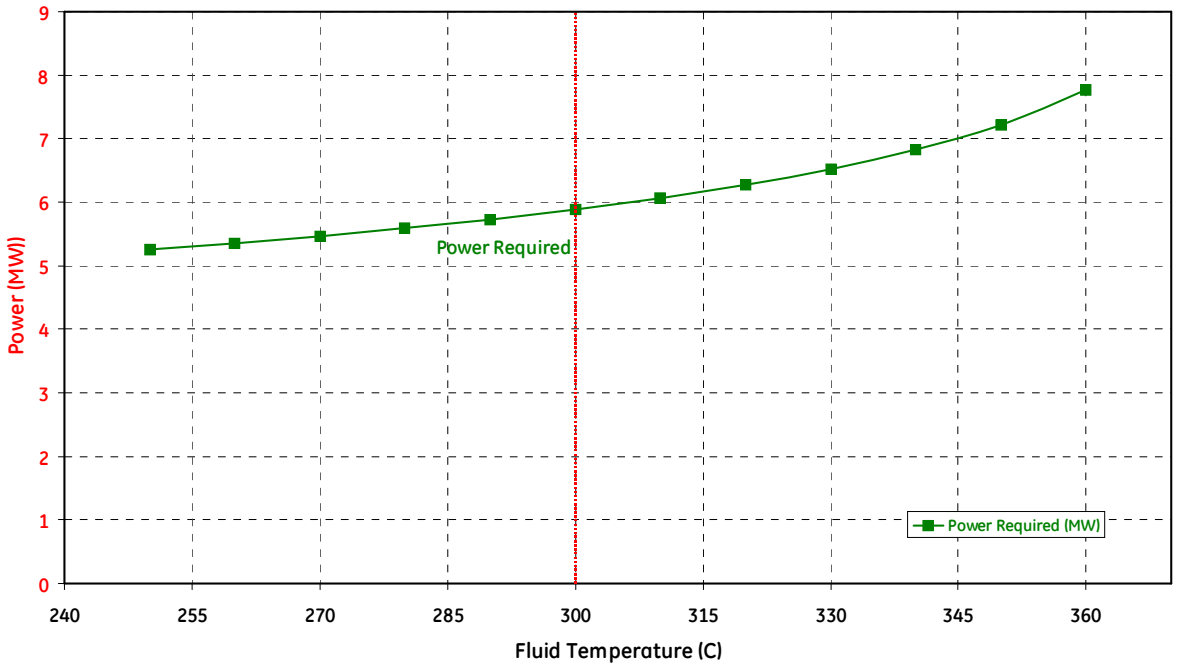

Figure 2.10 - Expected power consumption of a line shaft pump that meets the target specification as a function of the geothermal fluid temperature

Knowing the shaft power, one can estimate the shaft diameter required to transmit it by putting a limit on the maximum allowable shaft torsional stress. Also, one can determine the number of bearings required, stiffness of the bearings, etc. by imposing limits on the maximum allowable shaft deflection and rotor critical speeds. These are primarily design calculations, which will not be performed here. However, the calculations will show that the shaft diameter and shaft deflections will be unacceptably large for a line shaft pump operating at the depths required for an EGS well.

Line shaft pumps are generally less expensive than ESPs and are easier to install, though it is unknown whether the same holds for large-depth EGS applications. To be conservative, it is assumed that capital costs are the same in both cases.

The operating costs for a line shaft pump are likely to be higher than that of an ESP. The long drive shaft needs constant lubrication and the required power is higher (compared to ESP), leading to increased operating costs. However, the life of a line shaft pump is expected to be 4 years as opposed to 3 years for an ESP, which means that only ¼ of all line shaft pumps need to be removed and replaced as opposed to 1/3 of all ESPs in any given year. One can reasonably estimate that overall operating costs are likely to be higher with a line shaft pump.

Line shaft pumps are more reliable than ESPs. The primary risk with line shaft pumps is mechanical, whereas with ESPs it is primarily thermal (motor overheating) and electrical (brine leakage leading to short circuit). Industry experience shows that line shaft pumps have a higher operating life than ESPs.

Due to the presence of a downhole motor and the armored cable, corrosive contaminants (such as CO2, H2S) and abrasive contaminants (such as sand) pose a slightly bigger risk to ESPs as opposed to line shaft pumps.

2.2.14 Hydraulic Turbo Pump Performance

Two energy conversion processes occur in a hydraulic turbo pump accompanied by two sets of losses. The first conversion occurs at the turbine where pressure energy is converted to mechanical energy and the second occurs in the pump where the mechanical energy is converted back to pressure. In addition, an electric motor is used at the topside to compress the hydraulic power fluid to high pressure. Assuming similar efficiencies between the pump and the turbine, the power required at the pump shaft (to meet the target specification) is approximately 4.7 MW, whereas power lost by the hydraulic power liquid is ~6.5 MW. The amount of power liquid required depends strongly on the pressure at which it is supplied. The higher the supply pressure, the lower the quantity of the power fluid required to generate the desired glow and pressure boost. Hydraulic turbines also result in enthalpy dilution of the geothermal fluid as the lower temperature power fluid is usually mixed with the higher temperature geothermal fluid and both are pumped to the surface. Figure 2.11 shows the temperature drop of the geothermal fluid and the amount of power fluid required as a function of its pressure.

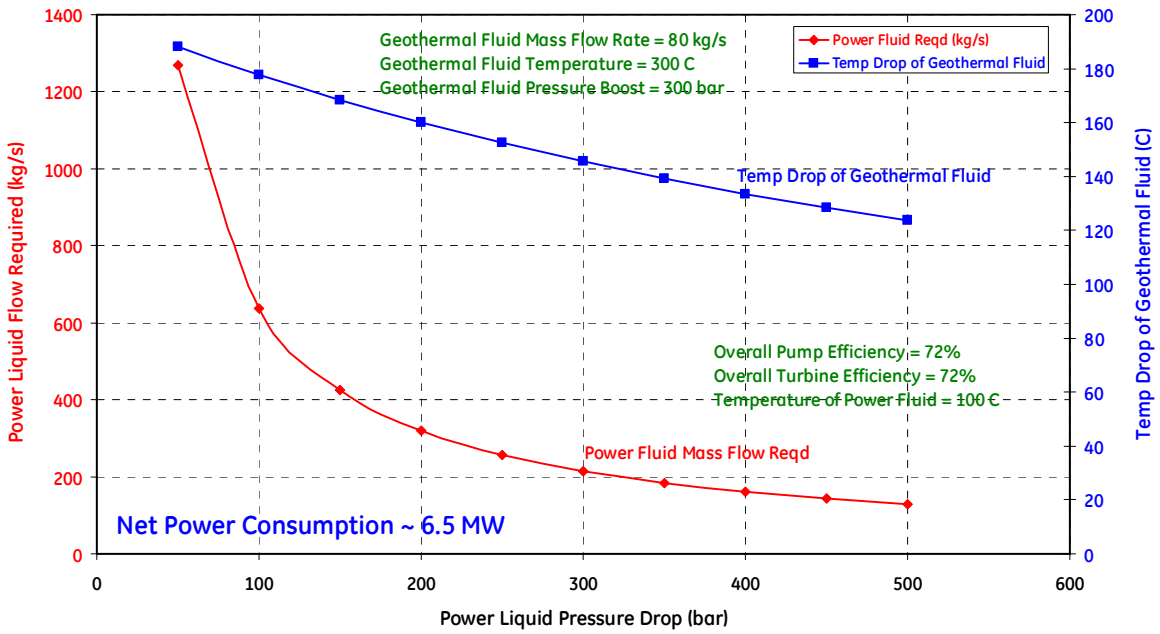

Figure 2.11 - Expected power consumption of a hydraulic turbo pump that meets the target specification

2.2.15 Reciprocating Rod Pump Performance

Reciprocating rod pumps cannot meet the depth, flow rate, and temperature requirements of an EGS well lifting system. The same considerations regarding the long drive shaft hold here as with a line shaft pump. In addition, the verticality requirement on the bore is unlikely to be met.

2.2.16 Gas Lift Performance

In making the calculations for a gas lift system, a key assumption is that the gas injection occurs in the bore at the minimum possible geothermal fluid pressure (saturation pressure * safety factor ~ 95 bar). The amount of airflow required to lift the geothermal fluid through a column equivalent to a 300 bar pressure boost is shown in Figure 2.12. If a source of high-pressure gas is readily available (as in case of oil & gas production where natural gas is readily available), gas lift can be an economical alternative. Otherwise, the parasitic load on the geothermal plant will be too high because of the cost associated with compressing ambient air. The surface pump power requirement is also shown in Fig. 2.12. It can be readily seen that the power requirement is 3 to 4 times as much as in the case of an ESP.

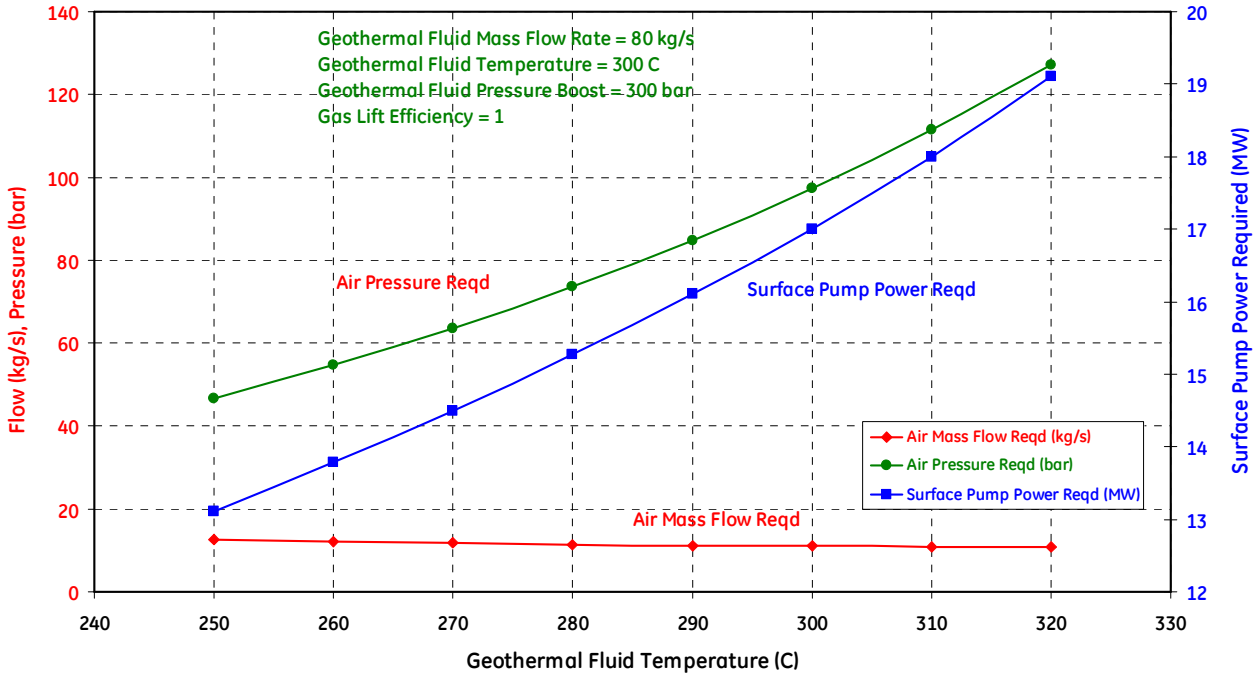

Figure 2.12 - Performance of a gas lift system. To meet the target specification, approximately 6.1 kg/s of compressed air at 98 bar is required.

2.2.17 Hydraulic Diaphragm/Piston Pump Performance

Hydraulic diaphragm/piston pumps cannot meet the depth, flow rate & temperature requirements of an EGS well lifting system.

2.2.18 Hydraulic Jet Pump Performance

Similar to the other lifting systems described above, the jet pump is also assumed to pump geothermal liquid that is close to its saturation pressure. With a small safety factor, it is assumed that the jet pump is required to provide a pressure boost of 300 bar to 80 kg/s flow of water at ~89 bar inlet pressure. Total energy required for this purpose is on the order of 3.4 MW. Jet pumps have very low efficiencies due to the inherently large mixing losses. Maximum possible efficiency is unlikely to exceed 40%. With this efficiency, the energy supplied by the motive fluid is about 8.2 MW.

The amount of power liquid (motive) required to transfer 8.2 MW of energy to the geothermal liquid being pumped is shown in Figure 2.13. The amount of power fluid needed varies with pressure drop. The higher the motive pressure drop, the lower the power fluid requirement. Also, the surface pump power required to pressurize the power fluid is shown in the same plot. It can be seen that this power requirement is ~3-10 times higher than in an ESP. Jet pumps also result in enthalpy dilution due to the mixing of the low temperature power liquid with the geothermal liquid at discharge, and the temperature drop seen is also plotted in Figure 2.13. For power liquid supplied at a temperature of 100ºC, the geothermal fluid temperature will drop in excess of 100°C. The higher the pressure of the hydraulic fluid, the better the performance of a jet pump will be.

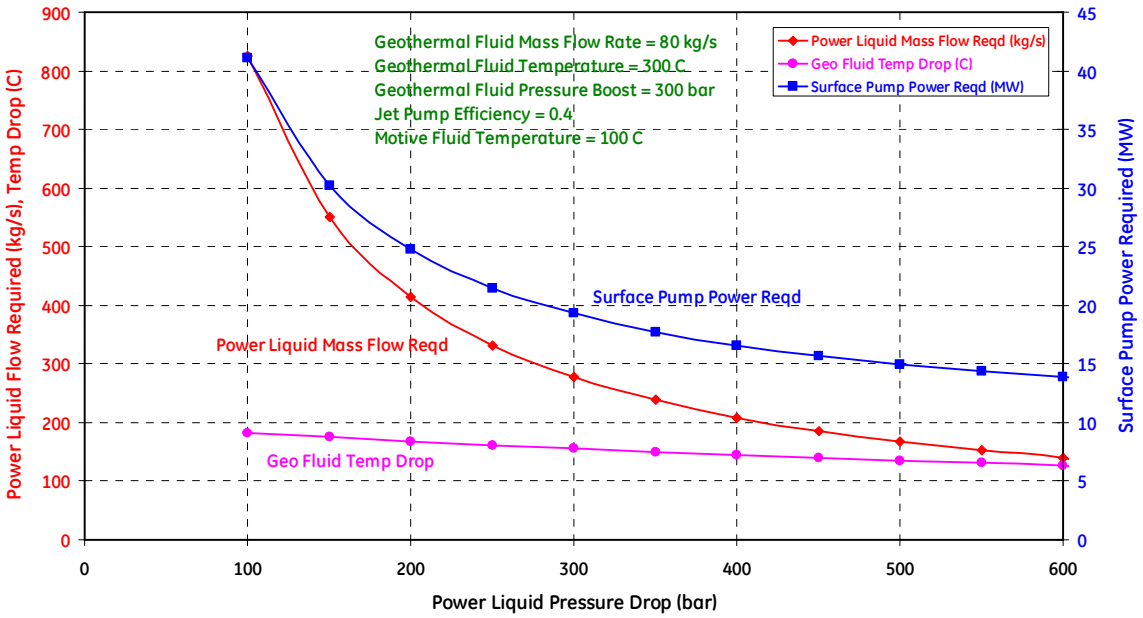

Figure 2.13 - Performance of a hydraulic jet pump – Power required, hydraulic fluid mass required and enthalpy dilution of geothermal fluid are shown as a function of pressure of the available hydraulic fluid.

2.2.19 Progressing Cavity Pump Performance

Progressing cavity pumps with a surface drive cannot meet the depth, flow rate, and temperature requirements of an EGS well lifting system. With a downhole electric drive, flow rate requirement cannot be met.

2.2.20 Discussion

Based on the preliminary analyses above, Table 2.3 is a comparison of the power requirements for each of the lifting technologies to meet the target specification.

Lifting Technology	Power required (original estimate)
Electric Submersible Pump	~ 5.2 MW
Line Shaft Pump	~ 5.9 MW
Hydraulic Turbo Pump	~ 6.5 MW
Gas Lift	~ 13 to 18 MW (assuming no available source of compressed gas)
Jet Pump	> 14 MW

Table 2.3 - Lifting system power requirements

As seen in the table, electrical submersible pumps provide the most efficient solution to lifting geothermal fluids from an EGS well. It should be readily apparent because in an ESP, electric power consumed is fed in the most direct manner (after conversion to mechanical power) to the pump with minimal losses. With a line shaft pump, mechanical losses are likely higher due to the increased bearing and seal losses due to the presence of the long drive shaft. With a turbo pump, electrical power is first converted to hydraulic power, which is in turn converted to mechanical power in the turbine. Each of these energy conversions is accompanied by a loss (mechanical, hydraulic, volumetric), essentially doubling the amount experienced in an ESP. Similar two-step conversion occurs in a jet pump with an even lower efficiency due to high mixing losses. With a gas lift system, there is a significant energy cost associated with compressing the air. Also the air is so dense at the required pressures (for EGS applications) that almost 3 times as much (by volume) compressed air is required for providing the specified lift. Positive displacement pumps (reciprocating rod, hydraulic diaphragm/piston pumps and progressing cavity pumps) cannot generate the flow rates desired from an EGS well. So, it can be concluded with reasonable confidence that ESPs offer the best choice in terms of the parasitic load on the power plant as well as in terms of the efficiency of the lifting process.

In terms of capital costs involved, ESPs are likely to be more expensive but not significantly. ESPs are currently being used in geothermal plants where line shaft pumps and turbo pumps could have been used as well, indicating that the capital costs are competitive or at most marginally higher. Turbo pumps, jet pumps and gas lift systems do not require expensive downhole equipment, but need substantial top side equipment (compressors, pumps, separators etc). It is

likely that these lifting technologies will require lower capital costs, but will incur high operating costs due to their inefficiencies.

Because of the high efficiency of ESPs, they provide the lowest operating cost in terms of the energy consumed from the power plant. ESPs do not have any other operating costs as opposed to line shaft pumps that require lubrication, or turbo pumps that require surface equipment maintenance as well as valve maintenance; the same holds true for jet pumps and gas lift systems.

Jet pumps and gas lift are likely the most reliable of all lifting systems because they require no downhole moving parts. As such downhole equipment will likely last much longer when compared to ESPs, line shaft pumps or turbo pumps, ESPs are likely to be the least reliable due to the motor cooling requirement and the sealing/pressure balance requirements on the motor and the cable joints.

Contaminants are likely to be better handled by any other lifting system when compared to ESPs. However, the risk is minimal in a closed loop geothermal system, especially after equilibrium is established. Any added risk due to contaminants particular to a site must be considered in the design phase itself, so an appropriate ESP system can be selected to handle the added contaminant risk.

Overall, ESPs score the highest in terms of power requirement, energy efficiency and operating costs. Capital costs may be higher but are comparable to some of the other lifting systems. Contaminants are not likely a serious issue for closed loop geothermal applications. As such, the most serious challenges in application of ESPs for EGS lifting applications are in the areas of reliability – protecting the motor from overheating, high temperature sealing of motor and cable, and design of a reliable motor protector system. Additional mechanical challenges are in the areas of supporting of the pump/motor assembly in the bore, bearing/seal/connector design, etc.

Based on all these considerations, it is concluded that an Electric Submersible Pump is the best lifting system for EGS wells, provided the technical challenges unique to EGS systems can be overcome.

3. Lifting System Configuration and Design

3.1 LIFTING SYSTEM CONFIGURATION

The conceptual design of the artificial lifting system (shown as Fig. 3.1) incorporates a submerged electric motor unit driving a multistage centrifugal pump to produce flow back to the surface. The design aims to lift large volumes of high temperature water against a pressure difference within the production well in which the system is installed.

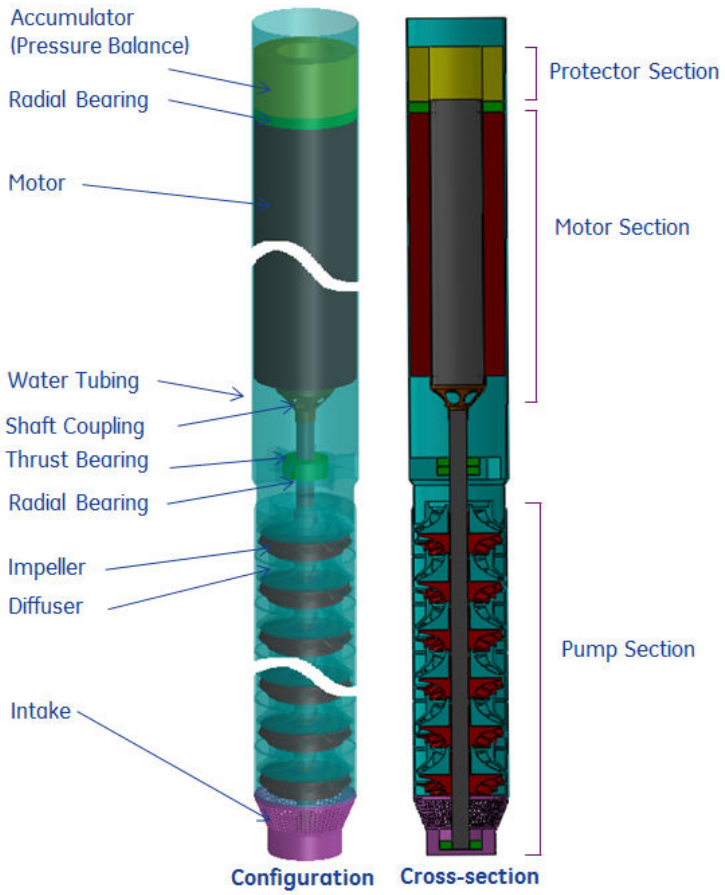

Figure 3.1 - Lifting system configuration

Generally, lift or head developed by a single stage centrifugal pump is relatively low, due to the limited well casing diameter. Thus, a multistage pump must consist of many stages stacked together in series to provide the desired lifting capability. Each stage consists of two basic components: a rotating set of impellers and a stationary diffuser, shown as Fig. 3.2. The geothermal fluid (water) from the previous stage enters the impeller in an axial direction at a relatively low velocity, and attains a higher velocity through the impeller due to the centrifugal force. The liquid then leaves the impeller with high kinetic energy that is converted into potential energy at the discharge of the diffuser, at higher pressure level than it was at the inlet of the

impeller. Since the diffuser redirects the flow into the next stage, the process repeats and the rotary action is finally converted to an increase of the fluid pressure. In this investigation, the multistage pump design aims to produce 300 bar pressure increase. Thrust washers must be placed at certain locations between impellers and diffusers to carry the thrust loads. A check valve is located above the pump discharge so that it closes on shut down of the unit, and prevents reverse rotation of the pump/motor due to the large column of downstream water. Details regarding the pump design, analysis and optimization can be found in a later section.

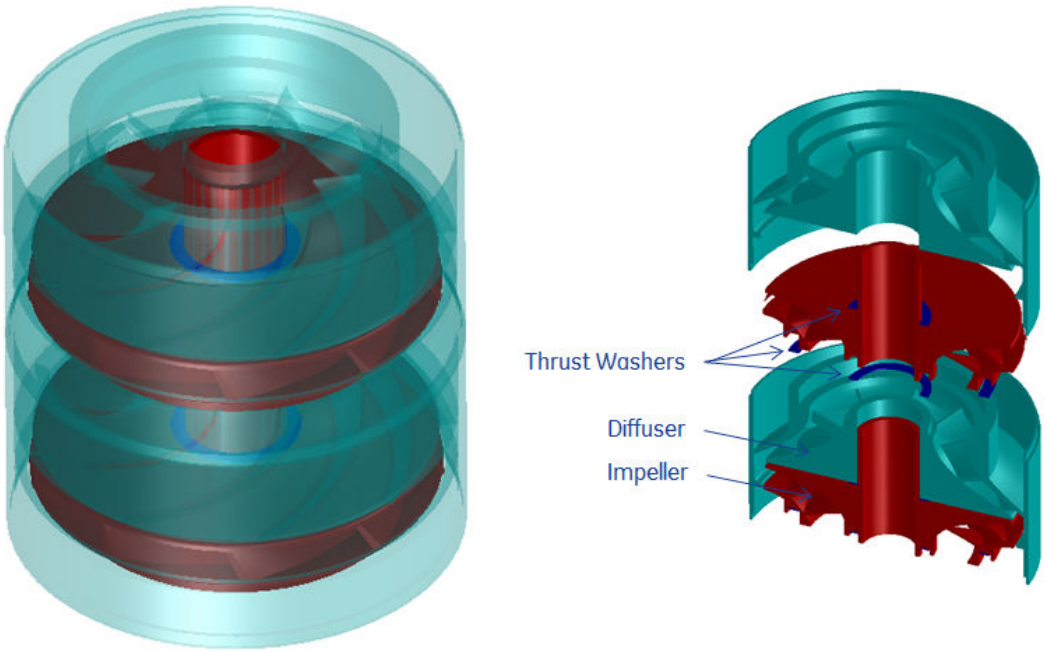

Figure 3.2 - Pump configuration

The conceptual lifting pump is driven by a submerged electric motor of the permanent magnet type (PM motor). Compared to a conventional induction motor, this type of motor enables superior power density and the capability of higher temperature operation. The motor is filled with dielectric oil for cooling and insulating purposes, and needs to be sealed from the well environment to prevent oil leakage and protect the bearings and motor internals. Process water passing through the motor shaft and outer diameter acts as a cooling agent. The power supply to the motor is from the surface via electric cables. These cables must be of relatively small size in order to fit in the annulus along the well bore tubing. The entire motor/cable assembly must be watertight, to maintain dielectric properties and be protected from the harsh well conditions. A novel feature of the configuration of the motor is a built-in cooling passage including one or more cooling impellers. The cooling impeller is driven by the rotating shaft and drives the circulation of the dielectric oil.

In the full scale system, the protector is installed above the drive motor. The main purpose of the protector is to prevent the process water from entering the electric motor, protecting the dielectric oil inside the motor from being contaminated by the production water. Furthermore, the protector provides an accumulator for the motor's dielectric oil when the oil expands due to the increasing internal temperature. A thrust bearing may be installed in the protector to carry a portion of the

vertical thrust developed by the pump, as well as the weight of the rotor shaft. Thrust bearings may also be spaced periodically along the pump/motor shaft system, with adjacent sections connected via couplings that allow relative axial movement.

3.2 SYSTEM ASSUMPTIONS AND CALCULATIONS

The assumptions and calculations of the overall system, pump and motor are listed as Tables 3.1, 3.2 and 3.3, respectively. Due to the complexity of the system and the downhole environment, certain assumptions may be subject to change in future investigations (and from site to site), affecting calculated values. The overall system design aims to meet the basic targets of mass flow rate (80 kg/s), pump boost (300 bar) and temperature of the produced fluid (300˚C). With these specific technical requirements, the system will require a power supply of approximately 4-5 MW.

During operation, the lifting system converts the electrical energy provided to the submersible motor into kinetic and potential (pressure) energy of the liquid being pumped. As the efficiency of energy transformation is inevitably less than 100%, energy losses are involved. It is assumed that all of these losses are converted to heat and absorbed by the water flowing within the pump and around the motor. Under steady-state conditions, the temperature increase of the produced water can be determined by the amount of wasted energy and the thermodynamic properties of the geothermal environment. The temperature rise of water from 300ºC ambient temperature is less than 10ºC due to the heat added by the lifting system. Thus the water's high heat capacity and low viscosity make it a good cooling agent for removing the heat from the system.

*F-Finalized; A-Assumption; C-Calculated

Mass flow rate	80	kg/s	F
DP	300	bar	F
Wellbore size (ID)	9.597	in	C
Water temperature	300	°C	F
Saturation Pressure @ 300C	85.88	bar	F
Water density @ P_sat, 300C	712.0	kg/m^3	F
Volumetric flow rate	0.1124	m^3/s	C F
	1780.8	gpm	C F
	61057	bpd	C F
System efficiency	0.5336		C A
Total power required	5.0	MW	C
Temperature rise of water	< 10	°C	C F

Table 3.1 – Overall system data

The water discharged by the multistage centrifugal pump should overcome the summation of pressure head occurring along the flow path at a certain flow rate. The total pressure head consists of the head due to wellhead pressure, hydrostatic head, and frictional head. In this study, the wellhead pressure is determined as the minimum pressure required on the top of the well that can maintain the 300ºC water as liquid in the entire flow path. The hydrostatic pressure acting on

the pump is due to the water column presented in the tubing above the pump. The frictional head is produced by the frictional loss occurring in the tubing as the water passes through. In order to provide 300 bar boost, the entire pump consists of 126 stages. The total length is approximately 19 meters and the total mass is around 3400 kg. The net power input through the shaft to the pump stages is 3.97 MW. A design tradeoff is made in the selection of rotational speed; a lower rotating speed helps to minimize the temperature rise within the motor, at the expense of requiring more pump stages.

*F-Finalized; A-Assumption; C-Calculated

Pump efficiency	0.78		A
Pump DP	300	bar	F
Total Head	4139.6	m	C
	13581	ft	C
Saturation pressure	85.88	bar	F
NPSH Required	5	bar	A
Safety factor	3	bar	A
Pressure @ suction	93.88	bar	C F
Pressure @ discharge	393.88	bar	C F
Density @ suction	713.94	kg/m^3	C F
Density @ discharge	763.56	kg/m^3	C F
Average density	738.75	kg/m^3	C F
Rotating speed	3150	rpm	C F
Single stage head	33	m	C
Number of pump stages	126		C
Total length	19	m	C
Estimated mass per unit length	177	kg/m	C
Estimated total mass	3363	kg	C
Total power output	3.1	MW	C F
Total (pump) power input	3.97	MW	C F

Table 3.2 – Pump data

The overall efficiency of the motor is determined by multiplying the electrical efficiency (95%) and the mechanical efficiency, which is calculated using 95% bearing efficiency and 90% interstage seals efficiency. Great effort has been taken to maximize the power density of the motor, while trying to minimize the number of motor stages and the total length. The proposed design of the single stage motor can produce 310 kW. Therefore, 13 motor stages are required to produce sufficient power for the centrifugal pump. The total length of the entire multi-stage motor will be approximately 26m.

Component failure due to extreme temperature is expected to be the primary cause of early motor failure for enhanced geothermal applications. The submersible electrical motor (in particular, the motor windings) must have exceptional capability to dissipate or withstand severe internal

temperatures. Thus, the winding temperature must be carefully evaluated so as to provide a guideline for the material selection of motor components. The skin temperature and winding temperature are two design criteria of the submersible motors. These temperatures are usually functions of geothermal fluid temperature, heat generation rate during operation, and the cooling effect of the production liquid flowing around the motor. Since the motor is surrounded by 300ºC water, the internal temperature will exceed that value. Therefore the rotor, stator winding, and the cooling passages must be properly designed to enhance the heat transfer rate. The motor design aims to maintain the maximum temperature within 330ºC.

*F-Finalized; A-Assumption; C-Calculated

Motor overall efficiency	0.795		A
Motor efficiency	0.95		A
Mechanical efficiency (bearings, seals, etc.)	0.837		A
Operating speed	3150	rpm	A
	329.87	rad/s	C
Power required	5.0	MW	C
Single stage motor power	310	kW	A
Number of motor stages	13		C
Total motor length	26	m	C
Motor Casing OD	9.44	in	C

Table 3.3 – Motor data

3.3 EGS WELL CONDITIONS AND OPERATION PROCESS

There are two types of wells in a typical geothermal field – production wells and injection wells. Production wells are those that connect to source of geothermal energy, while injection wells are designed to force water underground for the purpose of maintaining a steady supply of water in the geothermal system. At static conditions such as when the ESP is not working, the production well will be full of water without any flow. The well temperature will be approximately 300ºC and the static pressure approximately 4000 psi at 3 km depth. The field data obtained from two ongoing EGS wells display roughly linear trends of temperature and pressure.

Fig. 3.3 shows a set of curves showing the pertinent system conditions (such as pressures and temperatures) that the lifting system will be exposed to during all phases of its life: assembly, pressurization, installation, startup, steady state, shutdown, restart, re-shutdown, and removal from the well. The figure provides a consistent picture of all the conditions that must be satisfied for the multistage centrifugal pump and submersible motor. Due to the pressure balance system, the motor's internal pressure is always higher than its internal pressure so as to prevent the produced fluid from entering the motor. Since the motor is at the downstream of the pump section, the motor's external pressure always equals to the pump discharge pressure. The motor's internal temperature is controlled below 330°C for all phases of operation. The thermal management of the motor is presented in a later section.

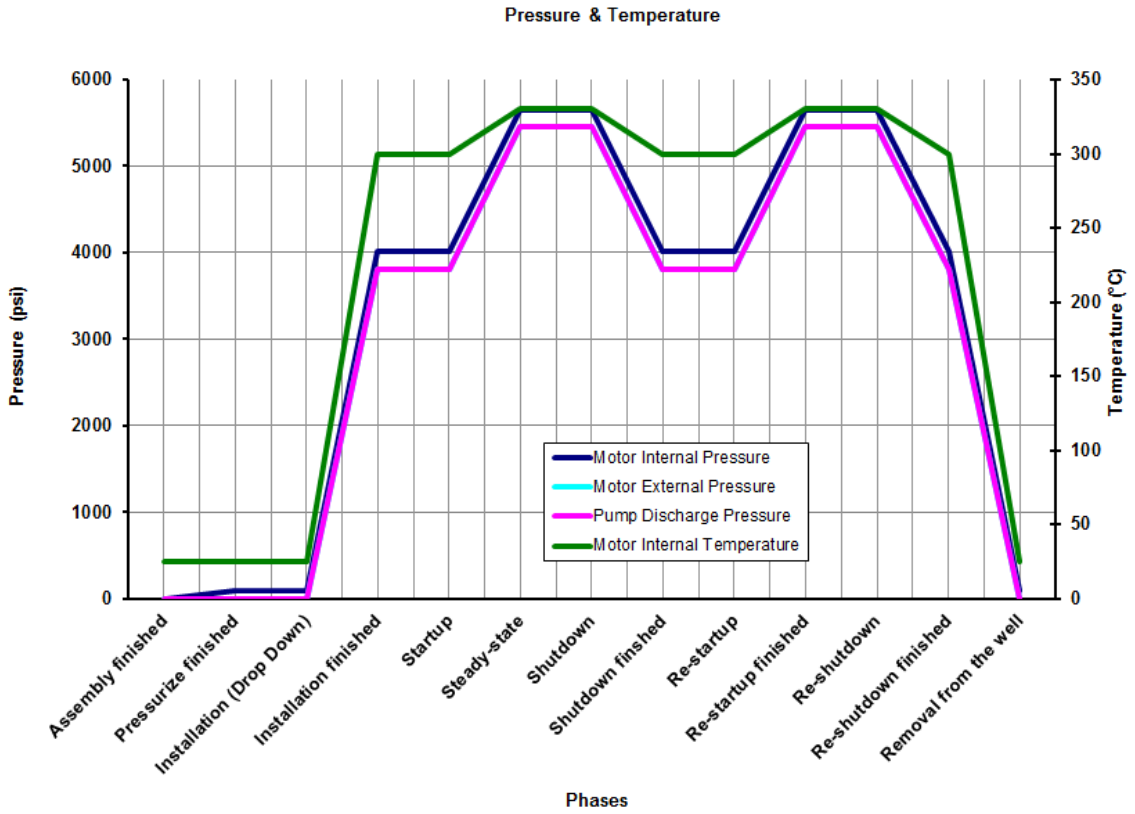

Figure 3.3 – Pressure and temperature at different system points

4. Lifting System Component Development

4.1 PUMP CONFIGURATION

4.1.1 Pump Design

As previously mentioned, a rotating impeller and a stationary diffuser constitute a single stage of the multistage centrifugal pump. The function of the impeller is to accelerate the produced water from a relatively low velocity to a higher velocity by the high-speed rotation. The kinetic energy of the liquid is then converted into potential energy at the discharge of the diffuser. As a single stage, the impeller and diffuser work together to create sufficient boost to conquer the resistance.

The impeller/diffuser configuration described in this section has been designed for a 10-5/8" wellbore, which is required by the U.S. Department of Energy for Enhanced Geothermal System (EGS) applications to improve the cost-effectiveness. It should be noted that a well bore diameter as large as 13-3/8" may be possible in some cases; this would greatly simplify the construction of the drive motor for the pump as it would relieve space constraints considerably. However, in the interest of meeting the target specification set forth in this program, the system has been designed to fit within a well bore of 10-5/8".

The conceptual design of the impeller/diffuser and stages are shown as Figs. 4.1 and 4.2, respectively. The meridional view of a single stage (impeller/diffuser assembly) is displayed as Fig. 4.3. The blue/red section represents the geometry of the blades in the meridional face.

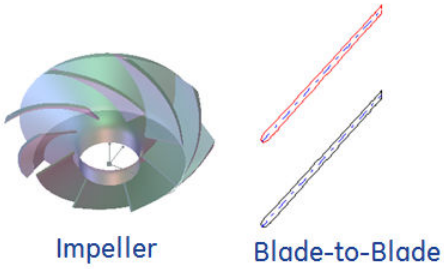

(a) Impeller

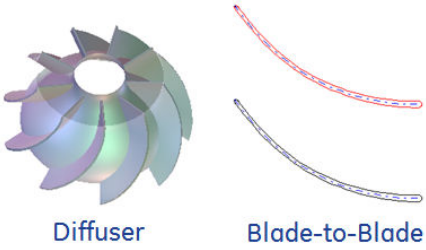

(b) Diffuser

Figure 4.1 – Conceptual design – impeller/diffuser

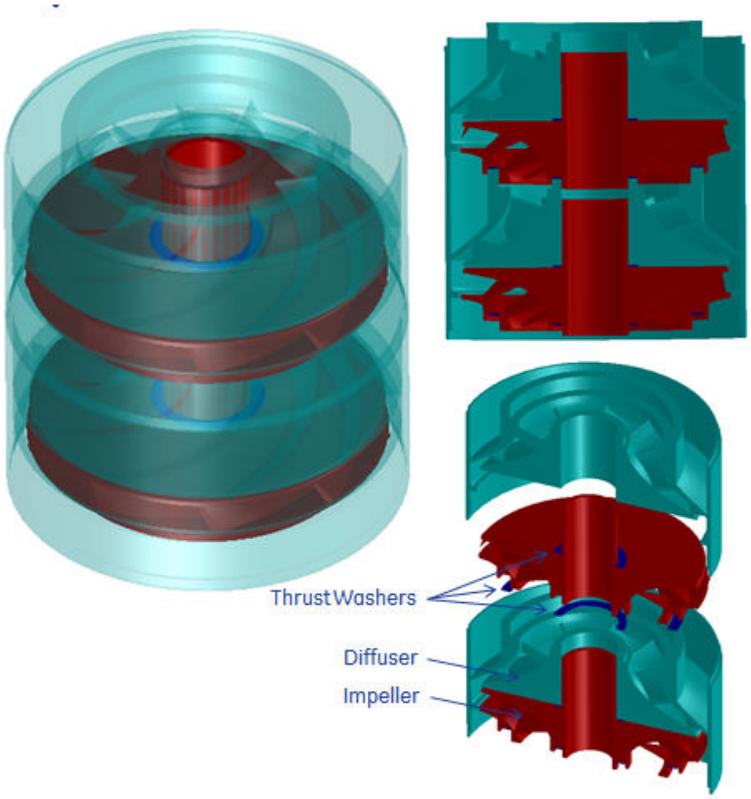

Figure 4.2 – Conceptual design – pump stages

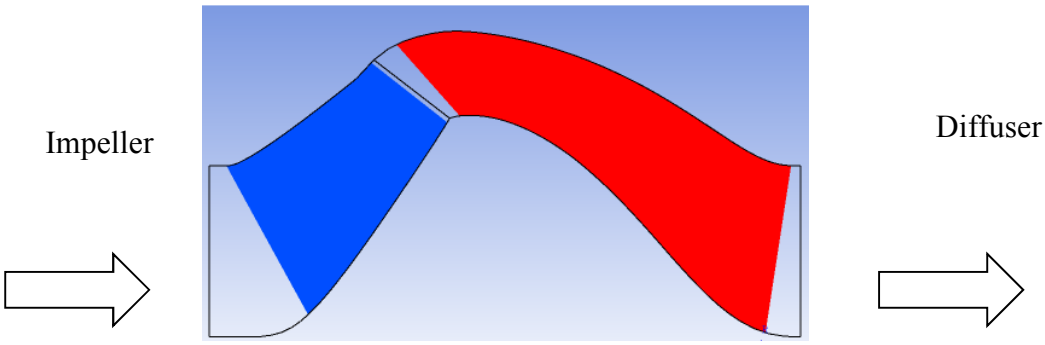

Figure 4.3 – Single stage meridional view

4.1.2 CFD Analysis and Performance Prediction

With the aid of Computational Fluid Dynamics (CFD), the complex internal flows in the impellers and diffusers can be well predicted, thus facilitating the design of pumps. This investigation presents a numerical simulation of the single phase three-dimensional flow in the impeller of a single stage centrifugal pump using CFD techniques and a commercial software, ANSYS®

CFX5® Release 13. The calculation predicts the performance curves of the impeller/diffuser stage.

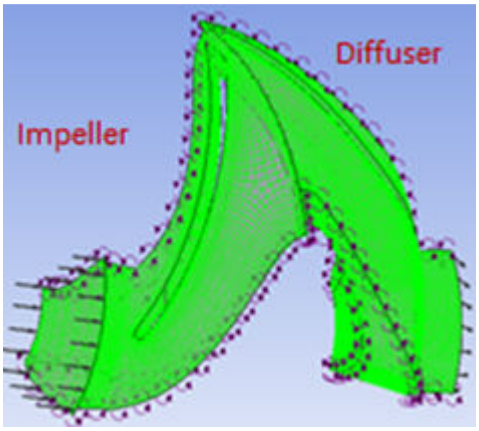

Figure 4.4 – Mesh model of fluid domain and boundary conditions

Figure 4.4 shows the 3D impeller/diffuser geometry and the meshed fluid domain. Due to the periodicity of the blades, it is only necessary to study the fluid domain around one blade and set the periodic boundary conditions as indicated in the figure. Other boundary conditions and inputs include:

1. Inlet: total pressure applied in the rotation axis direction = 90 bar
2. Outlet: mass flow rate = 80 kg/s
3. Wall: general boundary condition by default (roughness: 250e-6 in)
4. Fluid: Water at 300ºC
5. Rotational speed of impeller: 3150 rpm
6. Stationary diffuser

The calculation is carried out based on the standard k-ε turbulence model and shows good convergence after several hundred time-steps.

Figure 4.5 plots the velocity distribution at 50% span. It is found that the impeller/diffuser configuration is able to convert the mechanical energy of the rotation into the kinetic energy of the fluid very well for the given geothermal environment. A small amount of flow separation occurs at the trail edge of the diffuser due to the curved blade shape which is trying to guide the flow back to the axial direction. As a result, efficiency is compromised slightly at the first stage, but it is ensured that the flow direction is repeatable stage by stage so that every stage can have the same performance.

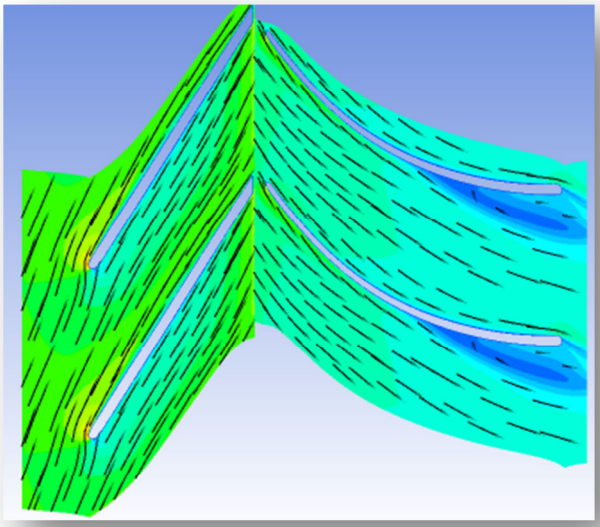

Figure 4.5 – Velocity distribution at 50% span

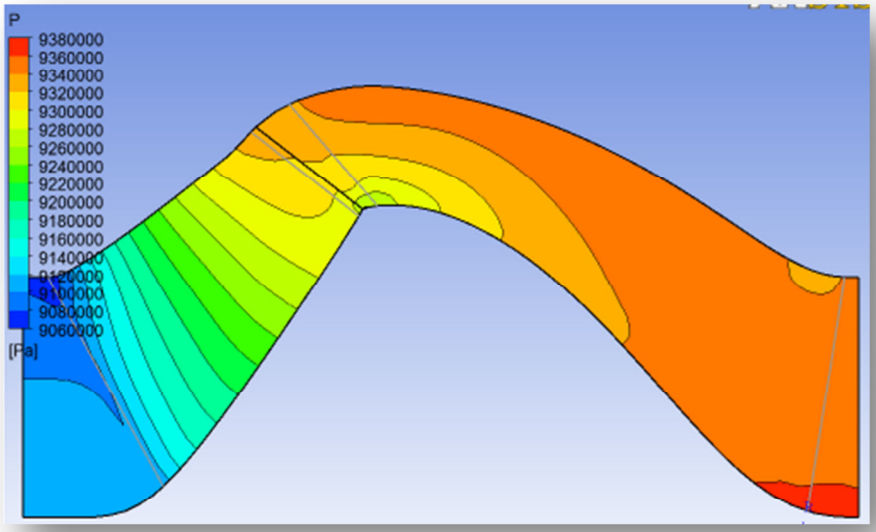

Figure 4.6 - Contour of area averaged static pressure on meridional surface

Figure 4.6 shows the predicted contour of area-averaged static pressure on meridional surface. It is observed that the static pressure increases by approximately 2.5 bar at the discharge of the stage, which results in a static head rise of 32m. In order to better evaluate the characteristic of the impeller/diffuser stage, the performance curves must be plotted to describe the relation between flow rate and head.

4.1.3 Performance Optimization

A Design of Experiments (DOE) was performed to further increase the performance of the stage. The main purpose of the DOE is to perturb various design parameters of the impeller/diffuser configuration and explore their effects on the boosting under the simulated environment. ANSYS® BladeModeler® and TurboGrid® tool kit are utilized to generate and mesh different geometries. There are certain parameters that play significant roles in determining a pump's performance such as blade count, splitter count, diameter, wrap angle, blade angle, vane angle, inlet and outlet width, etc. Their definitions and some examples are presented as Figs. 4.7 and 4.8. The DOE process aims to establish optimized configurations that can run at higher efficiency and generate higher head for a given set of constant boundary conditions.

Parameter	Description
B	Blade Count
S	Splitter Count
D	Impeller Dia.
θ	Wrap Angle
Δβ	Blade Angle
t	Blade Thickness
a	Inlet Width
b	Outlet Width
ϕ	Vane Angle
C_1 ~ C_4	Blade Start and end Coordinates

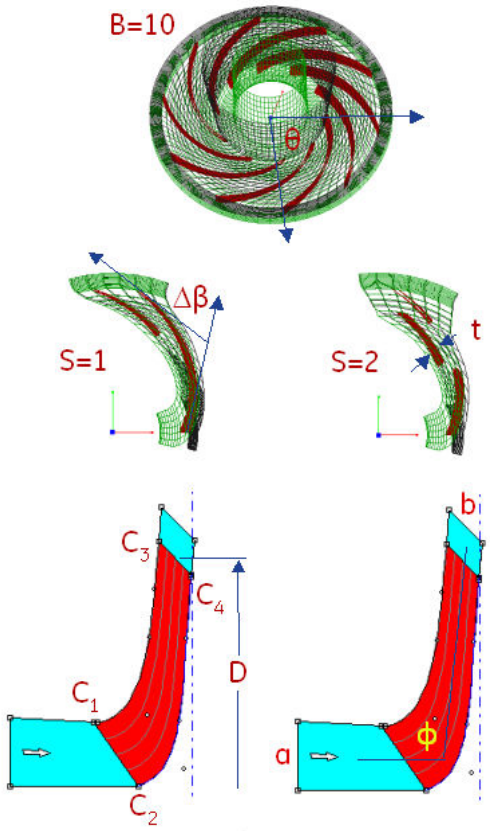

Figure 4.7 – Impeller/diffuser design parameters

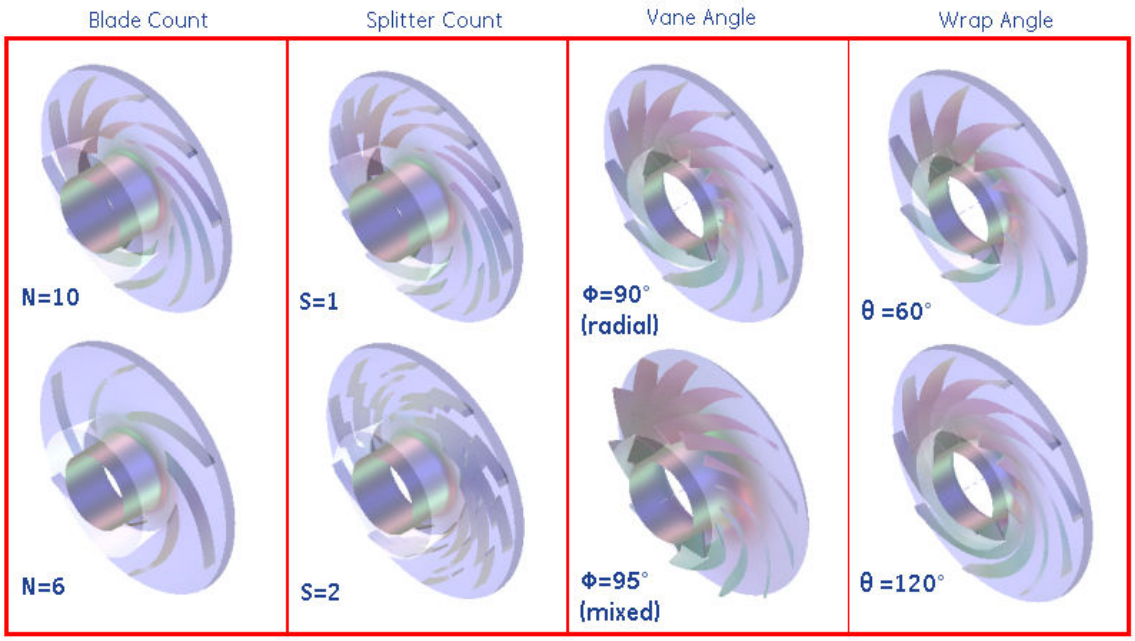

Figure 4.8 – Examples for different design parameters

The best efficiency of the stage occurs between 70 kg/s to 80 kg/s mass flow rate. For 80 kg/s, the efficiency is approximately 78%. A theoretical best efficiency of the stage is around 83% at 3150 rpm and the abovementioned flow conditions, but this efficiency requires the pump diameter to be greater than 10". For the limited wellbore diameter, 78% is the upper bound of impeller efficiency, and can be considered as a successful design. Furthermore, reducing wall surface roughness will be very helpful to increase efficiency. The wall roughness used in the simulation was from typical cast parts used in current electric submersible pumps.

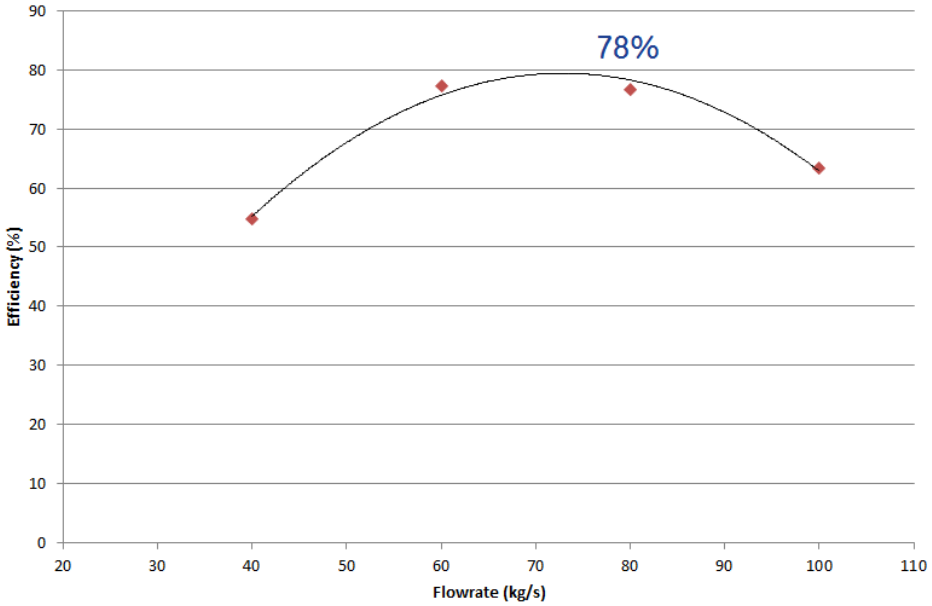

Figure 4.9 – Stage efficiency curve

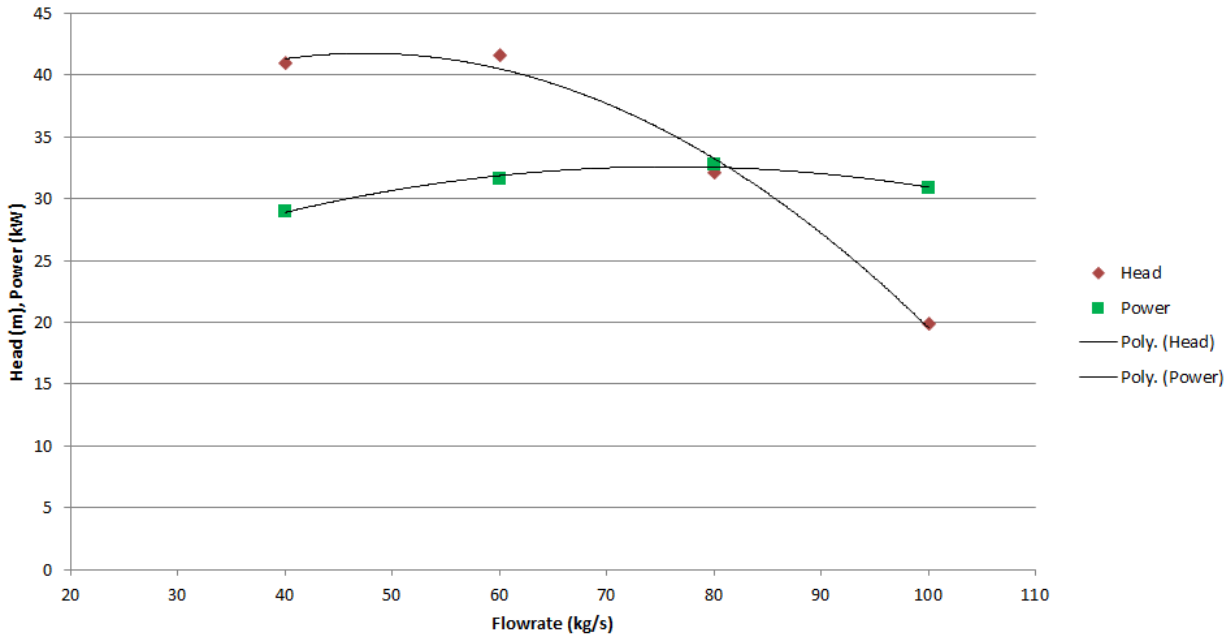

Figure 4.10 – Stage head rise and power curves

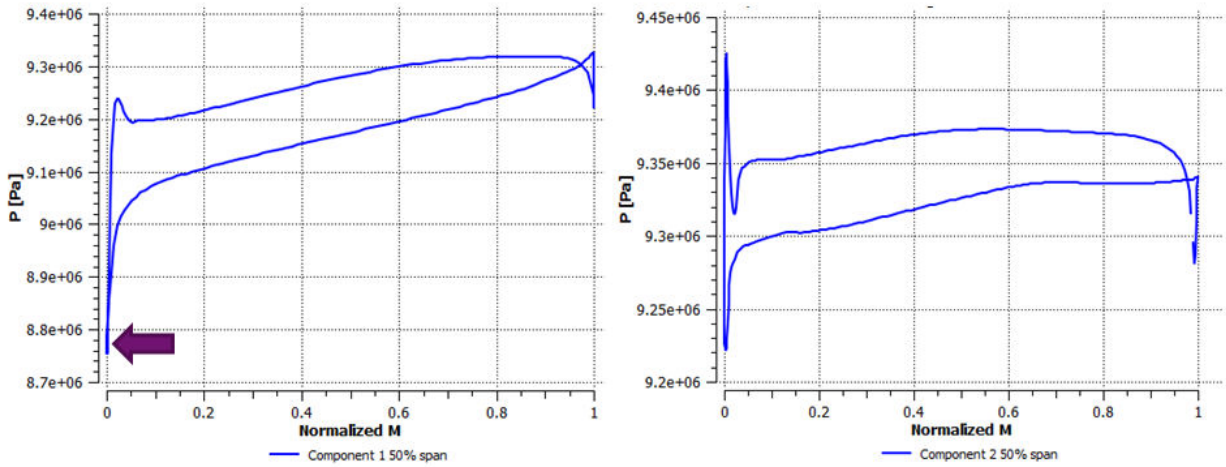

Figure 4.11 – Impeller/diffuser blade load

The blade load of the impeller and diffuser at their 50% span is shown as Fig. 4.11. It is seen that the pressure drop at the inlet of the stage is above 87.5 bar, which is higher than the saturated pressure of the 300°C water (86 bar). In addition, the load distribution along the blade is observed to be smooth. The DP across the blade is within 1 bar which results in relatively low structural loading.

Gas handling capability was also investigated for the stage. The proposed lifting system design aims to pump the process water with less than 2% gas volume fraction (GVF) with no significant pressure drop. It is observed from the multiphase CFD study, shown as Fig. 4.12, that no air bubbles attach to the blades, hub and shroud under 2% overall GVF. The static pressure only drops 1.8% compared to the pure liquid case. Therefore, the pump design can handle 2% GVF without adding any additional components. For the gassy wells where more than 2% gas is contained in the water, a gas separator can be placed in front of the intake of the pump.

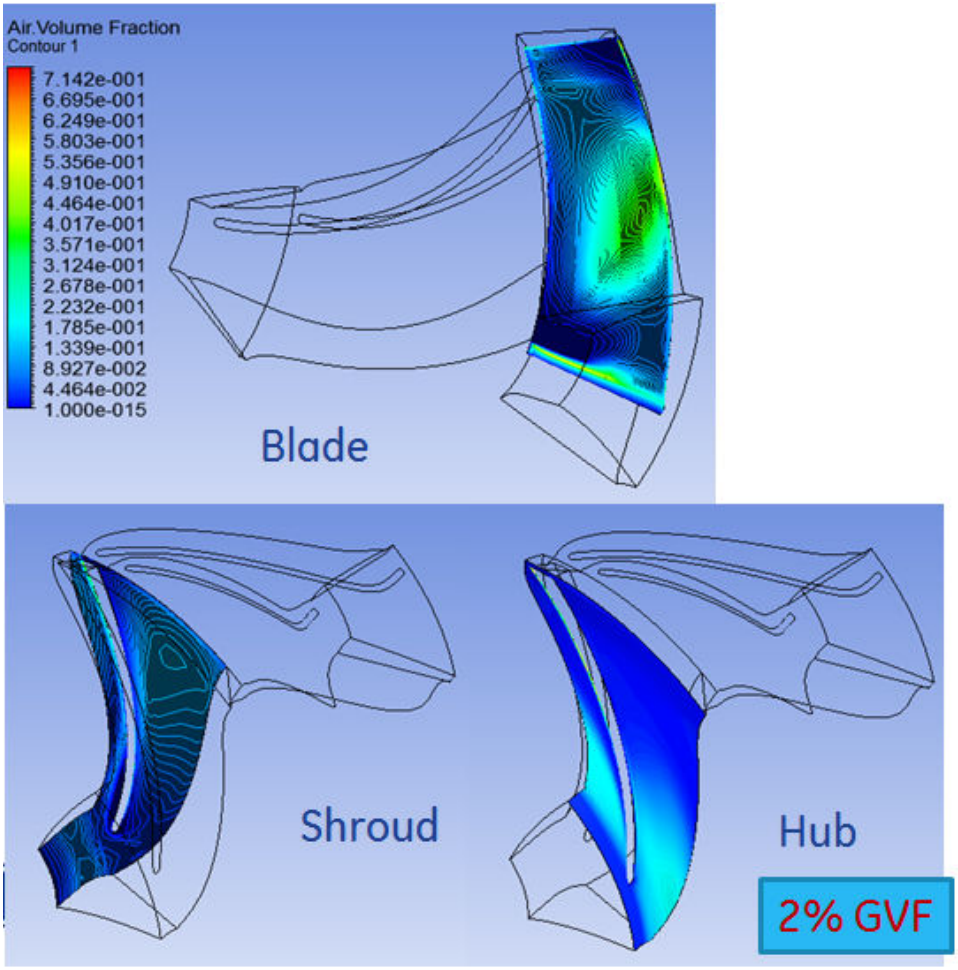

Figure 4.12 – Gas volume fraction on blades, hub and shroud

In order to validate the entire design process of the impeller and diffuser, the same design and analysis procedure was applied to an existing ESP design to compare the prediction and the experimental data. Figs 4.13 and 4.14 show the comparison of the efficiency and the head rise. It is observed that the prediction agrees with the experimental data very well. Both the error of the predicted efficiency and predicted head are within 2% compared to the actual values. Therefore, the single stage impeller/diffuser design procedure developed in this program has been demonstrated to be effective and accurate, at least for the operating range over which experimental data exists.

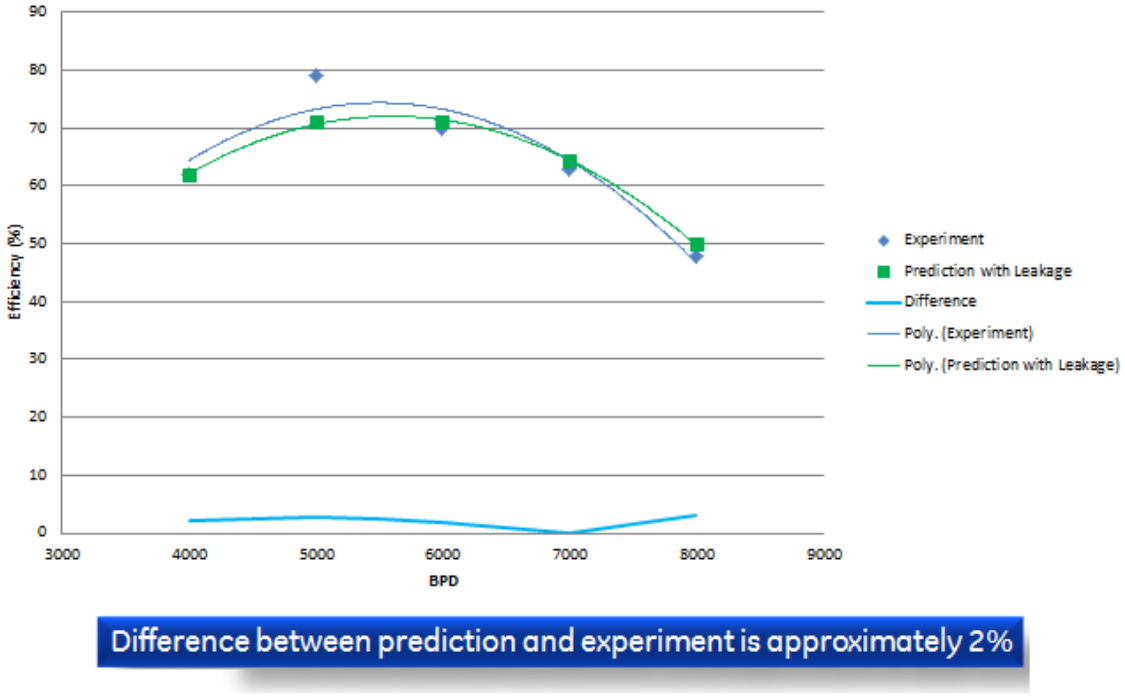

Figure 4.13 – Prediction vs. experiment – efficiency

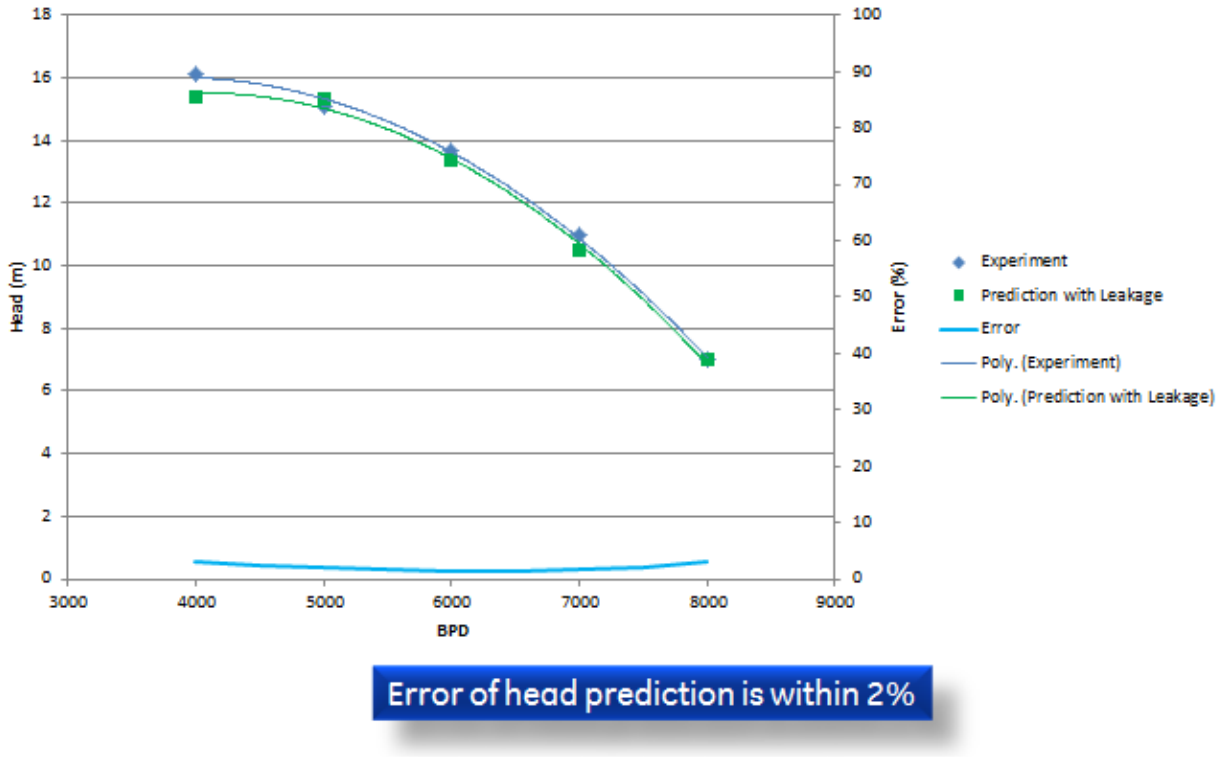

Figure 4.14 – Prediction vs. experiment – head rise

A comparison between the designed geothermal pump and an existing ESP pump is shown in Figure 4.15. Dimensionless coefficients, such as head coefficient, power coefficient and capacity coefficient, are compared. It is seen that the geothermal pump maintains high efficiency at a much wider span of capacity (flow rate) range. The best efficiency is also 5% higher than the existing ESP pump though operated at a lower rotating speed.

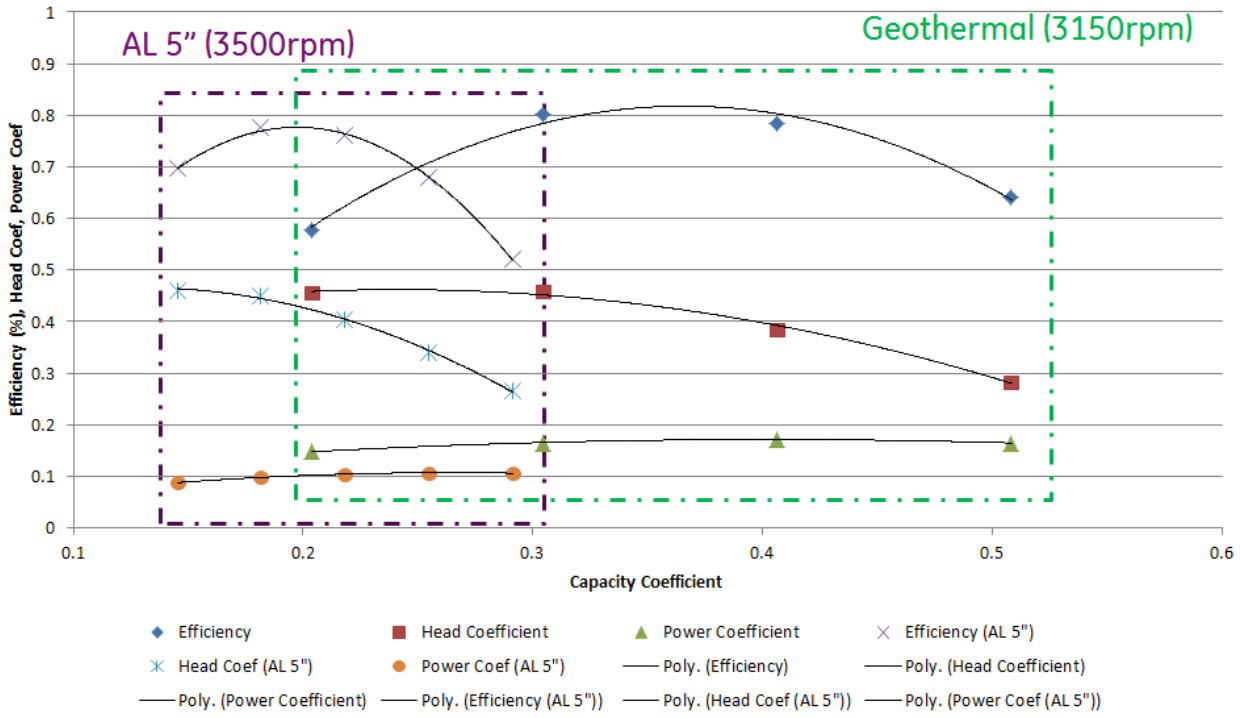

Figure 4.15 – Pump comparison

A sub-scale demonstrator of the pump section has been designed in order to prove the pump's performance at desired geothermal environment. The sub-scale pump keeps the same overall dimensions as the real pump, and is designed to be tested in 300°C water as can be seen by the actual pump. The only difference is that the flow passage has been narrowed down so that the pump can effectively lift water at 20 kg/s production rate, which is 25% of the actual pump. Figure 4.16 shows the stage performance curves of the sub-scale impeller and diffuser. It is seen that the efficiency and the head per stage are close to that of the actual pump.

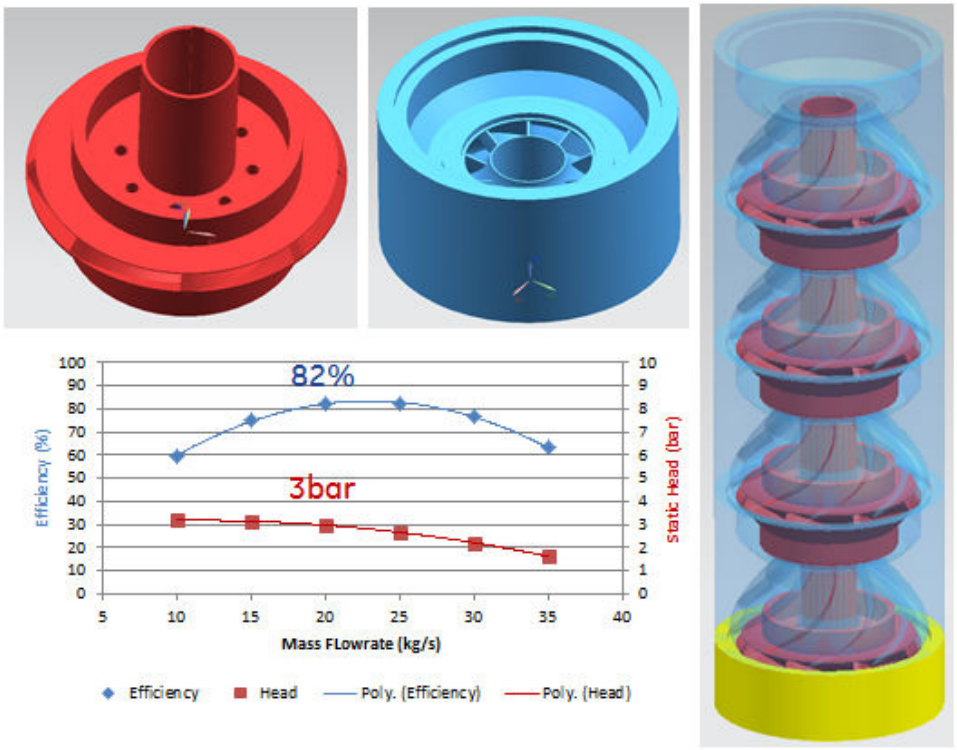

Figure 4.16 – Sub-scale pump configuration and performance curves

4.2 MOTOR CONFIGURATION

4.2.1 Motor Sizing

The motor design was originally developed to meet the performance requirements within a 13-3/8" well casing. One performance requirement having significant impact on the motor design was the need to deliver 80 kg/s (1704 gpm) water flow. Industrial experience indicated that metal surfaces will experience significant erosion rates for water flow velocities exceeding 25 ft/s (7.62 m/s). The required flow rate must then be passed through an area of at least 25 square inches to respect the erosion flow velocity limit. This represents approximately 20% of the cross sectional area available inside a 13-3/8" well casing. For a 10-5/8" well casing, the same water flow area represents nearly 35% of the available cross sectional area, posing a significant challenge. Designing a high power motor architecture that occupied less space became necessary.

4.2.2 Design Evolution

Power Capability of Small Diameter Motor

In order to provide the required water flow area around the outside of the motor within the smaller 10-5/8" well casing, the outer motor diameter had to be significantly reduced. Because the power generated by a motor varies with the square of the rotor diameter, the smaller diameter motor produces significantly less power per unit length. To achieve the same total power requirement,

the total length of the motor and number of motor modules must increase dramatically. For a greater number of modules, a greater number of power cables would be required and these would occupy space outside the motor. The space occupied by cables further reduces the space available for the rotor and stator. In order to protect the cables inside the oil-filled motor assembly and transfer heat from the cables to the flowing water, the design concept was to embed the cables inside cooling fins surrounding the periphery of the motor. The concept sketch in Figure 4.17 shows that the scaling of a finned motor with flow area sufficient for 80 kg/s of water is reasonably elegant for a 13-3/8" casing, but becomes less practical for the smaller 10-5/8" well casing.

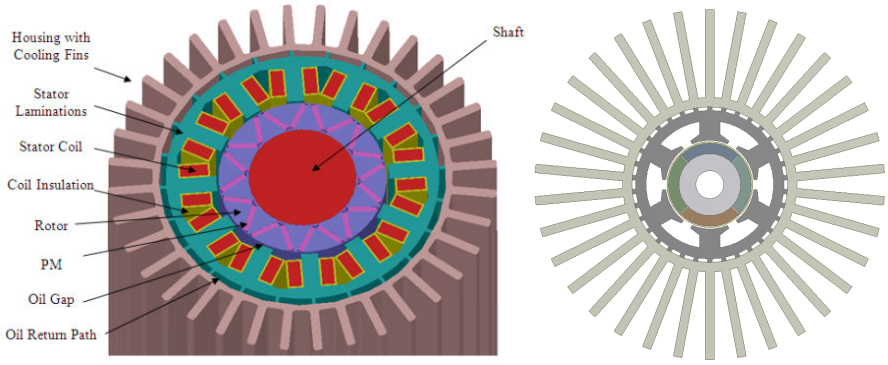

Figure 4.17 - Outside flow motor cross-section for well casing 13-3/8" (left) and 10-5/8" (right)

Accommodation of Motor Power Cables; Motor-on-Top

A traditional ESP system uses a small number of motor modules (<3) connected in tandem below the pump assembly. The motor(s) are then subjected only to the static downhole pressure without the dynamic pump head pressure. In this case the cables feeding electrical power to the motors are placed next to the pump within the well bore and extend down past the pump to the motor location.

For a high-power, high-flow ESP system, a larger number (>3) of motor modules will be needed and the space within the wellbore is limited. As illustrated by Figure 4.18, accommodating the large number of cables in protected oil-filled structure(s) would be complex and lead to reliability concerns. Furthermore, the space occupied by the cables would constrain the diameter of both the motor and the pump design - an undesirable situation. For this reason, a system configuration with the motor assembly placed above the pump design was considered. This allows the pump design to make use of the entire wellbore. The motor design must still accommodate power cable routing to supply power to each motor module in the tandem string, as shown in the right of Figure 4.18.

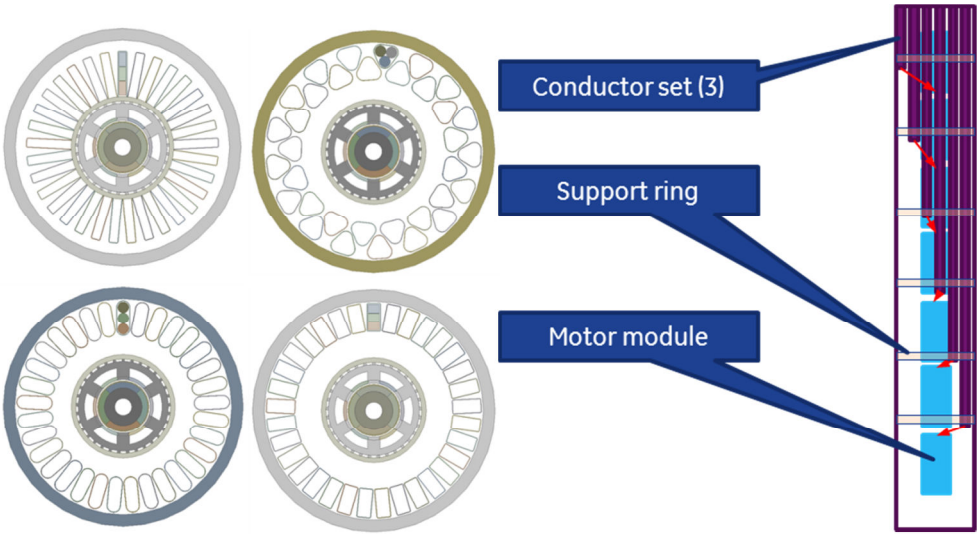

Figure 4.18 - Small diameter motor with cable routing options (left). Motor assembly with large number of modules each having power cables (right)

Rationale for a Large Diameter "Bore Flow" Motor

An alternative motor design was considered to reduce the total length of the motor. Recognizing that motor power varies with the square of the rotor diameter, and the bending stiffness of the rotor that determines rotordynamic stability and bearing spacing varies with the rotor diameter, there was motivation to maximize the diameter of the motor within the allowed well casing bore. Furthermore, the average flow velocity of the water was dominated by the area provided for water with no influence of diameter. A motor design was then considered where the motor elements (rotor, stator, and cables) were located at the maximum available diameter within the well bore. Area would then be provided at the bore of the rotor for water flow. A sketch of the concept is shown in Figure 4.19.

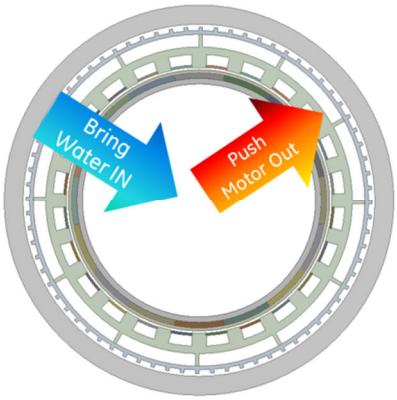

Figure 4.19 - Concept sketch of large diameter "Bore-Flow" motor cross-section

Large-Diameter Bore-Flow Motor

A modular motor design, shown as Fig. 4.20, was developed that would allow a high total power rating to be achieved by connecting individual motor modules in tandem. The limit on the length of a single element that can be handled at the well head with traditional rigs is approximately 35 feet, and the total motor length required to drive the geothermal pump was expected to be greater than this value. Once assembled, the motor modules would be sealed to one another and filled with a suitable fluid (e.g. dielectric oil) to provide mechanical support against the well fluid pressure. The majority of the well fluid (water) passes through the bore of the motor with some fluid flow around the outside of the motor. The rotor itself serves as a barrier between the well fluid and the motor fluid.

A large diameter motor was designed with enough water flow area to limit velocities below the erosion limit. On the outside of the motor casing are tabs to ensure that the motor casing will never be located tightly against the wellbore, and some fluid flow past the outer surface of the motor will always be available for heat removal. The motor casing is fitted over the motor stator. Power cables are positioned on the outside of the stator in a series of slots distributed around the periphery. Although it is preferable to bundle all three phases of the power cable together to reduce proximity heating from AC currents in the cables, a more compact arrangement was selected. Each phase of each cable could be produced in the form of a ribbon so that it occupies the least amount of radial space possible.

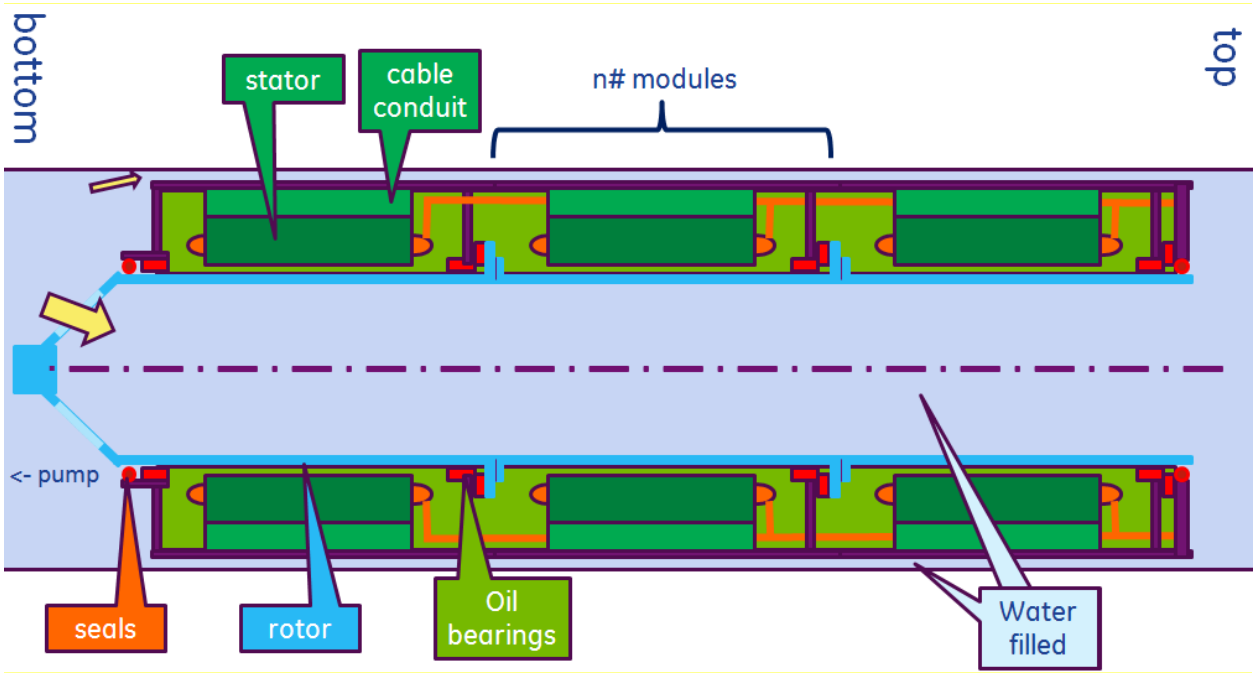

Figure 4.20 - Schematic axial cross-section of a large-diameter bore-flow motor

PM Motor Topology

As described above, the motor has process water flowing primarily through the bore of the rotor with the remainder flowing between the outer surface of the motor frame and the inner surface of the well casing. The outer process water flow removes heat resulting from all the motor stator losses plus the cable losses. Also, given the process water velocity limit as dictated by the erosion and corrosion of the contacting materials, the cross-sectional areas of both flow paths are appropriately sized based on historical data. As required by the project scope, the motor is to operate nominally at 300 bar and over 300°C in a dielectric oil-filled environment. The oil is used as the heat transfer medium to primarily remove the stator losses by pumping it through the air gap and the stator winding, and returning it to the stator back-iron outer surface by employing impellers mounted on the rotor shaft inside the motor on either side of the electromagnetically active zone. It is expected that the churning losses and rotor electrical losses will be transferred to the process water flowing through the rotor bore.

A number of non-traditional design aspects are considered in making this motor feasible. The insulation capability is estimated to be 330°C giving only 30°C for temperature rise (as the process water is expected to be at 300°C). The motor speed is fixed at 3150 RPM as a balance between power density and churning losses constrained by the capacity to remove the resulting heat. For the overall power requirements of approximately 4-5 MW, the motor cannot be built as one unit for two reasons. One is manufacturability, and the other is the rotordynamics. It is expected that 14 to 16 motors will be needed; each nominally rated around 300 kW. For these 3-phase motors, the cables are to be located between the outer surface of the stator back iron and the motor casing inner surface where they will be oil-cooled.

Design of power cable routing

The original design utilized wide, flat power cables for the purpose of minimizing the radial space occupied so that the outer diameter of the stator backiron could be as large as possible. A problem was identified for this arrangement related to delivery of oil to and from the passages outboard of the cables. The power cables must travel down the length of the entire motor assembly, passing from one module to the next. For each motor module to include a dedicated oil circulation path, the oil would have to pass between the cables in order to reach the outboard oil flow passages. The flat, wide cables provided only small gaps between them for oil to pass.

An alternative arrangement was designed to maintain the same cross sectional area for each cable, maintain the same total oil flow passage area, and change the form factor of the cable cross section. Rectangular cables are located outboard of each stator tooth. A pair of ligaments included as part of the stator lamination extends on both sides of the cable, providing a protective pocket in which to place the cable. A wide space between cables is available to pass oil to the passage outboard of the backiron, as desired. A cable of the same desired area can be arranged as described to allow the same oil flow passage cross sectional areas of the previous design without needing to reduce the stator backiron dimension.

Rotor Construction

The rotor construction viewed from a radial cross section shows a very simple arrangement of magnets placed on a round shaft, with a retaining ring fitted over the outside. The termination rings provide a self-supporting landing to capture each individual retaining ring segment. They also provide locations where weights can be added or subtracted for rotor balancing, because unlike the retaining ring, the termination rings will have low levels of stress.

Bearing Selection and Rotordynamics

Two journal bearing designs were considered for the prototype PM motor – tapered land and plain journal with two oil feed grooves. Both provide adequate load capacity and stability characteristics for the subscale prototype motor. Assuming a length/diameter ratio of 0.5 for both configurations, the margin of stability to oil whirl is 10x for the tapered land design and 2x for the plain journal design. The tapered land design is preferred for the vertical full-scale design as well, as it provides adequate radial preload to prevent instability even in the vertical "unloaded" condition. It is expected that standard bronze bearing material will suffice for the application. Dynamic coefficients for the selected bearings are shown in Figure 4.21.

The bearing model and rotor model can be combined to create the comprehensive dynamics model for any ESP system configuration. This is a full-train model that reflects the combined dynamics of the motor, pump and protector as a single unit. Damped natural frequencies, modal damping, unbalance response and a stability analysis (if necessary) can be performed. The output from these analyses is used to derive the proper bearing type and size.

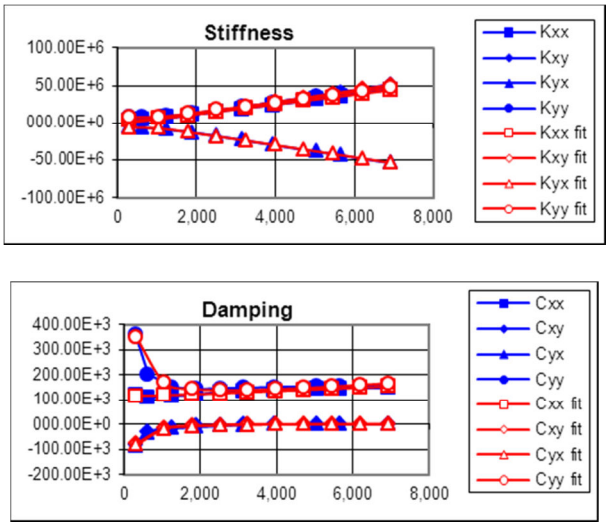

Figure 4.21 – Stiffness (N/m) and Damping (N-s/m) coefficients vs. Rotor Speed (RPM) for selected tapered land journal bearings

Modal analyses were conducted on the prototype stator to determine whether any coupled electro-mechanical resonances could be excited during operation. Since the prototype motor

operates as a 4-pole machine, the stator mode shape of interest contains eight nodes. The associated electromagnetic frequency was determined to be 1050 Hz.

A 2-D plane strain analysis of the stator was conducted, considering the out-of-plane lamination modulus to be approximately 1% of the in-plane modulus. The motor cables on the outer diameter of the stator back iron were also included in the model.

A number of conservative assumptions were made in the calculation of the stator natural frequencies. These included adjusting the material fill factor in the coils (80%), adjusting their density to account for the end-winding mass at both axial ends, and neglecting the large stiffness provided by the slot wedges that support the coils. The large mass and low stiffness assumptions result in an underestimate of the natural frequency which corresponds to a worst-case scenario.

The resulting frequencies and mode shapes were calculated. The eight-node mode that could potentially result in electro-mechanical resonances has a frequency of 1150 Hz which is 10% higher than the corresponding electromagnetic frequency. Since, in spite of the conservative assumptions outlined above, a comfortable separation margin exists the coupled vibrations were determined to be a low risk.

Even though the slot wedge stiffness was ignored for calculating the stator natural frequencies, its function of holding the coils in place is critical for the motor performance. In addition, its structural integrity is crucial since slot wedge failure would result in debris filling the air gap and potentially damaging the motor. As a result a static analysis was done to assess the slot wedge stresses under a sudden three-phase short circuit load. From electromagnetic analyses these loads were calculated to be approximately 40 N (~10 lbf) and to act in the radial direction under the coils. The results indicate that under static conditions, a maximum stress of 440 psi develops in the slot wedge. Since the load would act dynamically, an amplification factor of 2 was assumed, to result in a maximum stress of ~ 1000 psi. This results in a safety factor of nearly 14. Therefore, mechanical failure of the stator slot wedge is also a low risk item.

Rotor configuration and manufacturing process

The manufacturing sequence for the rotor was considered carefully to ensure that the rotor could be produced practically. The typical installation process for a retaining ring design of this type is to use elevated temperatures to thermally expand the retaining ring until sufficient clearance exists to slide the ring over the rotor. The proposed rotor design would be very long compared to its diameter, and so it would not be practical to assemble all of the magnets and discs to the rotor first and then install each retaining ring piece by sliding it over a relatively long distance to reach the final position. Attempting to do so would likely result in the retaining ring losing heat to the ambient and shrinking before reaching the intended final position. Even considering the option of using a retaining ring having a thickness much greater than required for the purpose of increasing thermal mass to hold heat and resist premature shrinkage, installing retaining rings over the entire rotor length was deemed impractical. As a result, a special fabrication method was developed to assemble the permanent magnet rotor.

Rotor mechanics analysis

Detailed mechanical analyses were conducted to verify the mechanical integrity of the prototype rotor at the operating speed of 3150 RPM and temperature of 330°C. The rotor structure is composed of a shaft, an array of permanent magnets, and centrifugal retaining rings.

The goal of the mechanical analysis is to ensure that rotor components are sized to produce a robust design. This is determined by three design criteria: (i) the equivalent stress on the retaining ring under maximum load must be lower than the yield strength at 330°C, (ii) the individual magnet pieces must remain under compressive pressure at all operating conditions to prevent lift-off, (iii) a manufacturing tolerance of 0.002 inch must be allowed for each radial dimension. Magnet lift-off results in motion of magnet masses which may change the rotor balance resulting in unexpected vibrations.

A representative unit was used in the mechanical analysis with symmetry conditions imposed on all faces except one edge of the retaining ring. Frictionless contacts are modeled among all parts. Since the operating temperature is significantly higher than in conventional applications, all rotor components use temperature-dependent thermal expansion coefficients and elastic properties at 330°C. The model was subjected to centrifugal acceleration under a speed of 3940 RPM at 330°C.

The results of the mechanical analysis are shown in Fig. 4.22. These show that the maximum equivalent stress experienced by the retaining ring is approximately 100 ksi at its maximum radial interference fit. This value is significantly lower than the yield limit at 330°C. Additional plots showing the stresses in the circumferential and axial directions are included. Figure 4.23 shows the radial stress at the base of the radial and circumferential magnets for the minimum radial interference fit. The results show that a minimum compressive stress of 300 psi is maintained to prevent magnet movement.

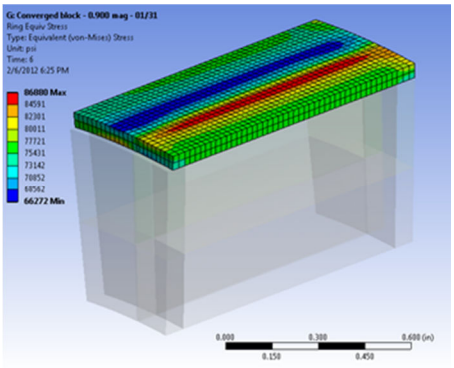

(a)

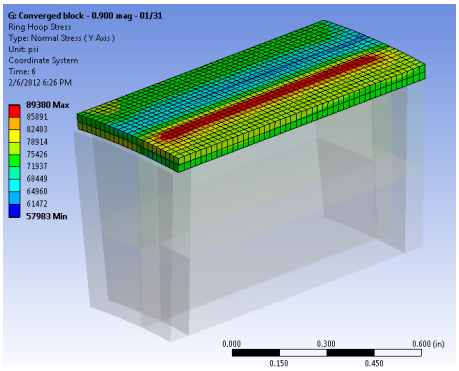

(b)

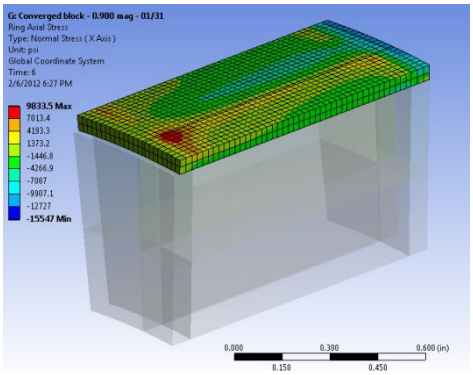

(c)

Figure 4.22: (a) Equivalent, (b) Circumferential and (c) Axial stress on centrifugal retaining ring

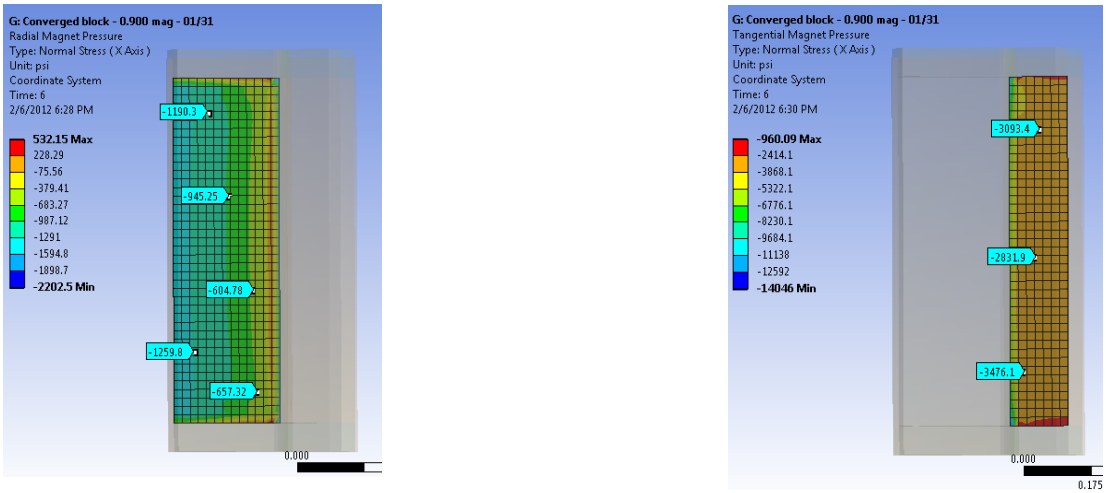

(a) (b)

Figure 4.23: Radial compressive stress on (a) radial and (b) circumferential magnet blocks

In order to facilitate the magnet placement on the shaft during rotor assembly, thin pockets are machined on the shaft surface as shown in Figure 4.24. Simple 2-D analyses were carried out to determine the stress concentrations resulting from these features. The results are shown in Figure 4.25 where a comparison between a shaft with and without the features is provided. In the absence of the pockets, the shaft stresses are in the order of 30 ksi, while introducing the features produces a stress concentration near the corners with a maximum stress of approximately 90 ksi. The high stress, however, decays to the baseline 30 ksi within a very short distance (~0.040 inch). As a result, a design decision was made to allow localized yielding of the shaft near the corners of the pockets.

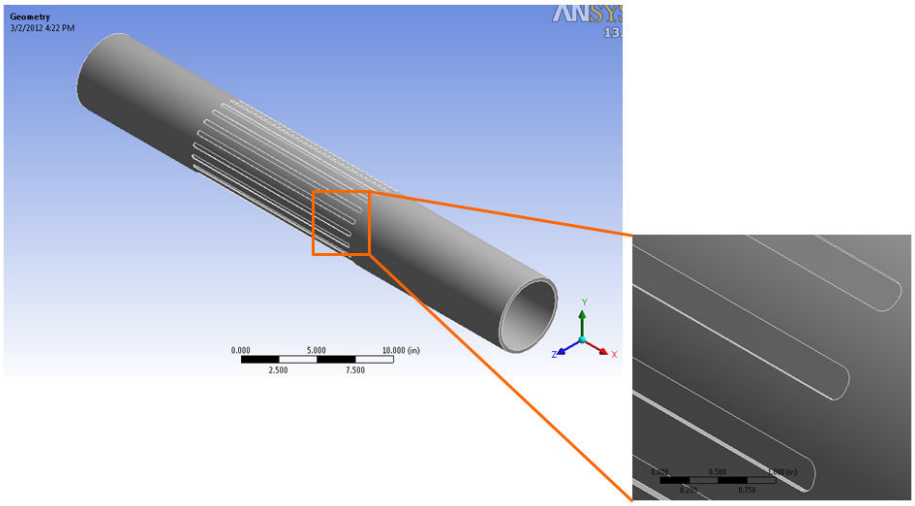

Figure 4.37: Detail of pockets machined on shaft surface to facilitate magnet placement

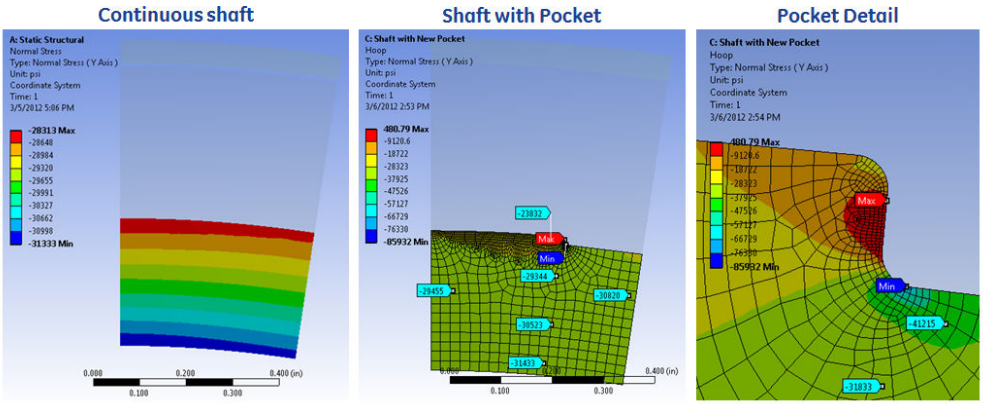

Figure 4.25: Comparison of rotor shaft stress with and without magnet placement features

Motor Layout

Figure 4.26 shows a CAD image of the geothermal motor prototype. On the left end, or pump end, are shown the rotating coupling connecting the pump and motor shafts, as well as the pump and motor casing coupling. Both coupling pieces feature several openings along their surface to allow water flow. The majority of the water is directed through the rotating coupling and subsequently through the motor shaft. A smaller fraction is directed through the stationary coupling to flow on the outside of the motor casing to cool the oil circuit that ventilates the motor.

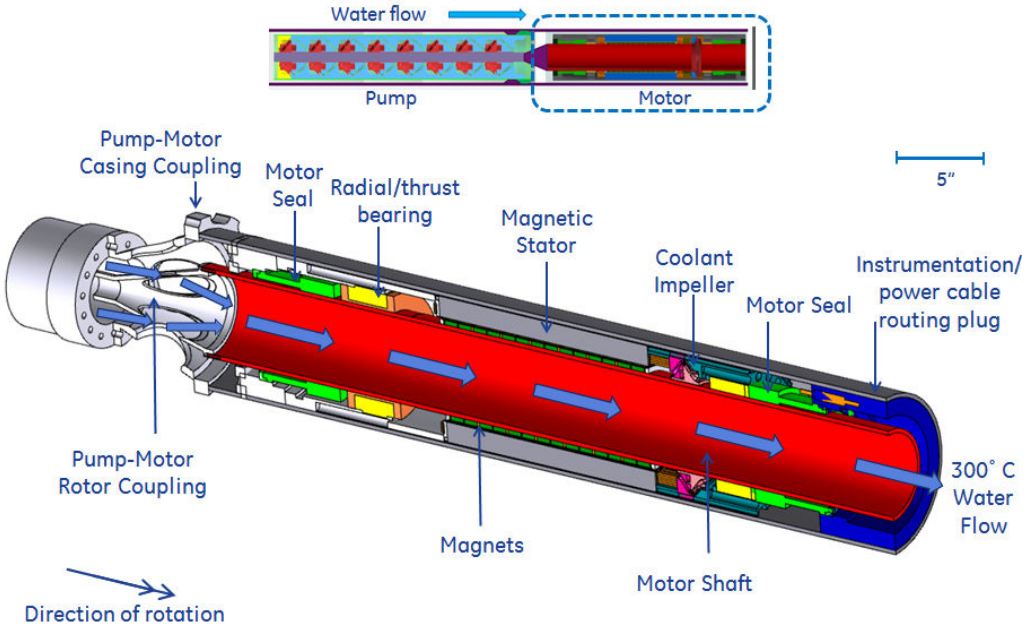

Figure 4.26: CAD model of geothermal motor prototype

Also shown in the figure is an integrated bearing to carry both radial and thrust loads. The bearing stator features thrust faces that act with thrust collar surfaces to carry the thrust loads of both the pump and motor. The radial-thrust bearing is located on the pump end of the motor for better axial clearance control within the pump. The thrust collars are an integrated piece that is shrunk-fit onto the shaft for ease of motor assembly. The figure also shows preliminary designs of the flow circulation channels that guide the coolant flow through the motor. Finally, the model shows the approach taken to lead the instrumentation and motor power cables out of the motor. This is done through a routing plug connected on the non-pump end of the motor which features radial channels that allow the wiring to exit the motor and flow loop.

Rotor Coupling

A preliminary design for the rotating coupling connecting the pump and motor shafts is shown in Figure 4.27. The coupling surface features four openings to allow water flow from the last pump stage diffuser through the rotor shaft. The main criterion in designing the pump was to provide sufficient access area for the water to flow to the motor shaft. As a result, the cumulative area of the coupling openings is 30 in^2 which is greater than the motor bore area of 23.75 in^2. As the figure shows, the coupling is connected to the pump shaft through a spline similar to the one employed in current GE Artificial Lift products. On its opposite end, the coupling is bolted to the motor shaft.

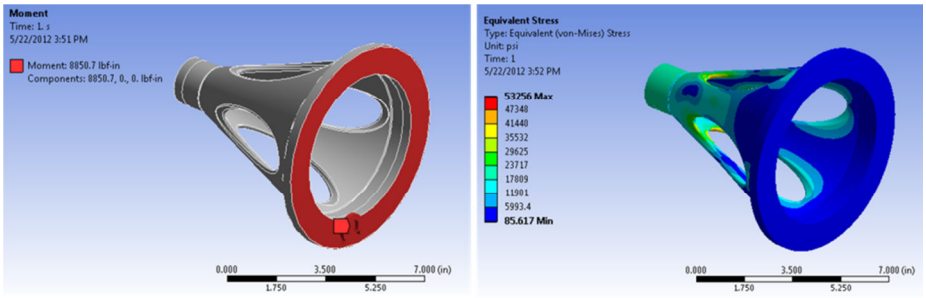

Pump torque at 3150 RPM ~1300 lbf-in
Coupling loaded with 8850 lbf-in to assess safety factor
Acceptable stresses (~50 ksi) under 7X expected torque

Figure 4.27: Static structural analysis setup and result for pump-motor coupling

In order to mechanically assess the coupling design, a static structural analysis was conducted subjecting the coupling to over seven times the torque seen during normal operation (1300 lb-in at 3150 RPM). Figure 4.27 shows a schematic of the analysis setup, and the resulting maximum equivalent stress of 53 ksi. Figure 4.28 shows the first three mode shapes of the coupling, which were computed to assess whether any natural frequencies existed near the running speed. The lowest frequency occurs at 1664 Hz which is over 30 times the running frequency, thus causing no risk of exciting a coupling resonance.

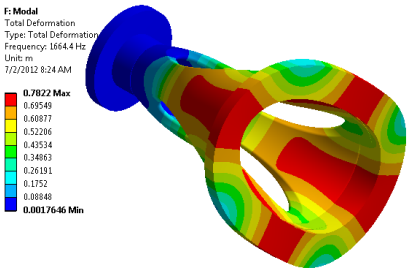

(a) First Mode at 1660 Hz

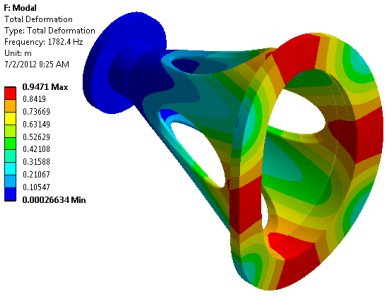

(b) Second mode at 1780 Hz

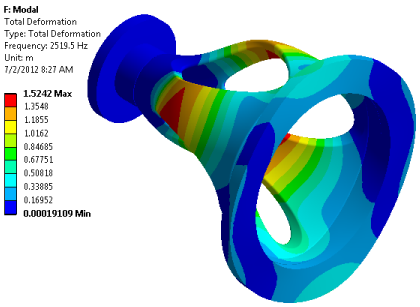

(c) Third mode at 2180 Hz

Figure 4.28: First three mode shapes of pump-motor shaft coupling

4.2.3 Thermal Management

4.2.3.1 Internal Cooling Path

To remove the heat produced within the motor, a forced fluid circulation cooling scheme was adopted. Fluid flow passages were provided down the length of the machine. It is important to note that the primary heat sink for the cooling system is the outer surface of the motor housing. In order to drive the oil through the desired flow passages, one or more impellers would be located at each end of the machine with a corresponding diffuser to direct the flow.

The current layout results in a compact and robust rotor where all components can be easily cooled.

One consequence of flowing water through the bore of the motor is that a passage must be provided for the water to enter the rotating shaft. A simple conical coupling with ported openings was modeled together with the rotating fluid passage inside the motor and non-rotating passage outside the motor. The preliminary CFD results showed that some fluid velocities would be high in local regions at the entrance but that the average fluid velocity would be within the desired limits. The geometry model and resulting fluid streamlines are shown in Fig. 4.28.

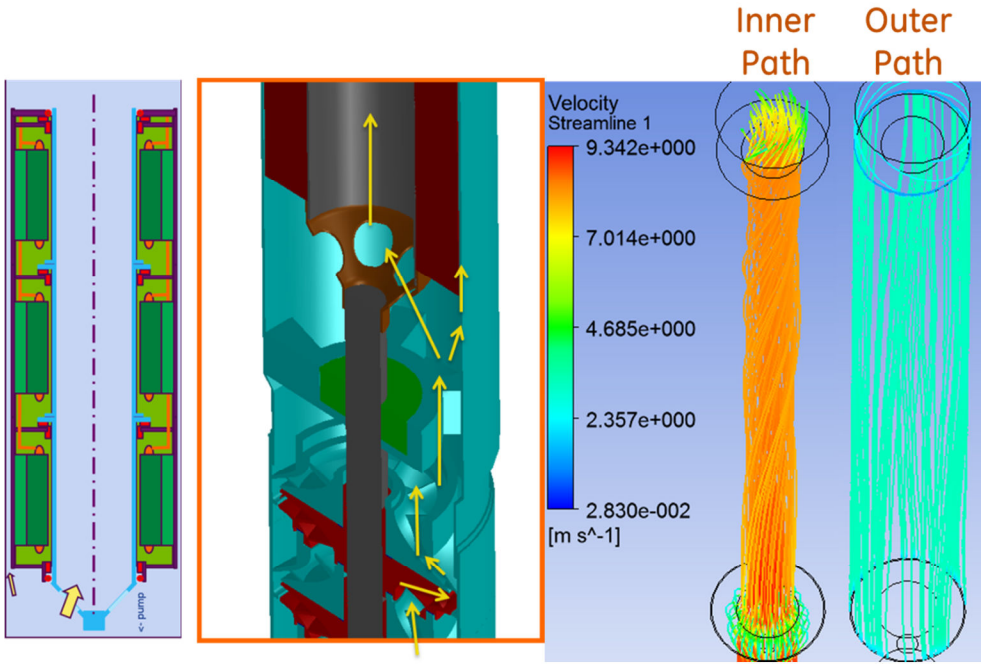

Figure 4.28 - Fluid flow model through rotating and non-rotating passages.

4.2.3.2 Internal Cooling Impeller

As mentioned above, the electric submersible motor designed for the geothermal application is a self-cooling electric motor with produced fluid flowing on the outside and an impeller-forced oil circulation system inside. A centrifugal impeller is attached to the shaft of the motor and spins with it, providing sufficient oil circulation to the motor's internal structure to aid in cooling. The cooling path consists of the impeller, oil gap between the rotor and stator, and oil passage between the windings, and a return path. During the recirculation, there will be a pressure drop (DP) due to the resistant in the flow path as shown in Figure 4.29. Therefore, a built-in cooling pump including an impeller and a diffuser has to be provided in order to provide sufficient boost to overcome the DP.

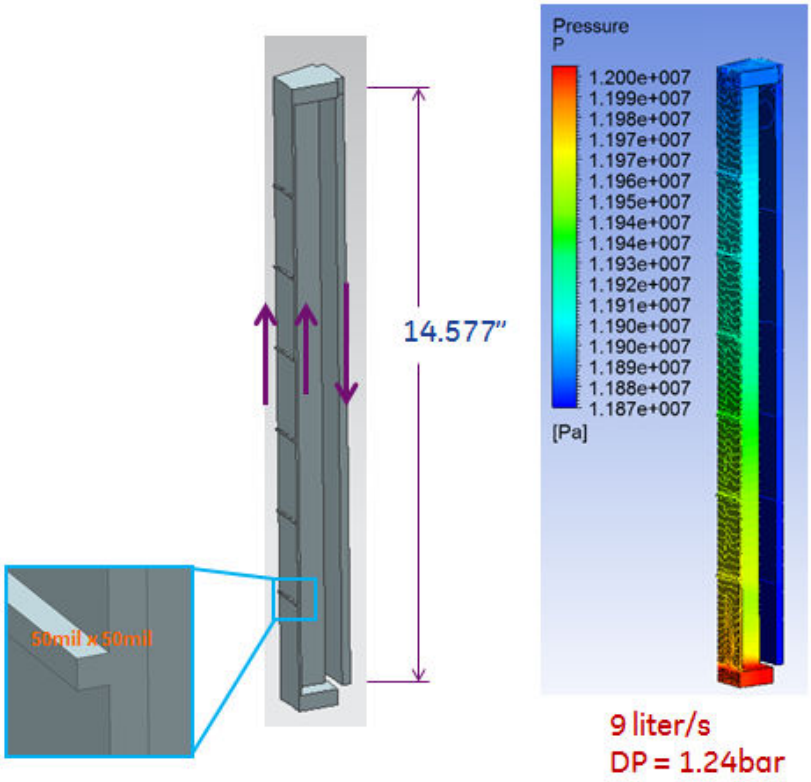

Figure 4.29 – Internal oil circulation and DP

The design variables of the current cooling pump include:

1. Operating speed
2. Shaft diameter
3. Pressure drop (DP)
4. Maximum diameter
5. Volumetric flow rate

In order to effectively use the limited radial space in the motor and generate sufficient head, a mixed-flow helical impeller has been designed. The configurations of the cooling impeller and diffuser are shown as Figure 4.30.

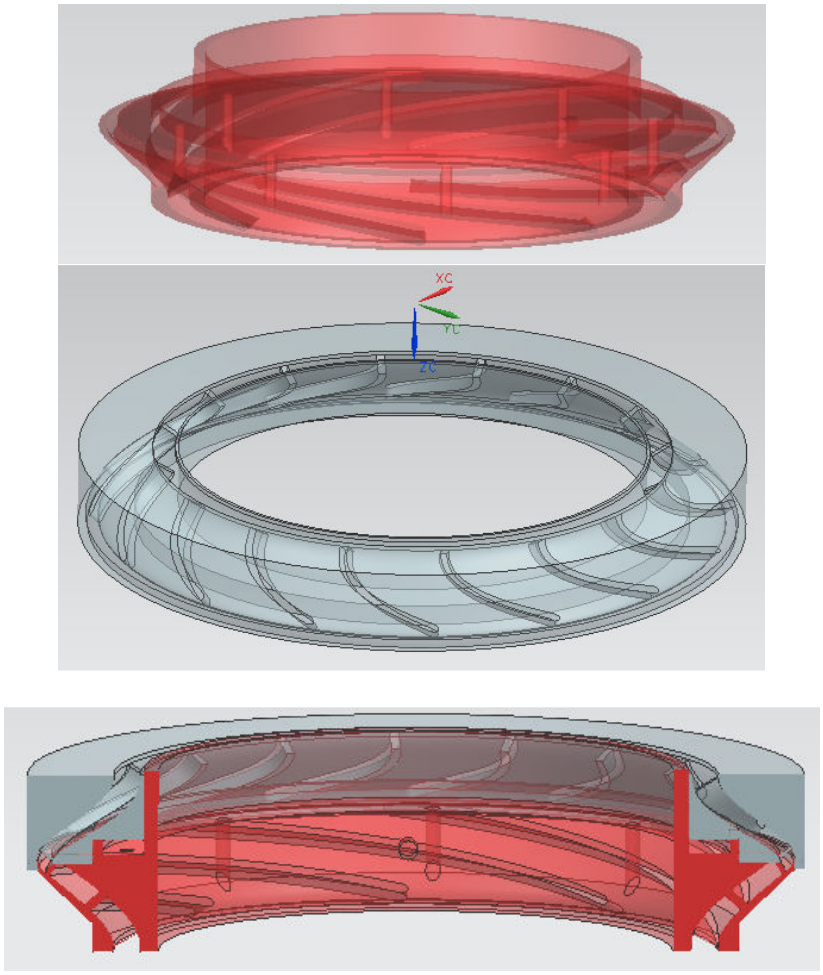

Figure 4.30 – Cooling impeller/diffuser configuration

During the oil circulation within the PM motor, churning losses are induced due to the rotation, pumping, and viscosity of the dielectric oil. Generally, this kind of loss is not insignificant for motors with relatively long active length and small oil gap, such as the ESP motors. Therefore, churning losses must be properly evaluated in order to optimize the motor design and manage the total power distribution. CFD analysis was performed to evaluate the performance of the cooling pump. Fig. 4.31 displays the performance curves including head, input power, DP of the oil passage and motor's churning losses. It is observed that the cooling pump will be working at about 9.7 liter/s, where the head equals the downstream DP. At this point, the power needed for the impeller is approximately 3.2 kW and the churning loss of the entire motor is 1.8 kW.

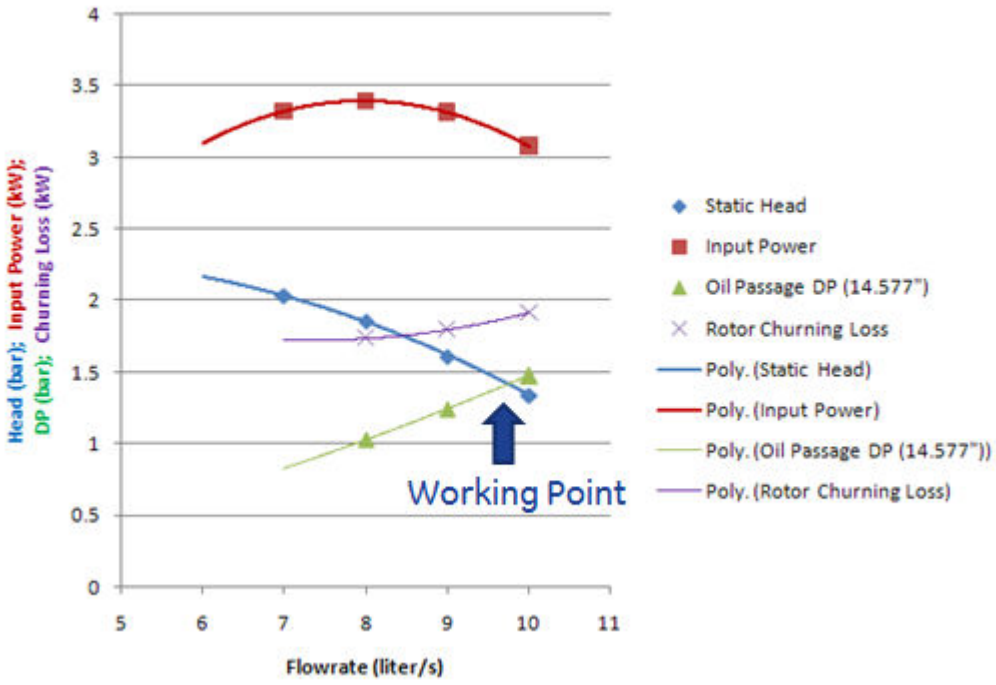

Figure 4.31 – Cooling pump performance curves

4.2.3.3 Thermal Analysis

The motor cooling design follows the method described in the previous sections, with the process water acting as the ultimate coolant and flowing through parallel paths to remove motor heat. From the inner bore of the rotor assembly, the process water directly cools the electromagnetic components of the rotor. At the stator outer bore, a cooling jacket with fin structures is attached. The outer fins of the cooling jacket and the well tube inner bore define the flow passages for the process water to cool the stator. Inside the motor assembly, dielectric oil is used to fill up the motor cavities. Dielectric oil passages are designed between the coil-side inside stator coil ground wall insulation. These passages, together with the air (oil) gap and the inner fins of the cooling jacket, form a circulation path for the dielectric oil. This path is sealed to avoid contamination from ambient process water. Shaft-mounted impellers are used to circulate the dielectric oil through this closed-loop flow path. The dielectric oil takes heat from locations with a higher thermal resistance to the process water, and dissipates the heat to the inner fins of the cooling jacket so the heat can be removed more effectively by the process liquid. The overall design enables a motor with significant advances in thermal performance and power rating.

Compared to the original design, the power cable location was redesigned to provide better cable packaging space. The friction drag in the air (oil) gap was also re-evaluated to reflect the updated gap geometry. The oil impeller was adjusted to provide adequate pumping pressure to circulate internal oil flow. Consequently the electromagnetic design, as well as the expected windage heating, are reflected in the motor finite element thermal model. The temperature of

the stator and the rotor components is been maintained at acceptable level following these design modifications.

4.2.4 FE-Based Design Optimization

For the design optimization, three key ratios are varied. These are the stator tooth width to stator tooth pitch, main rotor pole width (circumferential) to pole pitch, and split ratio defined by rotor radial height to the total motor radial height. They are shown in Figure 4.33. The finite element electromagnetic analysis uses time-transient simulation with rotor rotation. It accounts for eddy currents induced in all conductive materials (magnets, sleeve, stator casing and well casing) and calculates the associated losses. The goal is to maximize the torque per unit axial length while meeting the thermal constraints.

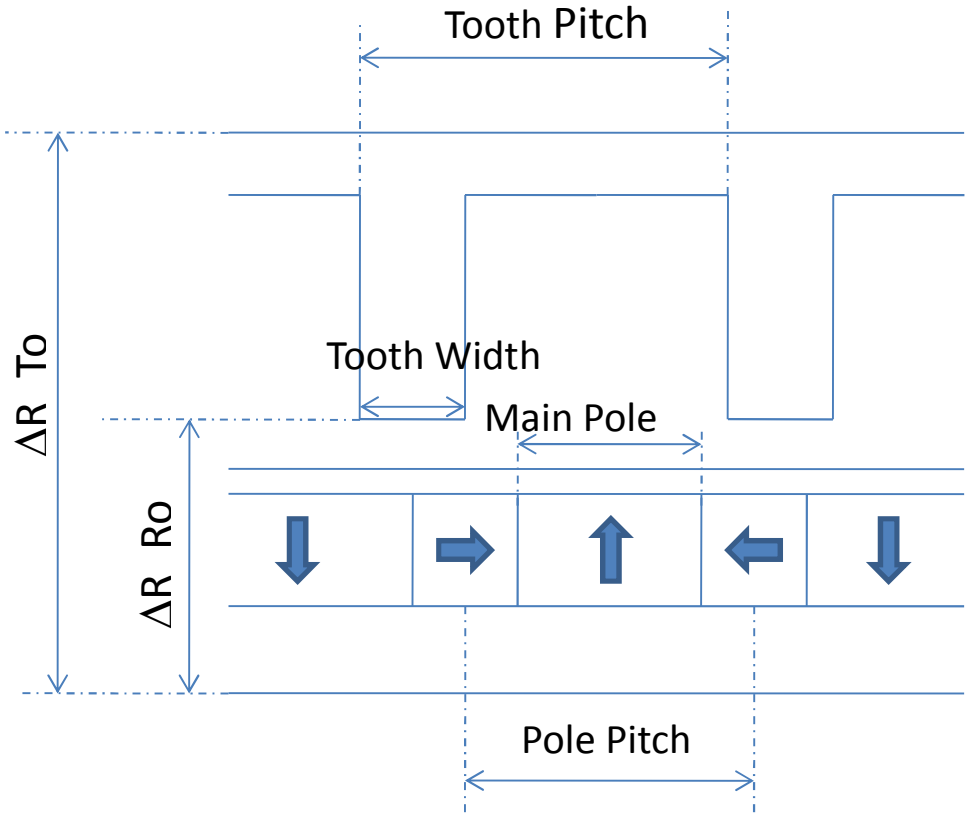

Figure 4.33 - Optimization variables

Figure 4.34 shows the torque waveform and Figure 4.35 the Line to Neutral and Line to Line voltages when the motor is fed by sinusoidal currents. The torque is smooth and the voltages under load are quite sinusoidal. The permanent magnets are chosen for their relative high energy density and ability to operate at high temperature.

The highest flux density level in the teeth is around 2T, allowing the design to take full advantage of the high permeability of the laminations. A demagnetization risk assessment has been carried out under a transient short circuit condition. Only tiny areas of the magnet pieces are at risk of permanent demagnetization. Thus, the post-event reduction in torque will be negligible. Finally, Table 4.1 summarizes the electromagnetic loss distribution of the optimized machine. These losses are used in the thermal model to validate the thermal design.

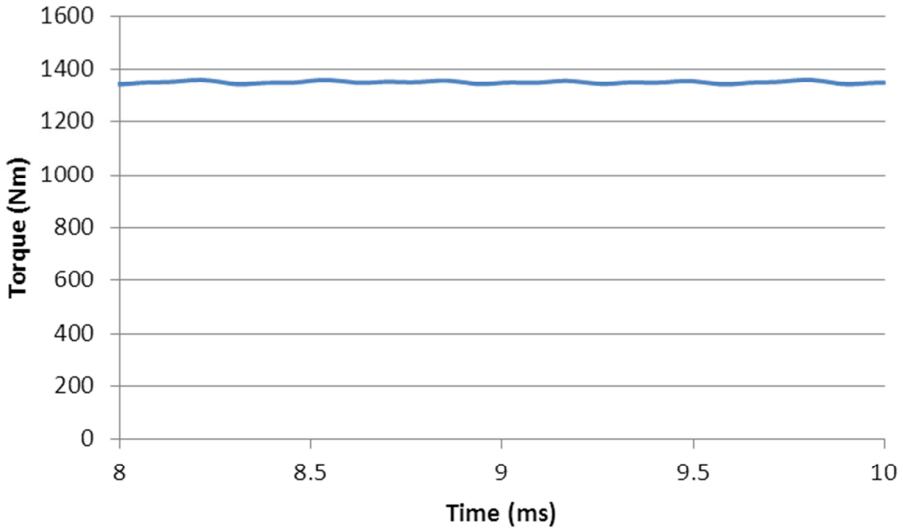

Figure 4.34 - Torque waveform

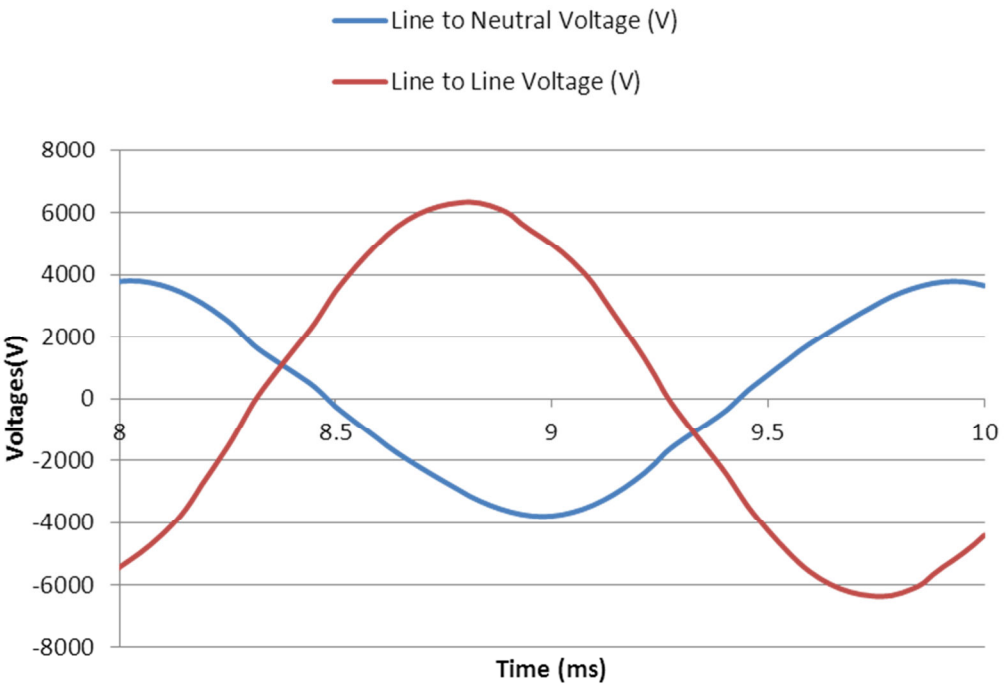

Figure 4.35 - Voltage waveforms

Speed (rpm)	3150.00
Axial Length (inch)	77
Active Axial Length (inch)	66
RMS current Density (A/mm^2)	5.40
Average Torque (Nm)	941
Stator Casing Losses (W)- assumed stainless steel	347
Stator Iron Losses (W)	4142
Overall Machine Copper Losses (W)	16128
Rotor Sleeve losses (W)	8083
rotor back iron/shaft losses (W)	936
Magnet Main Segment Losses if not segmented (W)	423
Magnet Circumferential Segment Losses if not segmented (W)	67
Well Losses(W)	123

Table 4.1 - Loss distribution

4.2.5 Motor Ground Wall Insulation

The geothermal motor cooling scheme requires high-velocity oil flow through the stator slots to maintain the temperature at or below 330°C. This flow poses an abrasion risk to the slot liner insulation which is in direct contact with the oil. The flow of any debris resulting from abrasion would potentially cause seal damage, among other adverse effects on the motor performance. As a result, alternative constructions were considered that would minimize the abrasion risk by ensuring there is no direct contact between the oil and the insulation.

5. Subscale Prototype Experiments

5.1 SUBSCALE PUMP

5.1.1 Pump Fabrication and Assembly

For the lab-scale high temperature flow loop demonstration, the production rate was scaled down to approximately 20 kg/s since pumping 80 kg/s geothermal fluid is not practical for a lab test. Furthermore, the primary goal of the demonstration is to validate the motor can work properly under 300°C. In a change to the original test plan, motor temperature capability can be demonstrated in a separate thermal test in air. The purpose of flow loop testing is to demonstrate the feasibility of the "flow-through-the-bore" motor configuration. Therefore, an existing 8-stage GE ESP pump, TJ12000, was leveraged for the lab-scale demonstration in order to cost-effectively test the motor.

The TJ12000 was not initially designed to work at 300°C. As stated above, the flow loop portion of the test program was modified to be done at a limited temperature of ~150°C (high temperature motor capability to 300°C to be demonstrated separately). This requires limited modification of certain pump components. The component level modifications are as follows:

1. As a general risk for high-temperature down-hole systems, clearance control is always vital to the performance. Therefore, it is very important to make sure the Thermal Expansion Coefficient (CTE) of each component has been considered and the clearances are good for the entire temperature range. Pump temperature will be limited to allow the use of standard bushings and sleeves between the rotating and stationary pump components. (Again, thermal testing of the motor can occur separately, in an open-air test without the TJ12000 pump.)
2. There are two static seals per stage between the OD of the diffuser and ID of the housing. The seal materials are temperature-limited and have been replaced by a material which is rated for 325°C.
3. The thrust washers between the impeller and diffuser are temperature-limited. These washers have been eliminated, and the axial thrust load will be carried by the dual-acting thrust bearing in the motor.

The new pump has been fabricated and is ready for testing (shown as Fig. 5.1). It is ready to be assembled and integrated with the motor section, pending successful completion of the motor thermal testing.

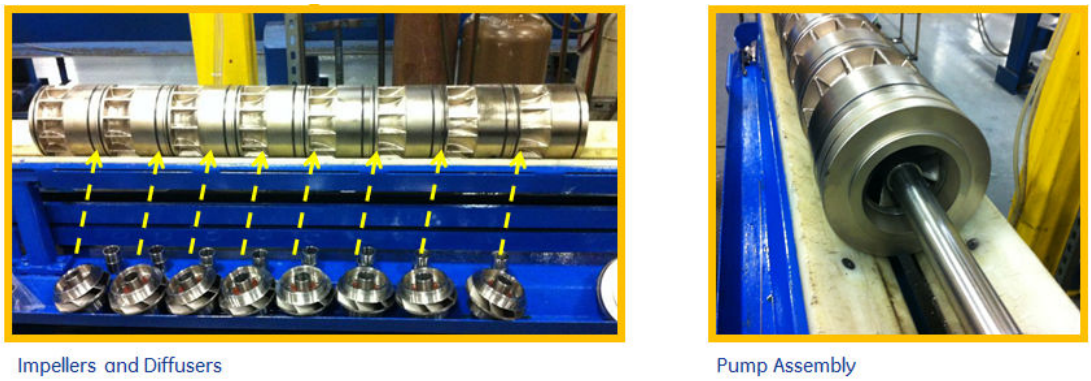

Figure 5.1 –TJ12000 pump assembly

For static O-ring seals between the pump and its housing, two high temperature O-ring materials were evaluated. The same materials were considered for the motor secondary seals, and these are exposed to the dielectric oil contained within the motor. Oil compatibility tests show that none of the O-ring materials indicate adverse behavior in the presence the candidate motor oils for 3 days at 70 psi pressure and at 300°C. The post test samples show there was no reaction between the O-ring materials and the motor oil.

Pump O-ring size was selected based on the O-ring groove geometry already machined into the TJ12000 pump housing. Figure 5.2 shows the O-rings and O-ring groove critical dimensions to aid in selection of the O-rings.

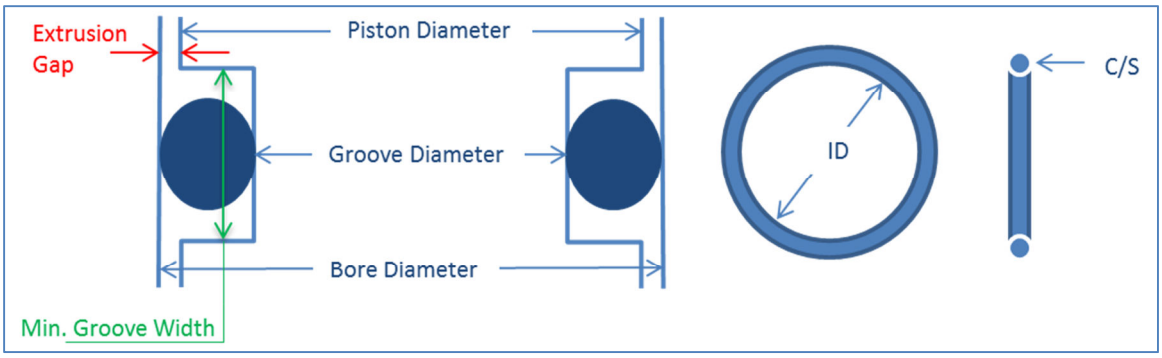

Fig. 5.2 – O-ring & groove critical dimensions

5.1.2 Pump Performance

The TJ12000 pump can achieve 80% efficiency at the best efficiency point (BEP). Though the flow rate at the BEP is 15.6 kg/s, 20 kg/s is within the best operation range of the pump (9.0kg/s ~ 21.6kg/s). In addition, the pump is able to boost 11.4 bar pressure at the BEP and requires 46kW power input.

5.1.3 Pump Bearings and Thrust Washers for High-Temperature Conditions

Pump Bearings

The geothermal prototype pump will operate with the process fluid as lubricant which, in the case of high temperature water, has very low viscosity. In addition, the test flow loop operates in a horizontal configuration resulting in a larger bearing load. As a result, an analysis was performed to determine the running eccentricity of the geothermal pump bearings and establish appropriate geometric tolerances to ensure proper functionality.

The water bearing flow regime at the design clearance (0.005'' radial) and running speed (3150 RPM) is fully turbulent as indicated by a Reynolds number of 15,800. This facilitates the horizontal operation of the water-lubricated bearing since turbulent conditions increase its load capacity. The bearing eccentricity was calculated using the XLLubGT software which is part of the XLTRC rotor dynamic suite maintained by the Turbomachinery Research Consortium. The tool is intended to calculate seal parameters, but is capable of calculating eccentricity and dynamic coefficients under loaded conditions. Figure 5.3 below shows an image of the analysis spreadsheet. Each diffuser pump bearing must support a static load of 5.5 lbf (25 N) resulting in an eccentricity of 0.74. As a result, the operating film thickness is expected to be 0.001'' which is in the conventional range for fluid film bearings.

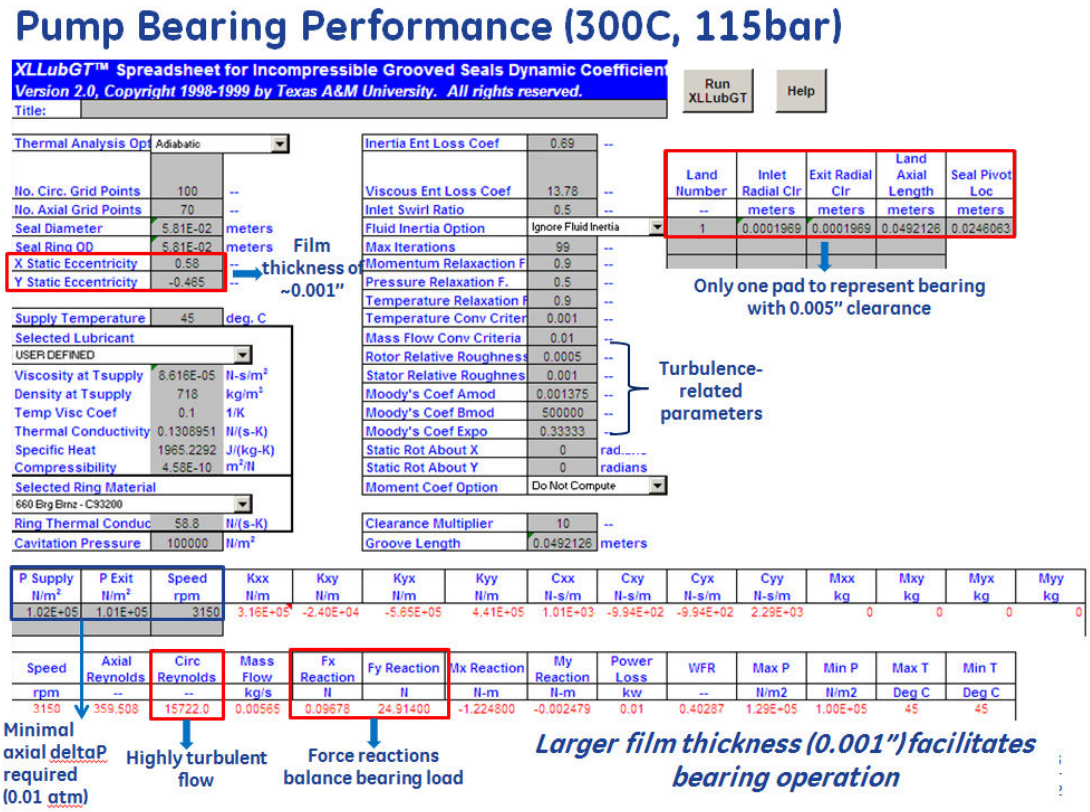

Figure 5.3 – XLLubGT interface showing results for geothermal pump bearings

Thrust Washers

Thrust washers in each stage of the pump must operate in an environment that is 300°C and potentially exposed to sand. As part of the selection process for suitable materials, wet and dry specimen wear tests were conducted on a Falex wear tester using the thrust washer specimen configuration shown in Fig. 5.4.

The rig is capable of:

- Contact Stress: 4000psi
- Speed: 14-4420rpm
- Temperature (dry): 260C

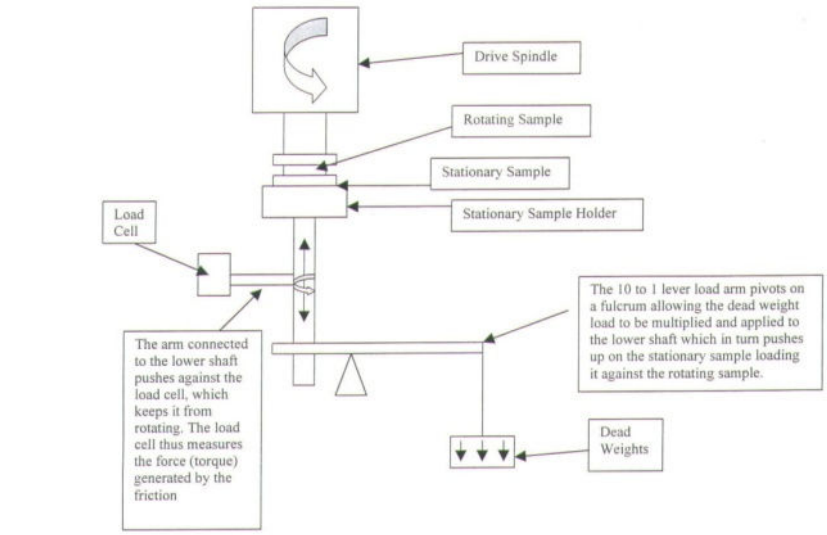

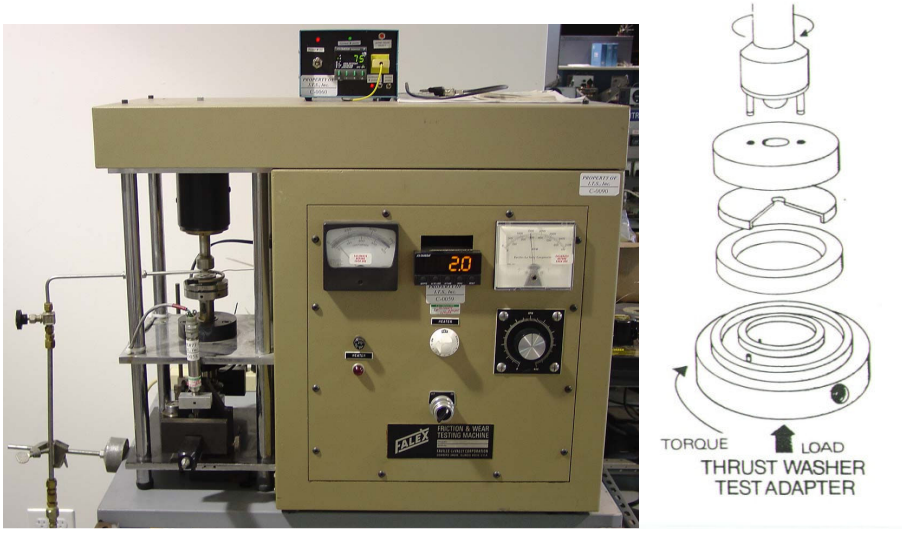

Figure 5.4 – Falex Wear Tester

Thrust washer materials considered include bronze bearing alloys and cemented carbides. The counter face material is the standard diffuser material.

Two types of tests are considered:

1. Wet tests using water as lubricant at room temperature, whereby the test starts with a minimum load at a nominal speed. Load is then added at regular time intervals and held for a set period of time until a load is reached where the lubricant film between the thrust washer wear specimens is broken, leading to scuffing. This load is recorder as the scuffing threshold. Friction/torque as well as temperature rise due to frictional heating is measured throughout the load cycle.

2. Dry tests at 260°C at a nominal load and speed where friction/torque, temperature and wear rate are recorded.

Scuffing threshold under wet condition tests, friction and torque as well as frictional heating are the basis for material selection for prototype test in sub-scale loop. Tests were conducted on the Falex rig using water as lubricant and at 10.5 ft/sec surface velocity. The same diffuser material was used for each test. The test conditions are shown as Table 5.1 below.

Test #	Sationary	Rotating	Lubricated step test at room temperature					Additional comments
			Load 1	Load 2	Load 3	Load 4	etc.	
1	Diffuser material	Material A	Increasing load --->				until scuffing occurs	All bearing surface will be of the same nominal finish (TBD). lubricating fluid: water
2	Diffuser material	Material B						
3	Diffuser material	Material C						
4	Diffuser material	Material D						
			High temperature dry test					
5	Diffuser material	Material A	Dry test at 260C at one nominal load to measure wear rate.					Load will be defined to produce normal oxidative wear. 260C temperature is the limit of the test rig.
6	Diffuser material	Material B						
7	Diffuser material	Material C						
8	Diffuser material	Material D						

Table 5.1 – Thrust washer test conditions

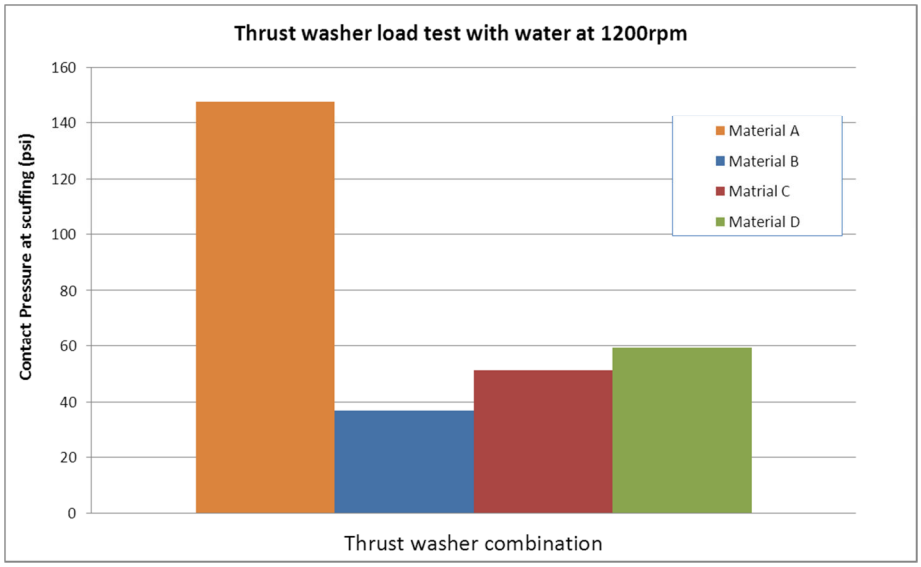

Figure 5.5 – Scuffing contact pressure for different material pair in wet step tests

The scuffing threshold is shown in Fig. 5.5 in terms of contact stress for each material pair. Clearly, Material A against the diffuser material shows the highest scuffing contact pressure. Fig. 5.6 shows the corresponding temperature profiles for each pair during the test. Recorded temperature profiles also confirm the same ranking whereby Material A with highest scuffing contact pressure threshold shows the lowest frictional heating build up throughout the test.

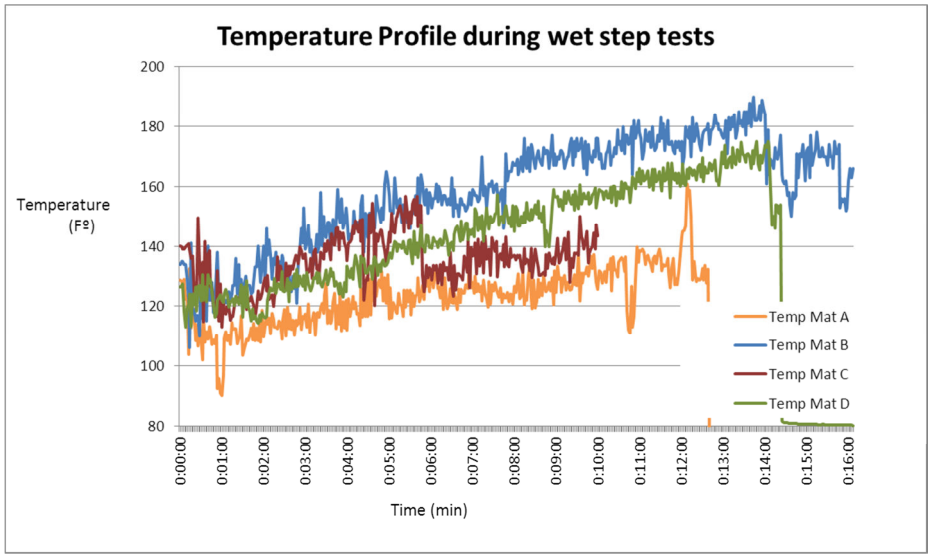

Figure 5.6 – Temperature profiles during wet tests

Fig. 5.7 provides torque data for each of the tests also confirming Material A to have to lowest torque amongst the tested pairs.

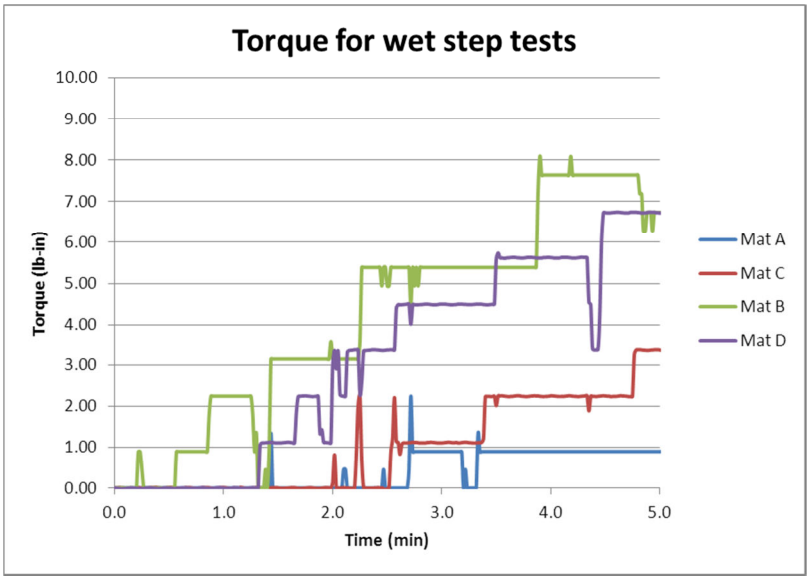

Figure 5.7 – Torque associated with each pair of materials tested

Fig. 5.8 shows roughness of all bearing surfaces before and after wet step tests. All surfaces' starting roughness Ra is within 13-15 micro-inches; however, Material A does not seem to have the lowest Ra after scuffing against the diffuser material.

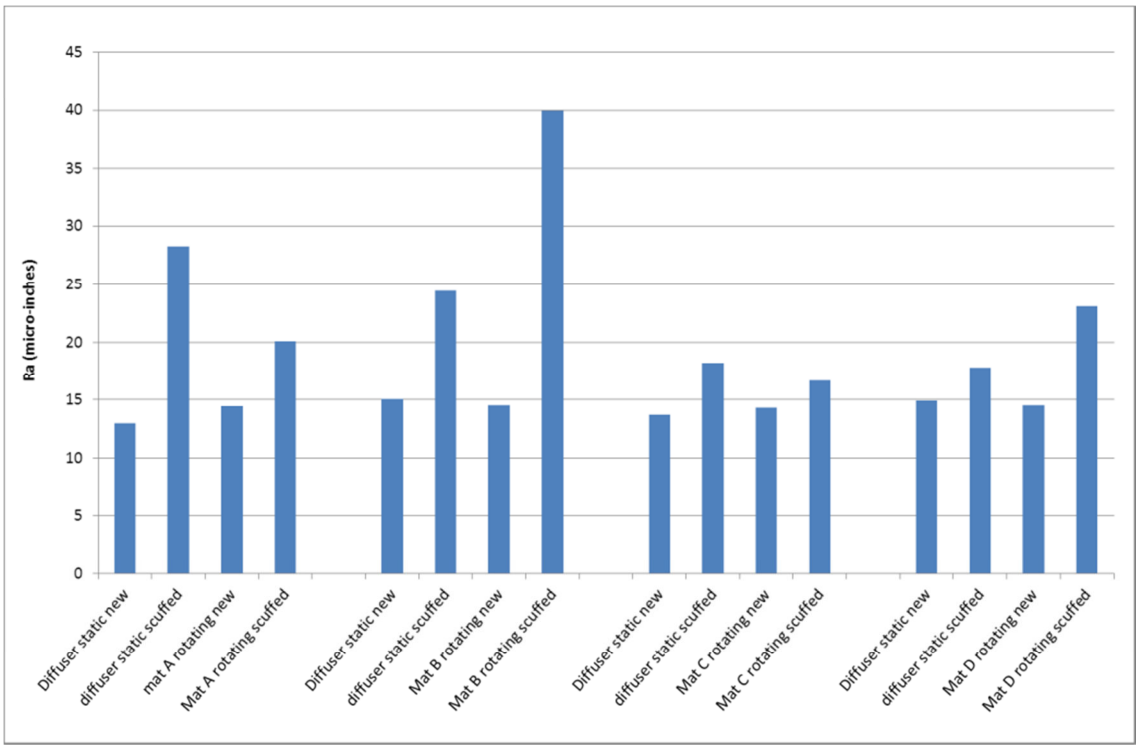

Figure 5.8 – Roughness before and after wet step tests on static & rotating faces

Fig. 5.9 provides an image of Material A before and after the wet step test. The after-test scuffed region is marked.

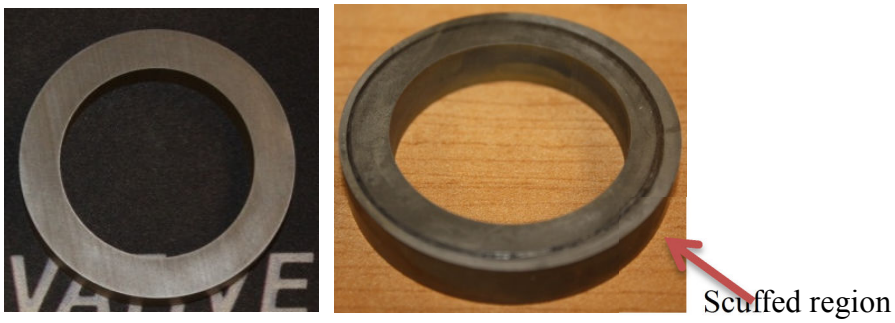

Figure 5.9 – Example of test thrust washer Material A before and after

Dry wear tests were completed on thrust washer materials as described in Table 5.2 below. The aim of the dry tests at a single load is to establish a wear rate for each pair of bearing material under dry, oxidative wear condition. This information is used as a guide for selecting the bearing/thrust washer pair in conjunction with lubricated step scuffing tests. It must be noted that dry tests and dry test data on their own have little relevance to the bearing behavior in this configuration. However, the dry test data is a useful and complementary guide to the selection process.

Test #	Sationary	Rotating	High temperature dry test	Additional comments
5	Diffuser material	Material B	Dry test at 260C at one nominal load to measure wear rate.	Chose a nominal load of 25lb to produce normal oxidative wear. This corresponds to 25psi contact stress. 260C temperature is the limit of the test rig.
6	Diffuser material	Material C		
7	Diffuser material	Material D		
8	Diffuser material	Material A		

Table 5.2 – Thrust washer test conditions

A test load of 25 lbf was selected based on the previously reported lubricated step scuffing tests. Material B in lubricated step scuffing tests showed the lowest scuffing threshold which was about 37 psi. Therefore, the selected dry test load to measure wear rates had to be below this threshold to allow measurement of wear rate in an oxidative wear regime.

Figure 5.10 provides the wear rates for each of the tests. Test 5 which is material B against the diffuser material shows the highest wear rate which in fact was the same material combination that showed the lowest scuffing threshold in lubricated step scuffing tests. Tests 6, 7 and 8 all show low wear rates, however test 8 in particular shows both stator and rotor with lowest collective wear rate. Test 8 (as in the lubricated step scuffing tests) is with Material A against the diffuser material and shows the lowest wear rate and the highest scuffing threshold in lubricated tests.

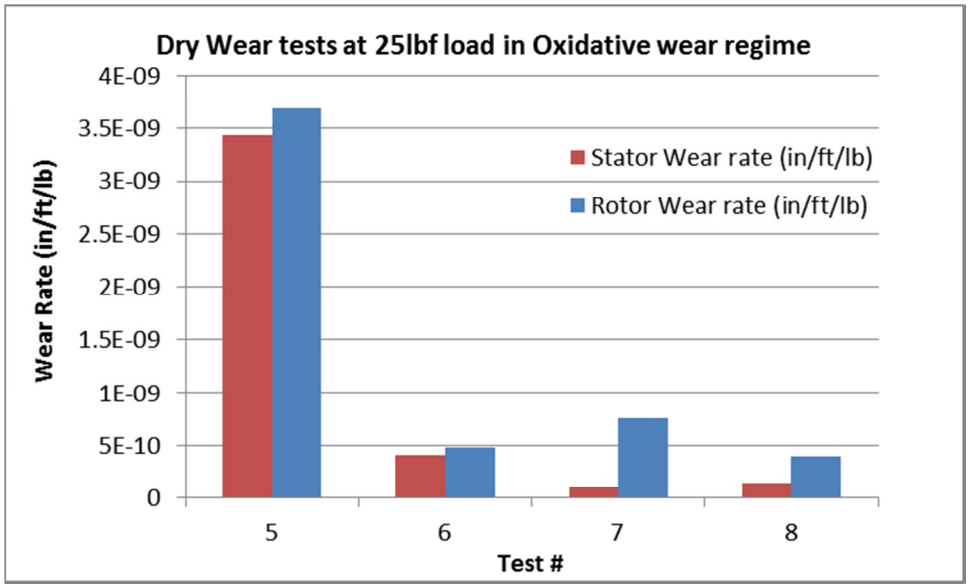

Figure 5.10 - Dry wear rate test data

5.2 SUBSCALE MOTOR

5.2.1 Rotor Fabrication and Assembly

The construction of the magnetic rotor has been completed. Figure 5.11 shows a view of the magnets assembled on the shaft after being ground to their final dimension. Figure 5.12 shows the completed magnetic rotor with all retaining rings assembled over the magnets.

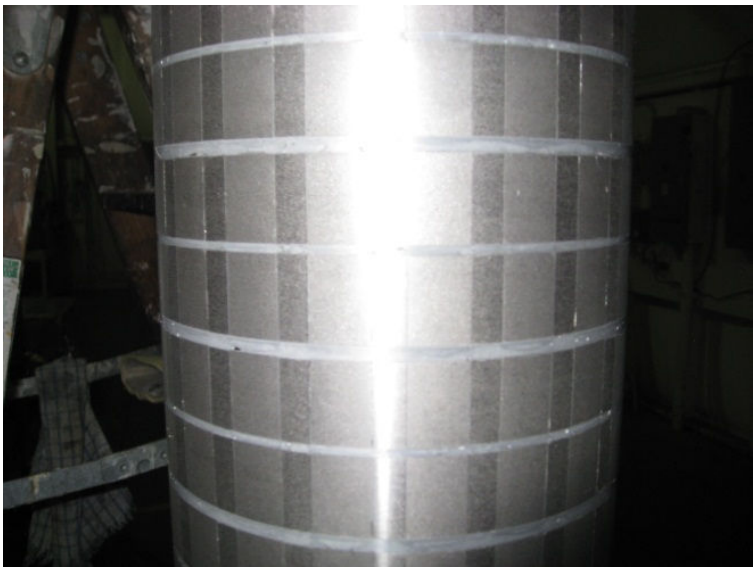

Figure 5.11: Magnets assembled on shaft after grinding to final dimensions

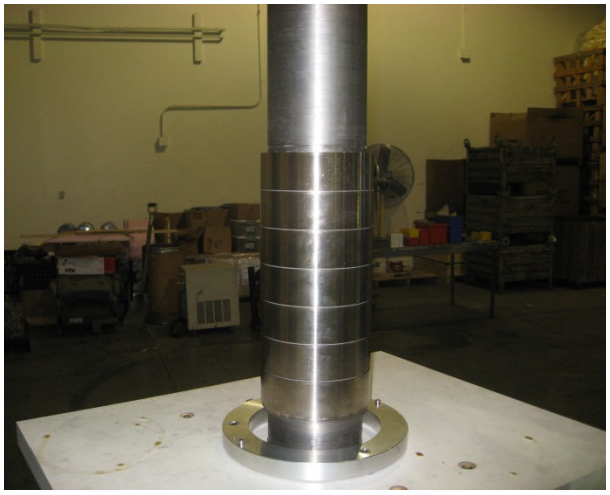

Figure 5.12: Completed magnetic rotor assembly

5.2.2 Stator Fabrication and Assembly

The most challenging process of the motor fabrication, assembly of the stator, is described below.

The stator coils are wrapped to avoid abrasion damage to the insulation. This abrasion may be caused by the high velocity oil flow required for ventilation. The insulated coil is shown in Figure 5.13, while Figure 5.14 shows a set of coils being formed in a custom fixture. In order to maintain the high-velocity oil flow required for proper ventilation, a gap between the coils assembled in the stator must exist at all times. The current motor design ensures this by placing a custom-designed mechanical spring between the coils at various locations along the length of the coil. Finally, Figures 5.15 and 5.16 show the journal bearings and one of the two mechanical face seals, respectively.

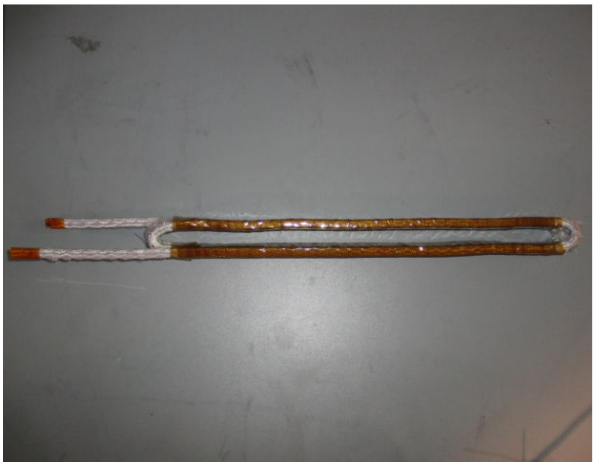

Figure 5.13: Sample coil

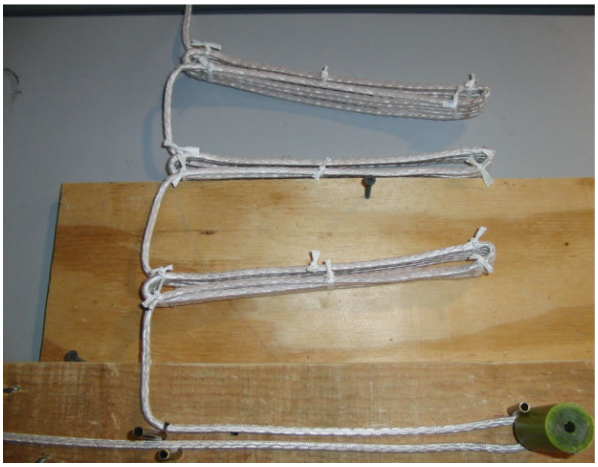

Figure 5.14: Stator windings

Figure 5.15: (Left) Radial-thrust bearing showing thrust faces; (Right) radial bearing

Figure 5.16: Mechanical face seal

Once the stator core is assembled, the slot liner insulation, coils and wedges must be inserted in the slots. Springs are placed between adjacent coils to ensure a proper gap is maintained to allow cooling flow circulation. A snug fit between the wedges and the stator laminations will ensure that no axial displacement occurs during operation.

As described in the test plan, the temperature of the stator windings can be monitored during testing using high-temperature thermocouples embedded in the coils. Figures 5.17 and 5.18 show a sample coil with the thermocouple attached near its center. Additional thermocouples are attached to monitor the temperature near the end turn region in a similar manner.

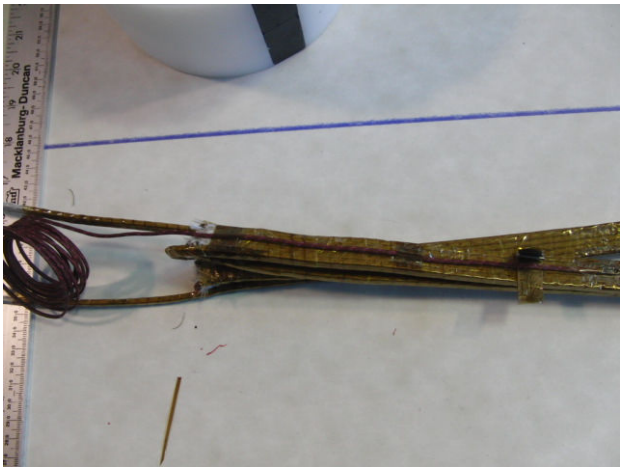

Figure 5.17: Sample coil instrumented with high-temperature thermocouple

Figure 5.18: Detail of thermocouple attached to stator coil

Most of the retaining wedges are slid into the slots as well to hold the windings in place. Also note that the wedges create a smooth cylindrical surface at the ID of the stator where the rotor will be inserted. There are also six lead wires that extend beyond the stator to connect with the electric power supply. A neutral is formed inside the motor with three-phase leads exiting the motor for external power connections.

The motor is a 3-phase machine. The power conversion takes place at the 5^{th} space harmonic of the stator. This requires the winding to be connected in the manner shown in Figure 5.19. In this schematic, all "T"s are teeth, and the letters A, B and C represent the 3-phases and the manner in which they are to be connected, with the "-" showing the negative or reverse polarity. This pattern is completely reversed for the next set of teeth. Then the whole pattern repeats.

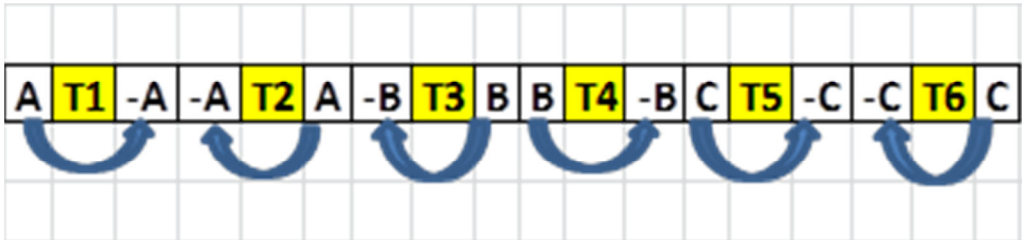

Figure 5.19: 3-phase windings connections

The three phases were connected and an EM test completed with a dummy rotor. Figure 5.20 shows that the voltage waveforms from the three phases. It is seen that each waveform is 120-degrees apart from the other two as intended. Also, for each single phase, the polarity reverses every 90 mechanical degrees or 180 electrical degrees. The test results confirm that the coil connections are correct. Figure 5.21 shows the relation between a phase voltage and its corresponding flux linkage. It proves that the flux linkage varies through each coil as the magnets rotate past it, implying that the phases are connected correctly as well.

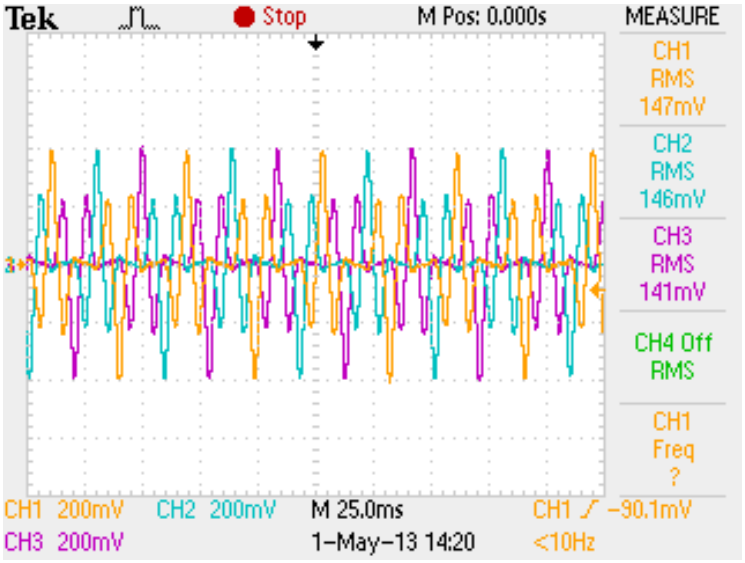

Figure 5.20: Stator EM test waveform with a dummy rotor

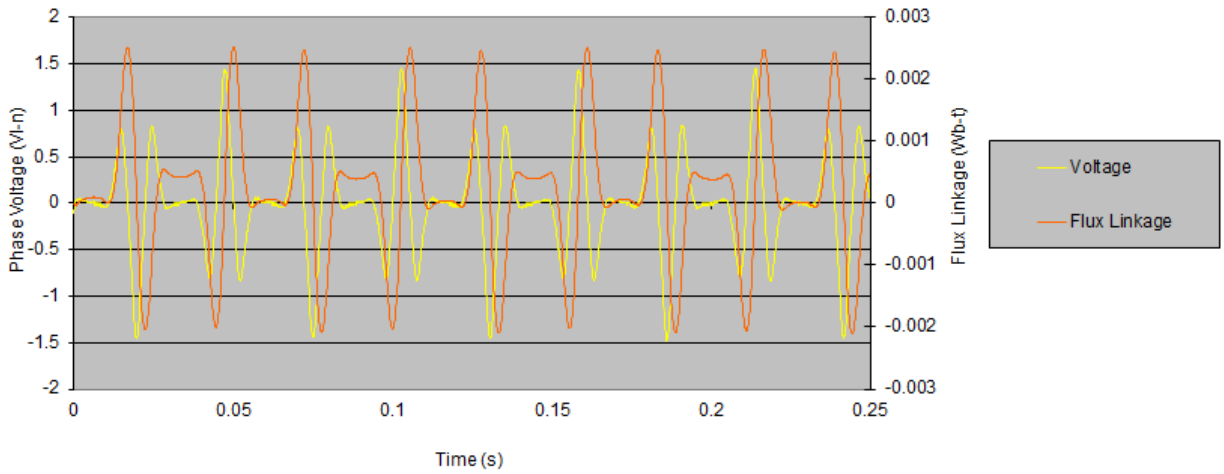

Figure 5.21: Stator EM test flux with a dummy rotor

5.2.3 Motor Assembly and Lessons Learned

Figures 5.22 and 5.23 show the completed motor housing. In order to increase the heat transfer surface area, multiple shallow fins were machined on its outer surface as shown in detail in Fig. 5.23. This process doubled the surface area and is expected to greatly enhance the heat transfer to the cooling air during the motor thermal test.

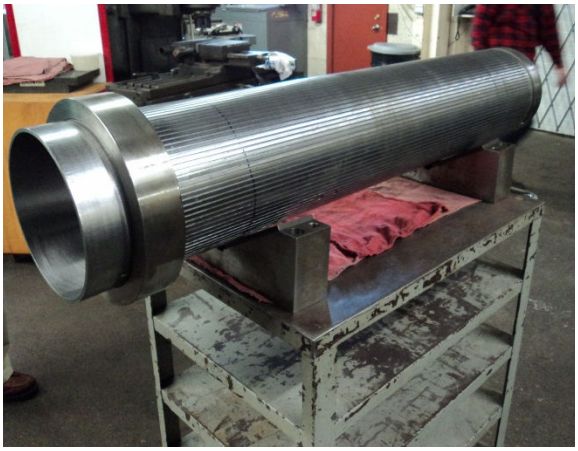

Figure 5.22: Geothermal motor housing

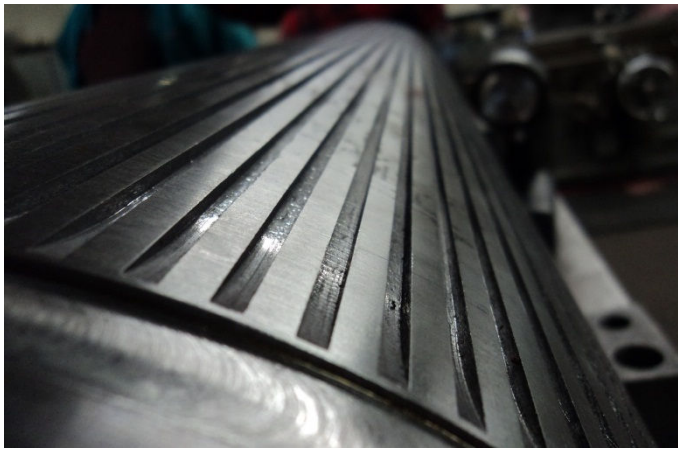

Figure 5.23: Detail of fins machined on housing OD

The stator must be fixed within the housing both axially and circumferentially; thus a stator key is inserted between two stator teeth to prevent the stator from rotating when subjected to EM torque.

In addition, an extra insulation layer is applied to the six leads to provide additional electrical safety margin as these have to pass through the slots during assembly and finally exit out of the machine for power source connections. Also, the root of each lead is fixed to the nearby winding end turns to prevent relative motion.

With the stator assembly completed and installed inside the motor housing, and the lead wires protected by additional layers of insulation, the next step is to insert the rotor into the stator. Due to the unique structure of this permanent magnet motor, there are certain technical challenges associated with the insertion process:

1. As previously mentioned, the rotor has 5.5" diameter and is hollow in the center to allow the geothermal fluid flowing through for cooling purposes. Therefore, the rotor is much larger compared to a rotor in a conventional ESP, which is around 1" to 2" in diameter. While the larger diameter results in higher power density, it also results in a much stronger magnetic force that increases the difficulty of inserting the rotor in a controllable way.
2. The air gap to rotor diameter ratio is extremely small compared other conventional PM machines. Thus the insertion has much higher requirement on concentricity between the rotor and the stator.

To address these challenges, a guide pipe with 4.5" OD was fixed concentrically with the stator on a work bench, shown as Figure 5.24. The strategy was to insert the rotor from the drive end of the machine with the support from the guide pipe.

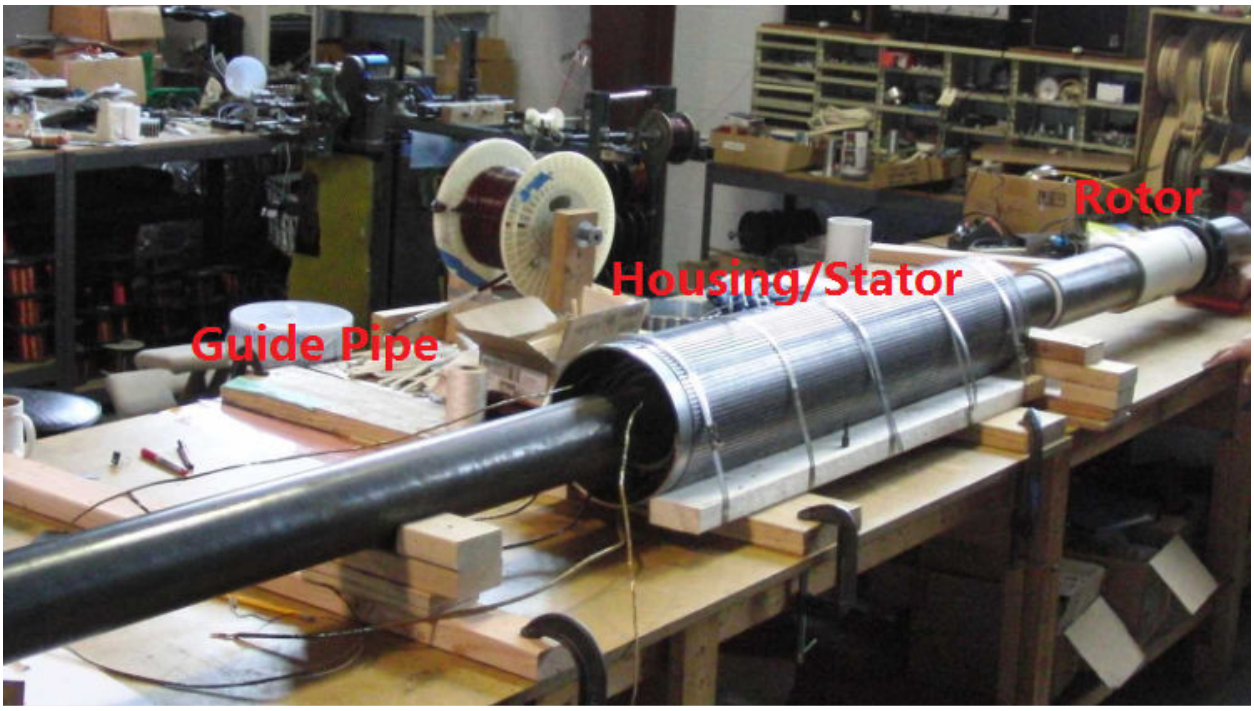

Figure 5.24: Rotor insertion work bench

A few attempts of insertion were made but the deflection in the middle of the guide pipe prevented the rotor from going all the way through. In addition, the magnets touched the wedges due to the deflection, leading to a fear of potentially damaging the wedges and scratching the rotor surface. The deflection was caused by two main factors: (1) the strong magnetic force from the permanent magnets on the rotor, and (2) the weight of the rotor. One solution proposed was to reduce the axial span of the two supports from 10' to 5', which could theoretically decrease the deflection to 1/8 of the initial value. However, one of the supports had to be an internal support inside the housing because the length of the housing is greater than 5'.

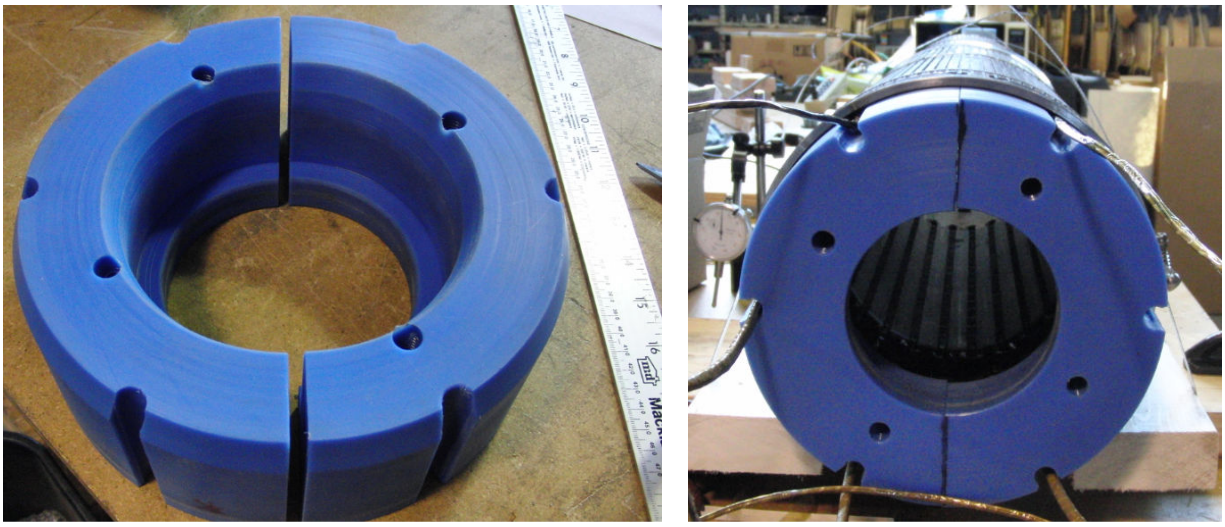

Figure 5.25: Teflon internal support for rotor insertion

A two-piece Teflon support was fabricated shown as Figure 5.25. This part could be installed inside the motor housing and has a 4.5" bore to provide sufficient support to the guide pipe. It also features six guide channels on the OD to protect the lead wires during rotor insertion. Another function of this part is to assist the installation of the oil diffuser, impeller, bearing holder and the other pieces on each end of the machine.

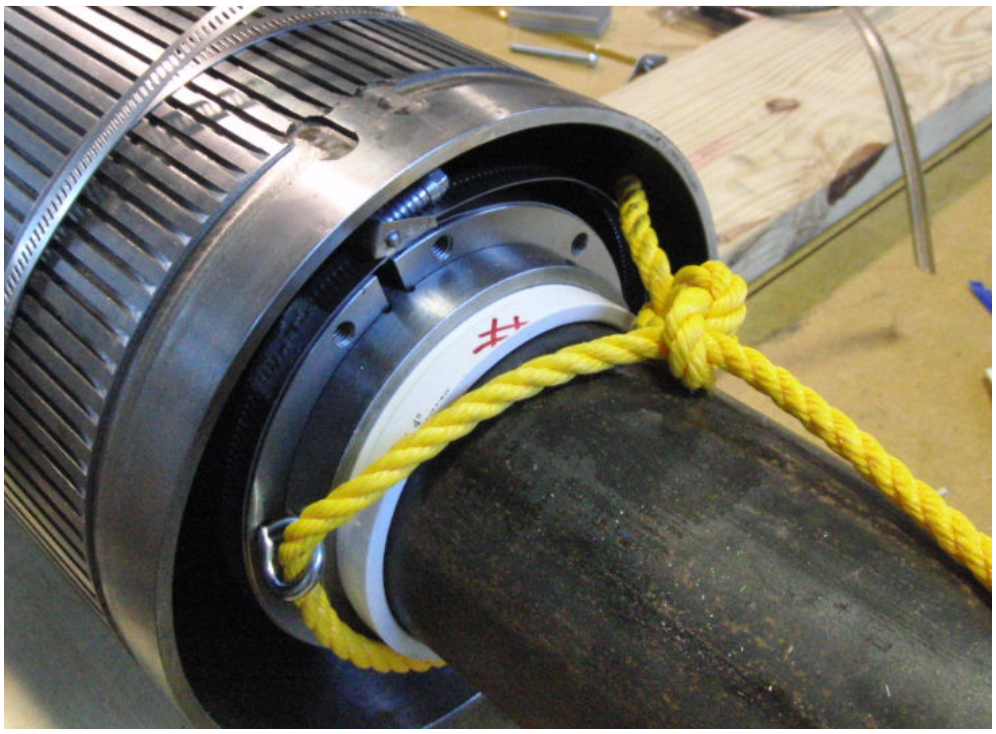

Figure 5.26: Fixture with rope to assist rotor insertion

On the drive end, from which the rotor was inserted, a fixture with a rope was installed on the rotor (Figure 5.26). As mentioned above, the force from the permanent magnets could suddenly pull the rotor into the stator and damage the wedges, wire insulation and especially the pieces on the stator end. The rope and the fixture were aimed at applying a resistive force against the magnetic force so that the speed and the progress of the insertion could be managed.

Special care has to be taken at each step to ensure proper protection of the wire insulation. Short circuit checks were performed regularly to detect any potential problems as the assembly progressed. The check includes a 1kV Megger test and a 600 volt HiPot test. The wire insulation itself is designed to withstand a 2-2.5kV Megger test. However, given the working conditions and the special fabrication and assembly process of the motor, a 1kV test was recommended.

It was discovered after the first attempt of the diffuser installation that the machine couldn't pass the 1kV Megger test, indicating a short circuit at one or more places on the lead wires. The diffuser was thus removed and a short length of insulation was found to be peeled off by the edge of the lead wire channels.

As a result of this setback, several measures were taken to make the necessary repairs and to make the remaining assembly steps go more smoothly:

1. Necessary repairs to the winding insulation were made. Multiple wraps of insulating tape were added around the area where the short occurred and at the outside of the end turn winding. For each layer of insulation, at least a 50% overlap was achieved. The process was repeated three times to add three extra layers of insulation, providing sufficient redundancy.
2. An undercut was made in each of the diffuser's lead wire channels to allow for more room as the leads transition from a smaller inner radius to a larger radius. The edge of the channels was filed to avoid any possible sharp corners that could cut the insulation.
3. A 0.020-inch lamination stack was inserted, which was used as a spacer between the coil end turn spacer and the diffuser.
4. The OD of the diffuser was machined down by 0.010 inch to make the re-installation go more smoothly.
5. As previously mentioned, the diffuser installation was not visible as it was deep into the motor housing. A borescope camera was used to view the end turns and inspect the insulation for damage but the result was inconclusive. Thus a decision was made to push the stator all the way to the lead wire end of the housing, allowing full visibility and inspection of the assembly process. In addition, it also provided an opportunity to fully clean the stator OD and the housing ID where the dust could form due to the oily surfaces exposed to the shop environment.

By following these procedures, the oil diffuser was successfully installed onto the stator. All lead wires passed through the channels smoothly without damaging any winding insulation. The Megger and HiPot tests were performed frequently during this process. The machine passed both tests every time with very high resistance values.

The other components on the lead wire end, such as the oil impeller, journal bearing and its holder, mechanical seal housing, oil separator and lead wire protection tubes, were all successfully installed. Megger and HiPot tests were performed and passed after installing each piece to ensure the integrity of the winding insulation. The motor power leads and the thermocouple leads successfully exited the machine's end plate. The bulkhead, which is the last piece to be installed on this end of the machine, completes the work. The lead wire end and the power lead feed through are shown as Fig. 5.27.

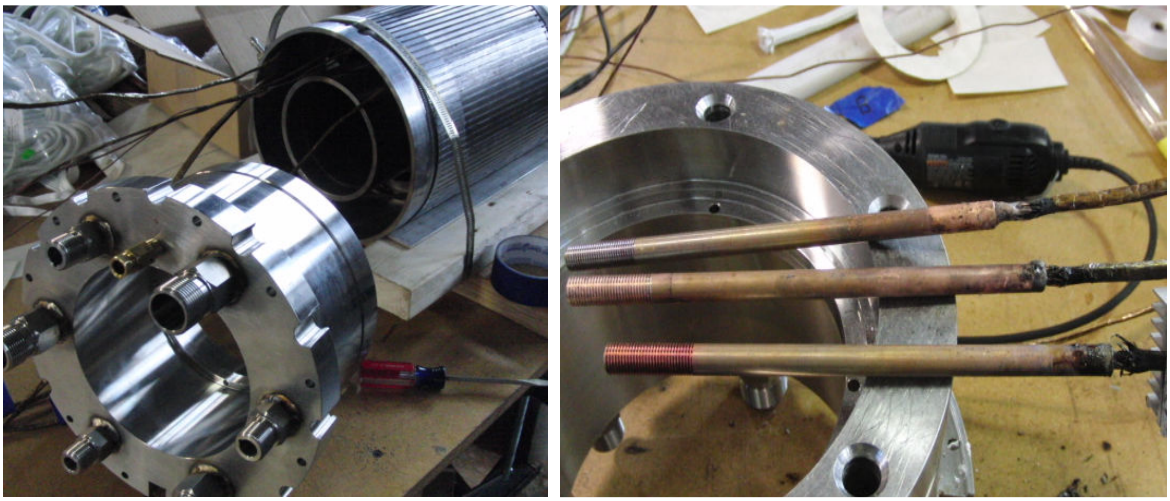

Figure 5.27: Lead wire end bulkhead and lead feed-through

On the non-lead end of the machine, the assembly became considerably easier than the lead end for several reasons: (1) No lead wires passed through the non-lead end and thus the operator had no need to worry about the potential damage to the lead wire insulation; (2) Because of (1) there is no need to run Megger or HiPot tests; (3) The number of components and the complexity on this end of the machine is much less than the lead end. The key components at this end are the thrust bearing and the mechanical seal which had already been installed onto the rotor.

The finished non-lead end of the motor, with the bulkhead assembled, is shown as Fig. 5.28. The fabrication and assembly of the entire 300°C EGS motor prototype has been successfully finished at this point, shown as Fig. 5.29.

Figure 5.28: Finished non-lead end of the motor

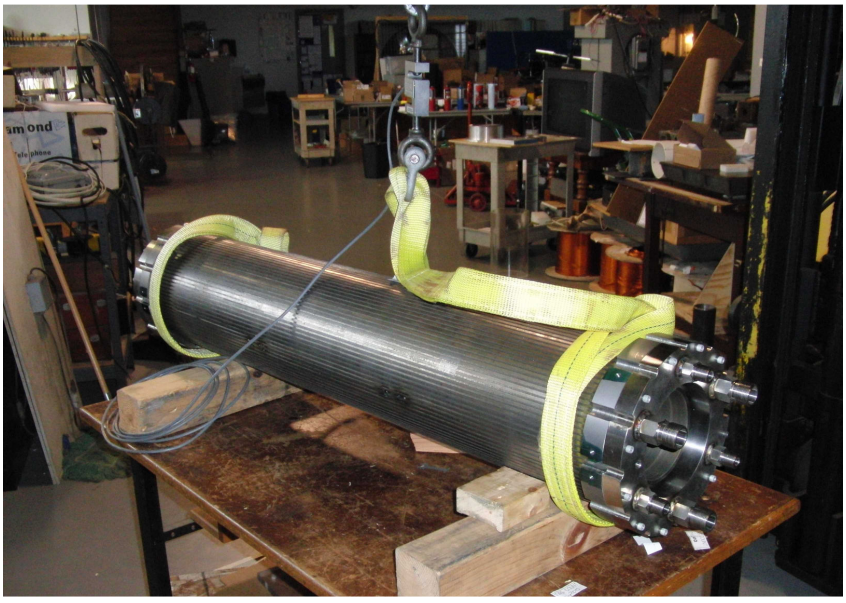

Figure 5.29: Completed prototype geothermal motor

As described in this section, the engineering team of this program has conquered all the technical challenges associated with assembly of this unique high technology motor that serves the EGS applications.

5.2.4 Motor Testing

5.2.4.1 High-Temperature Insulation Material Tests

Slot Liner –Ground Wall Insulation

To determine if the materials are suitable for ESP motors at high temperature conditions, accelerated thermal aging tests were performed. Several candidate materials were aged at 350°C for different intervals in air; electrical and mechanical tests were then conducted on these samples to evaluate if any degradation in properties occurred. Results are summarized in this section.

Figure 5.30 shows a comparison of breakdown strength of Material A before and after thermal aging at 350°C for one week and three weeks. The data were analyzed with Weibull statistics using the two-parameter Weibull expression: $\mathbf{F_p=1-exp(-E_{bd}/E_c)^s}$, where F_p is the breakdown failure probability, E_{bd} and E_c are measurement and characteristic breakdown values, and s is the scale parameter, which determines the reliability of the data. Table 5.3 summarizes the test results of both Materials A and B. They show good retention of electrical performance after thermal aging. However, Material A has higher breakdown strength than Material B.

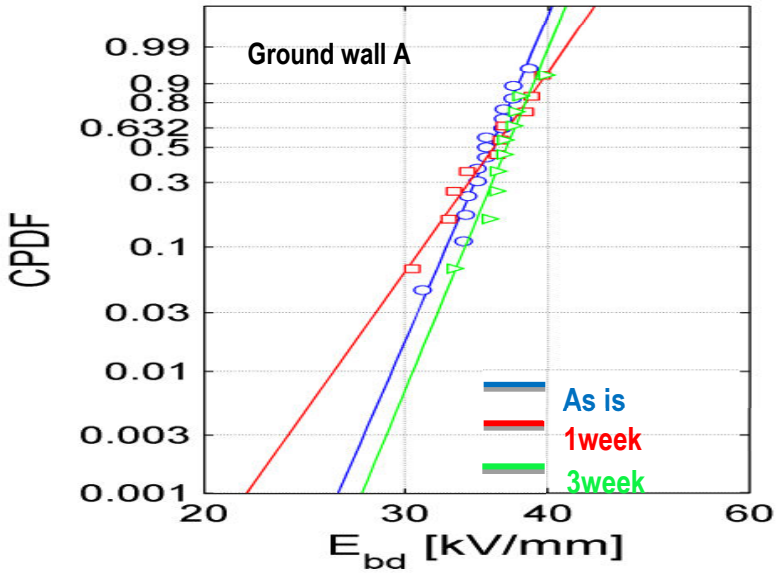

Figure 5.30 – Breakdown data of as-is and aged ground wall material

Table 5.3 - Weibull parameters for breakdown data of samples

Material	Breakdown properties		Aging condition	Test condition
	E_c [kV/mm]	s		
Ground wall A	36.2	21.3	As received	@RT
	36.9	13.1	Aged 1week @350°C	@RT
	37.4	22.4	Aged 3 weeks @350°C	@RT
Ground wall B	25.1	23.0	As received	@RT
	25.4	17.8	Aged 1week @350°C	@RT
	26.0	29.0	Aged 3 weeks @350°C	@RT

Similarly, the mechanical data obtained from tensile measurements were analyzed with Weibull statistics, as shown in Figure 5.31. The data are summarized in Table 5.4. The maximum stress was used to determine the condition of the sample after aging. Although the mechanical properties changed significantly compared to the electrical ones, it is anticipated that the samples will not experience any stress in the longitudinal direction. The tests showed that both Materials A and B, evaluated in air, warrant further evaluation in oil in an autoclave as slot liners or ground wall insulation for the ESP motor.

Table 5.4 - Weibull parameters for the mechanical properties

Material	Mechanical properties		Aging condition	Test condition
	M_c [lb]	m		
Ground wall A	90.5	7.1	As received	@RT
	37.5	17.4	Aged 1week @350°C	@RT
Ground wall B	256.5	9.0	As received	@RT
	131.1	7.8	Aged 1week @350°C	@RT

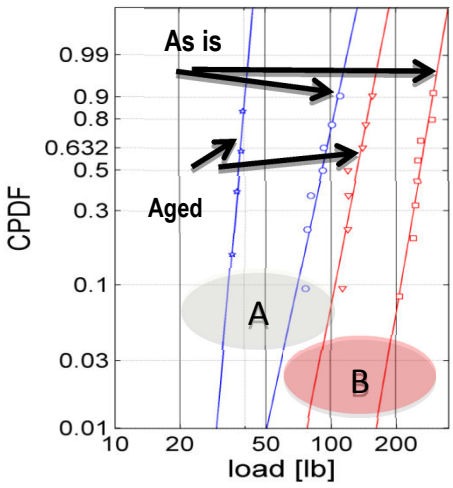

Figure 5.31 – Mechanical properties of samples A and B, before and after aging

Winding Insulation – Magnet Wire

Currently, the limiting thermal component of the state of art ESP motor is its wire insulation. The highest thermal class insulation commercially available is the polyimide enameled wire, which has thermal class of 240°C. GE has developed an HT wire that shows significant improvement in thermal performance. Ten twisted pairs of wire were thermally aged at various temperatures for different periods of time, and underwent voltage proof tests to check wire quality according to ASTM D2307. Figure 5.32 shows comparative thermal aging results of HT wire and commercial polyimide wire. All ten polyimide wire samples failed after aging at 320°C for 7 days, their insulation coating having completely degraded. In contrast, the GE-developed HT wire survived 70 days at 320°C without any failure; insulation coating remained intact without any sign of degradation. Figure 5.33 shows life versus thermal stress based on twisted pair tests in air. The degradation of insulation is expected to be much lower in an oil environment with no/minimal oxygen level. Therefore, thermal performance of the HT wire is expected to be even better.

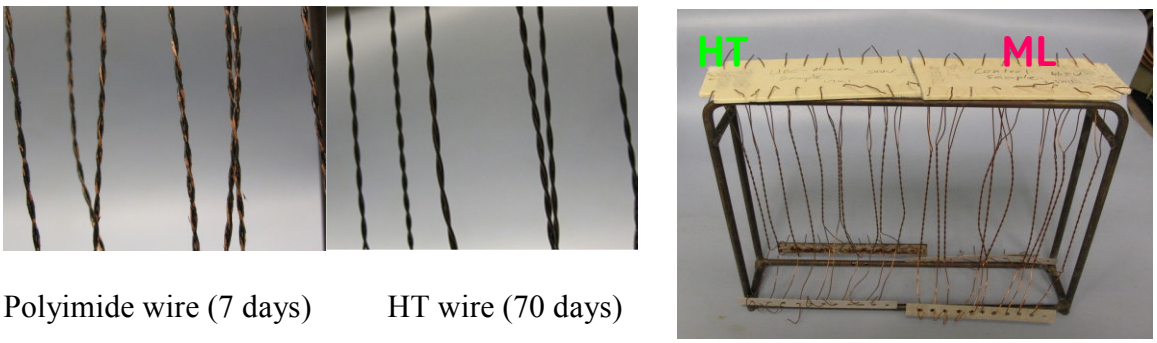

Polyimide wire (7 days) HT wire (70 days)

Figure 5.32 - Comparison of HT wire and polyimide wire after thermal aging at 320°C

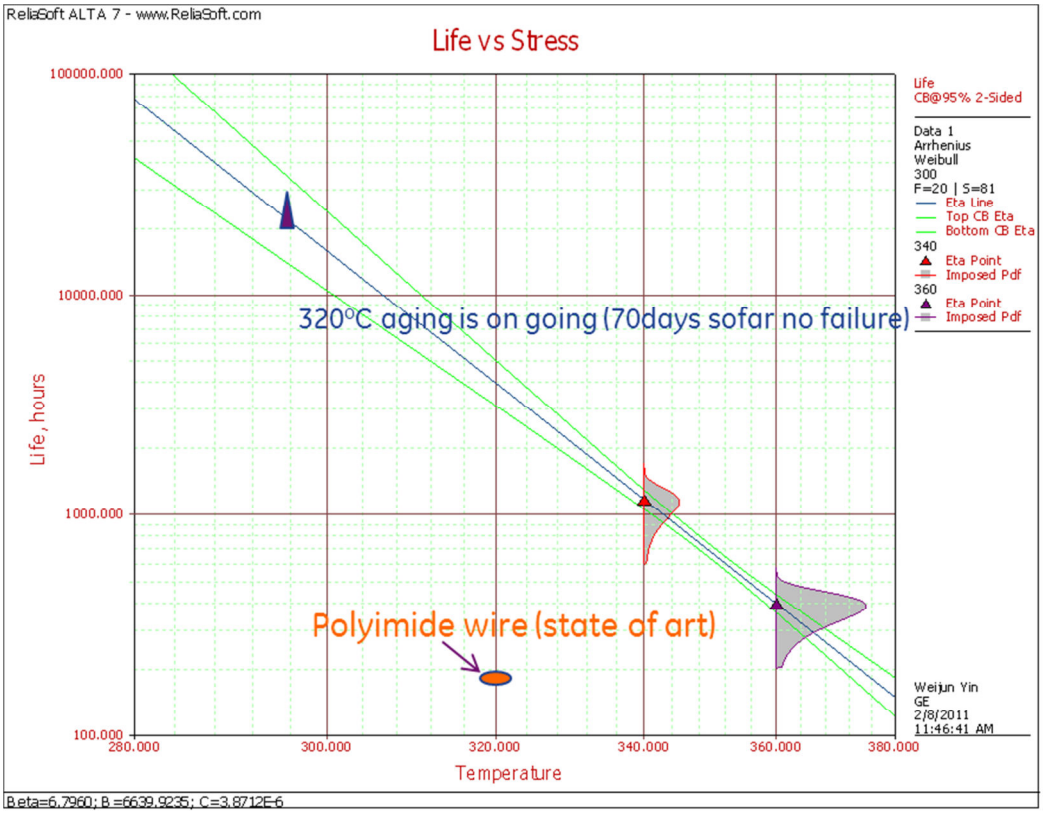

Figure 5.33- Comparison of thermal aging of 22AWG of HT wires and polyimide enameled wires

5.2.4.2 Mechanical Seal Tests

Fundamental mechanical seal configuration is a function of rotor speed and rotor outside diameter. For the geothermal ESP these parameters have been frozen at:

- Motor speed: 3150 rpm
- Shaft outside diameter: 5.5 inches

As a result, the seal configuration is such that the flexible bellows are part of the stationary section of the seal. Seal features are:

- Outside diameter pressurized seal, polished faces and all metallic bellows
- Flexible static “secondary” seals
- Designed for up to 5000 ft/min (25 m/s), 325°C & 8 bar differential pressure
- Estimated mass of 700 grams
- Estimated leakage range of 3 to 17 ml/hr, operating at 1.3 um film thickness

The geothermal ESP design requires one seal on either end of the motor. Critical parameters related to the seal are summarized in Table 5.5 below.

Table 5.5 – Mechanical seal design parameters

Critical Parameter	**Description**
Maximum allowable axial travel	+/- .045” from nominal set dimension
Maximum allowable radial travel	~.002”/ inch of seal size (~.0125”)
Maximum allowable differential pressure	600 psig (41 bar)
Maximum allowable reverse pressure	450 psig (31 bar); Note: This is a calculated value. Maximum tested reverse pressure with this type of seal has been up to 250 psig.
Fluid flow/flush rate limits	Recommend minimum of 3.5 GPM. API 682 has a 2X factor when determining flush rates, which equates to 7 GPM on the high end.
Maximum allowable dry running time	Seal is not designed for dry running. Damage to face(s) and bellows can occur in seconds in case of dry running.
Minimum speed to form film at faces	No minimum speed requirement. As long as there is 20 psig, faces will have sufficient lubricant film.
Fluid film break-down	Lubricant/fluid coking affects seal performance – Coking is solid residue remaining after oil exposure to severe temperatures and oxidation

The seal fixture design has been prepared (Figure 5.34) to allow for assembly and testing the stationary bellows seal configuration. The fixture is assembled onto an existing base test rig with a 5.5 inch diameter rotor.

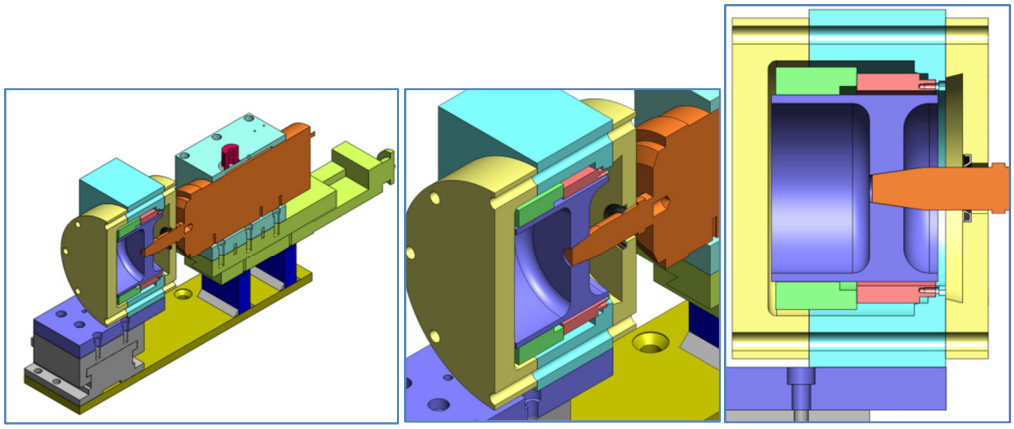

Figure 5.34 - Mechanical seal fixture design in test rig

As part of the rig set up an oil/barrier fluid skid was designed and manufactured (Fig. 5.35). The barrier fluid skid is comprised of a motor & pump, valves, pressure gauge, heater and temperature control unit. The barrier fluid skid provides fluid to the seal cavity at the required flow rate,

pressure and temperature. The fluid leakage from the seal is captured from a drain point while the remainder and majority of the fluid recirculate through a return line, chiller and pumped back to the seal cavity.

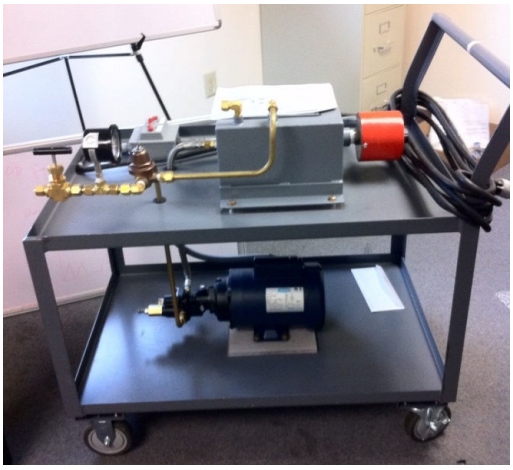

Figure 5.35 – Barrier fluid skid

The seal has been designed based on the motor and pump designs described above. Figure 5.36 provides images of the mechanical face seal in its un-assembled form and after assembly in the 5 inch rig.

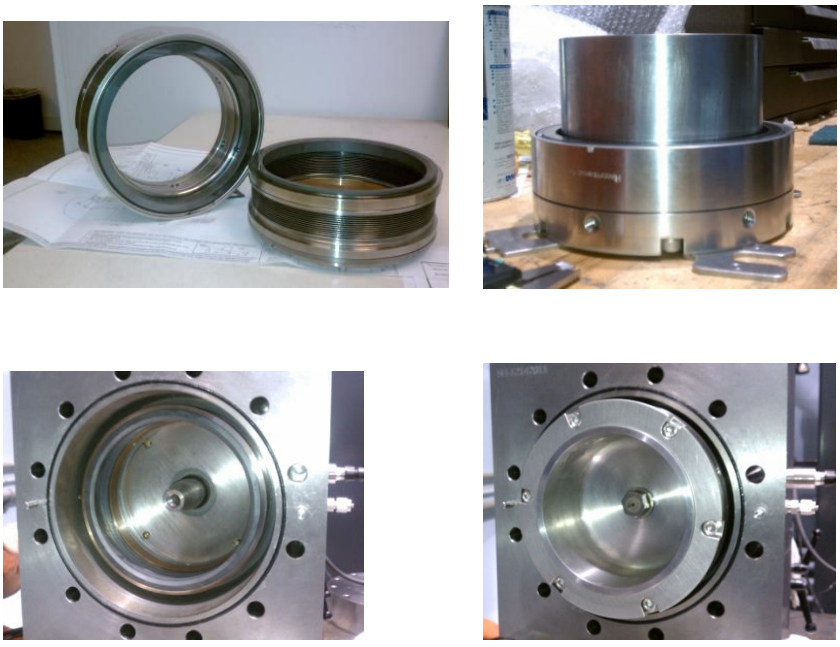

Figure 5.36 – Seal before and after assembly in 5-inch rig

Tests were run at 1600 rpm and maximum pressure of 45 psi (3.1bar). In order to overcome the large breakaway torque within the limits of the test rig drive motor, seal pre-load was reduced

from the recommended 0.225” to about half of that value. This reduces the breakaway torque to about 3 lbf-ft. This is done by moving the slide on the motor. Once the desired speed is achieved, the slide is pushed back against the seal until the required preload on the seal is achieved. Fig. 5.37 shows the rig configuration and the motor slide. During the time this procedure was being followed, no oil pressure was applied to the seal.

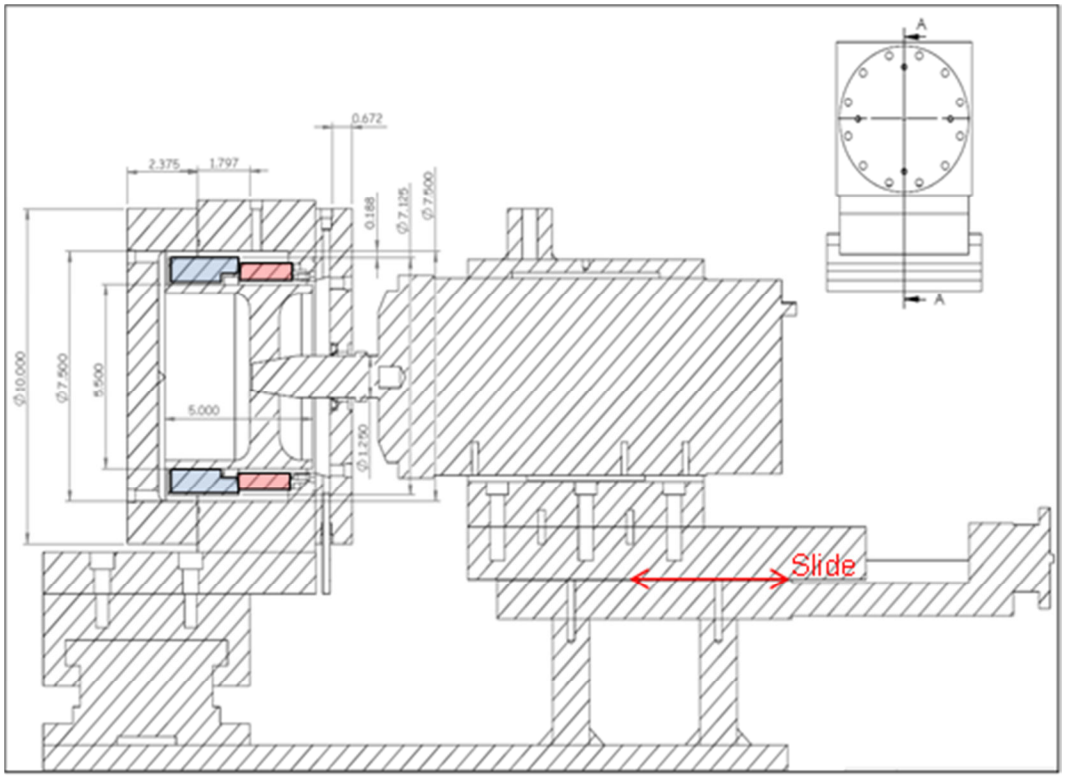

Figure 5.37 – Rig set up and motor slide to adjust seal preload

During tests it was also noted that secondary seals were susceptible to damage either during assembly or more often when seal was subject to repeated axial loads as the motor slide was moved to reduce seal pre-load. Overall seal leakage test data and a typical example of the secondary seal damage may be seen in Fig. 5.38.

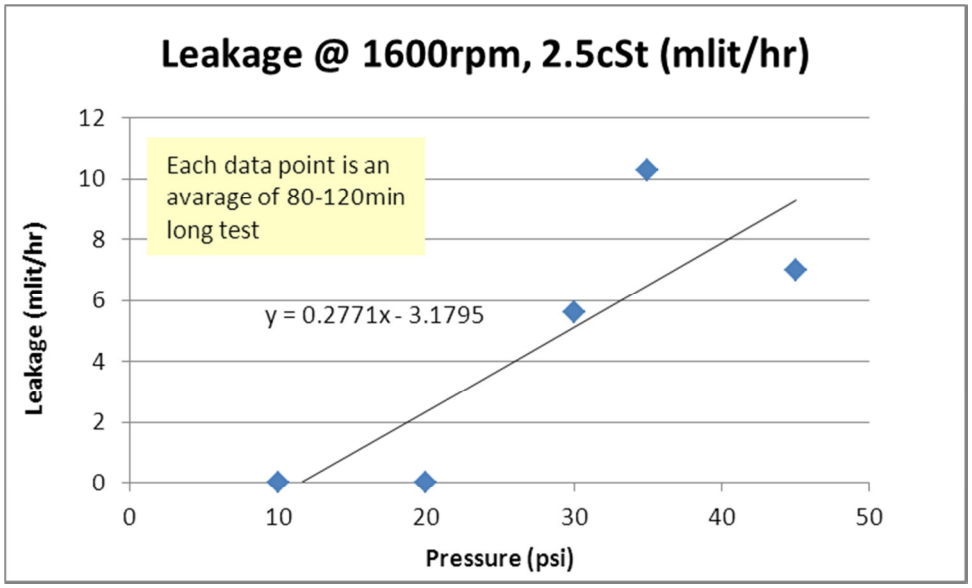

Figure 5.38 – Overall seal test data and damaged secondary seal

Therefore, it is important to note that the leakage values measured, in some cases, could include a certain amount of leakage from the secondary seal. In all tests oil temperature was allowed to reach about 155°F (~68°C) before leakage values were recorded. At this temperature, oil viscosity is about 2.5 cSt.

Additional static tests were also conducted when seal pre-load was about 50% of the required pre-load. This data showed no difference in leakage values compared to full pre-load.

Data indicates the following:

- Measured leakage with 2.5 cSt viscosity fluid is in-line with estimated values
- Seal leakage has little sensitivity to reduced bellows preload (0.100")
- No damage to seal with no oil pressure for 5 minutes
- Single seal with full pre-load requires 6-7 lbf-ft breakaway torque
- Static seals are sensitive to axial travel & will affect overall leakage

5.2.4.3 Oil Resistivity and Viscosity Tests at Elevated Temperature

The GE ESP design features an oil-cooled motor that will operate at 300°C and 300 bar. Four candidate oils were selected. The viscosity and resistivity of candidate oils were measured and data were populated for down-selection of the coolant. Measurement results are shown below in Figure 5.39. Each color represents a different oil and arrangement of the experimental setup. Note that one candidate oil in particular had much higher viscosity than the others at low temperatures. The solid line in the figure is used to estimate the viscosity of the oils from the experimental setup.

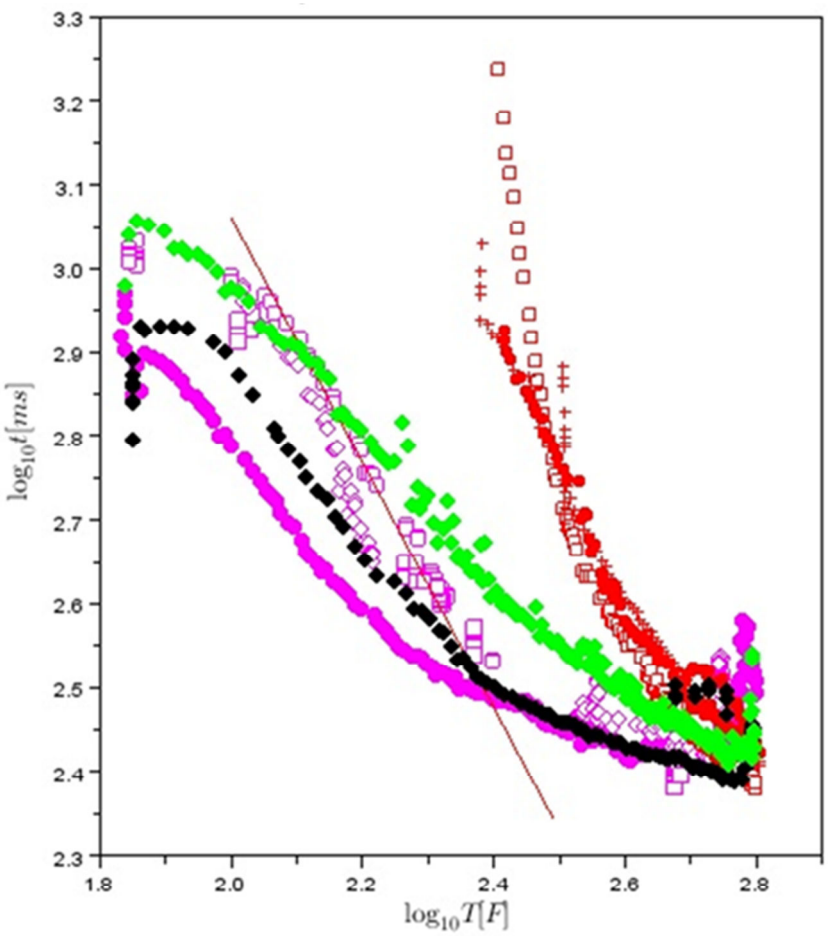

Figure 5.39 - Time-to-fail as a function of temperature for different oils. Color coding indicates various oils considered in the measurements.

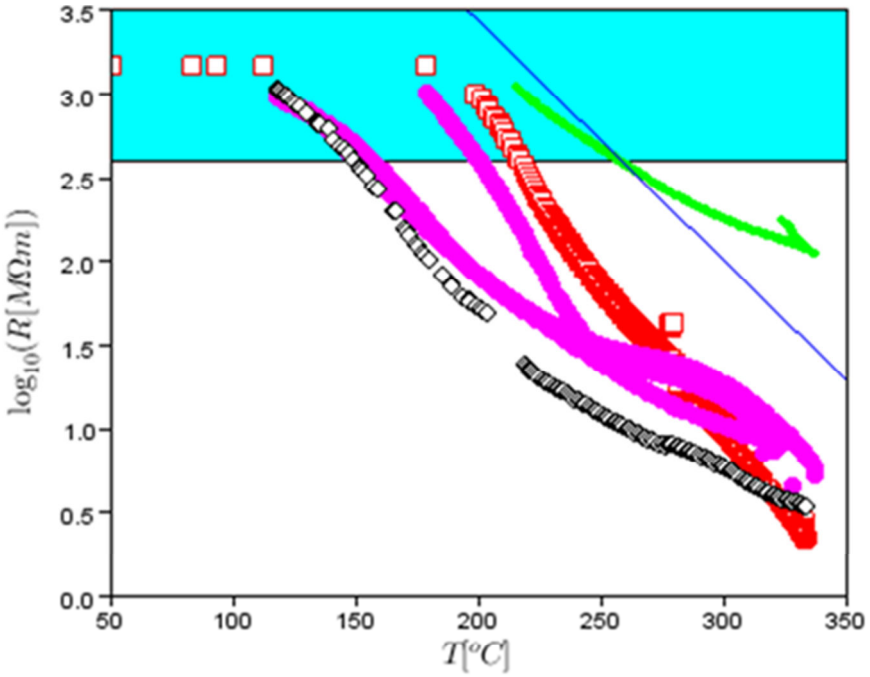

Figure 5.40 - Resistivity of oils as a function of temperature. Color coding indicates different candidate oils.

The resistivities of four oils were measured to determine the electrical losses due to electrical leakage. The experimental setup used a guarded electrode and a resistance meter (Agilent 34410A). The resistances were converted to resistivity using the geometry of the measuring electrodes. Results are illustrated in Figure 5.40. The shaded region represents the desired losses for the insulation. None of the oils have the desired resistivity value. However, one of the oils could be selected due to its resistivity value which exceeds the recommended value by the ASTM 2442--- shown in the figure with the solid line.

Some of the oils were aged at elevated temperatures and pressures to examine their aging behavior. It was shown that depending the on the temperature, in this case around 350°C, the oil degrades and its color changes. However, its electrical properties and dielectric strength do not change significantly. In the tests, different components are added to the oils to determine the effect of any cross-contamination on the electrical properties. Figure 5.41 below indicates the color change in one of the oils that experienced high temperatures (approx. 360°C for 3 days). The clear, transparent nature of the oil changed to a black, slightly translucent color. Electrical properties and dielectric strength do not change significantly.

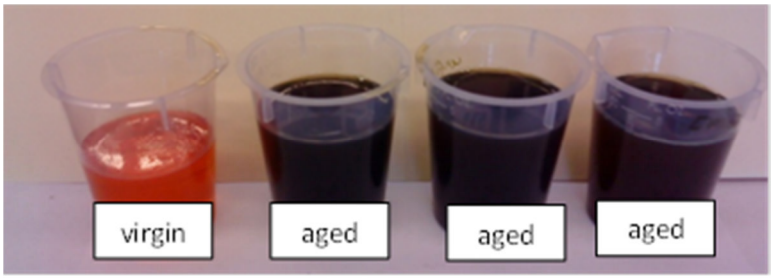

Figure 5.41 - Aging studies in oils. The color of the oil becomes dark when it is heated to 350°C at 300 bar.

Data obtained on the oil that was aged for 3 days shows promising breakdown properties. Breakdown values of the oil with different components introduced are between 11kV/mm and 20kV/mm. Figure 5.42 shows the breakdown values of the magnet wire as a Probability of Failure (%) vs. AC Breakdown Volgate (kV), indicating some improvement with aging in an oil environment at high temperatures and pressures.

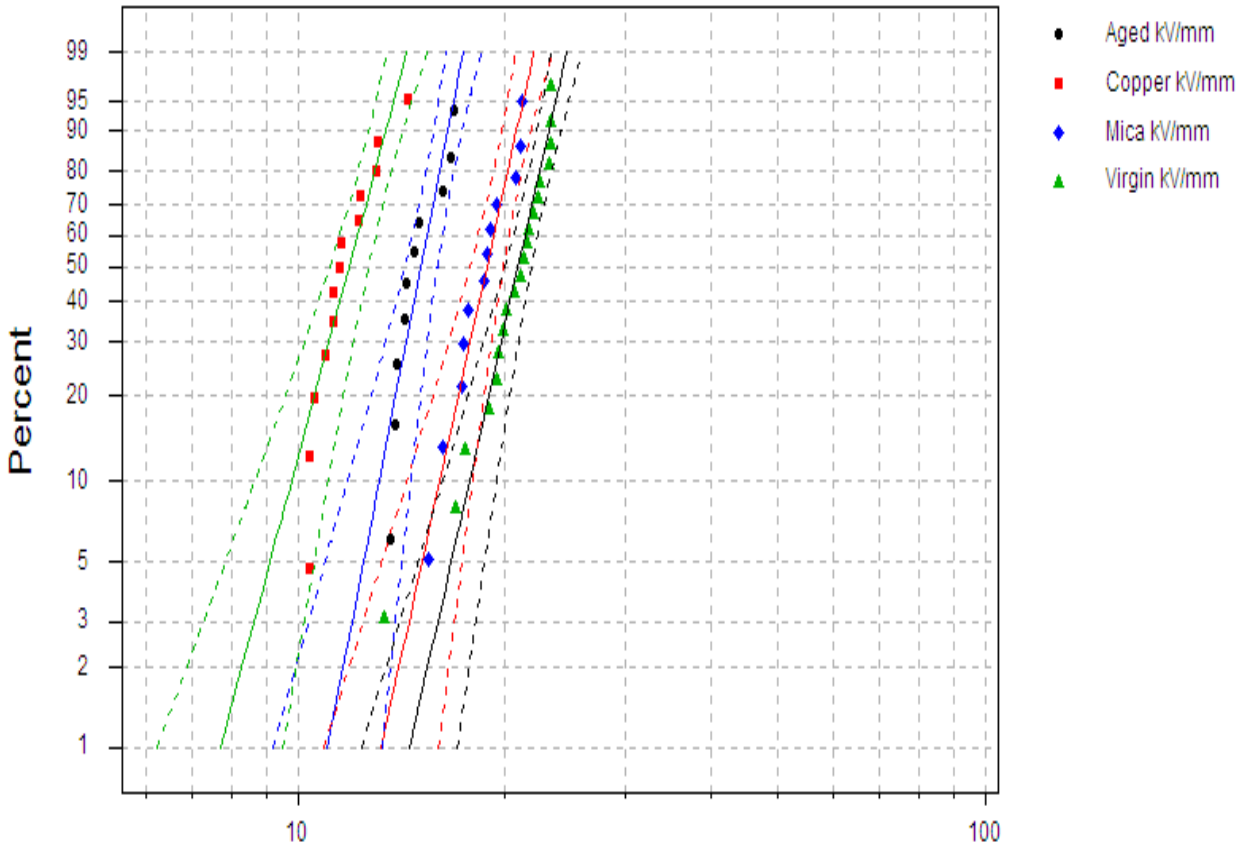

Figure 5.42 - Dielectric breakdown of oils and a candidate wire.

5.2.4.4 High-Temperature Oil Compatibility Test

The ESP electrical insulation system needs to be qualified for reliable long term and operation. Selected insulation materials were characterized for oil compatibility using initially screened oils A and B. The compatibility tests were performed at 330°C and 400 psi. After samples were aged for three weeks at 330°C and 400 psi, the oil samples and solid insulation and wire samples were visually examined for differences, and breakdown values were compared with the virgin sample to check whether any degradation had occurred. Figure 5.43 compares two oil candidates, where one of the oils (B) created deposits of a black substance floating inside the oil and on the insulation material. Oil (A) showed darker color than the virgin oil but without any obvious sludge formation or viscosity change. Figure 5.44 shows the breakdown value of oil (A) before and after aging; it shows little degradation in dielectric performance, therefore oil (A) could be a potential candidate for the current ESP design. HT wire was also placed in oil (A) aged at 330°C and 400 psi for three weeks; the AC breakdown value of both virgin wires and aged wires were tested and compared as shown in Figure 5.45. The dielectric performance of the aged wire does not show any degradation, again demonstrating that HT wire can be a potential candidate for the ESP motor application.

Figure 5.43 - Oil comparison after thermal aging at 330°C and 400 psi for three weeks; oils (A) and (B) in the left and right containers respectively. The insulation materials tested show different surface characteristics due to deposited black-substance. The insulation on the left has a clear surface.

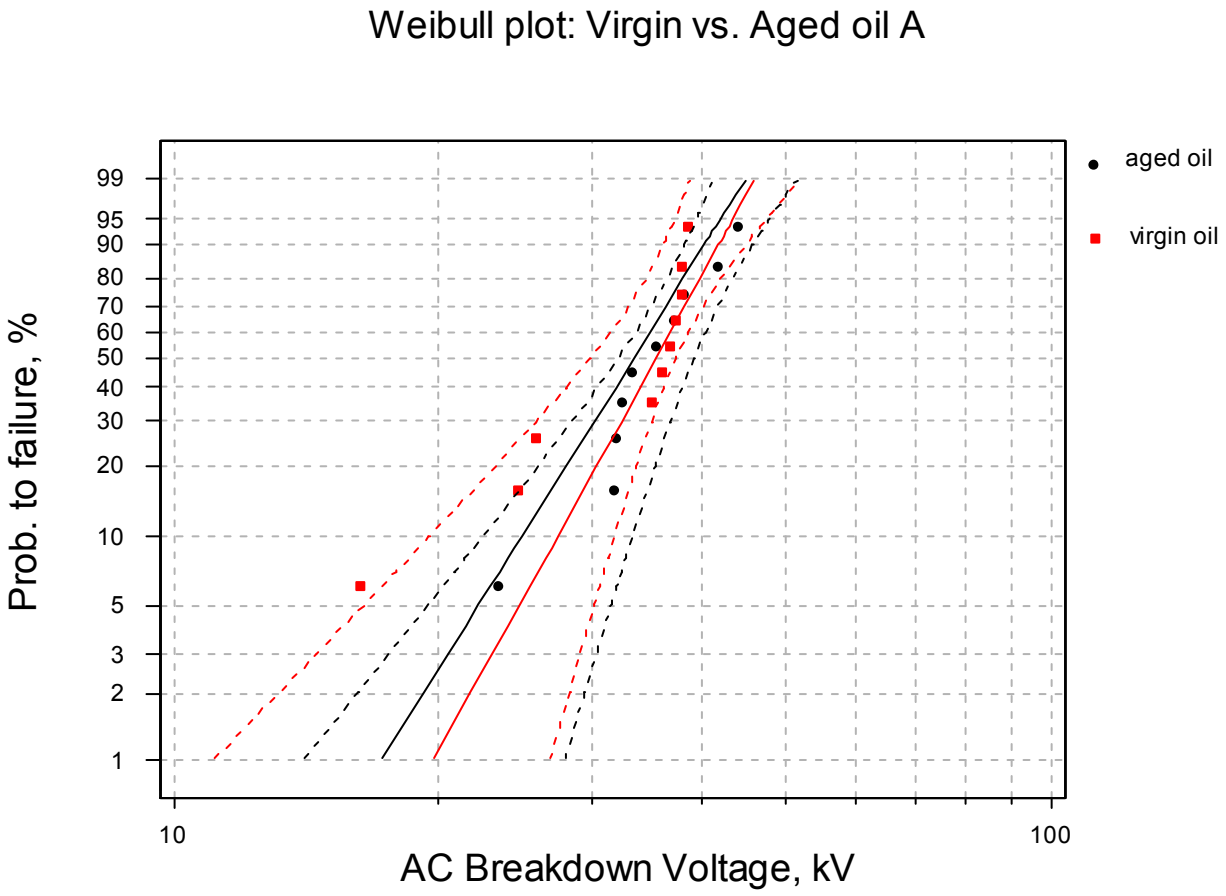

Figure 5.44 - AC breakdown comparison of oil (A) before and after thermal aging at 330°C, 400 psi for three weeks

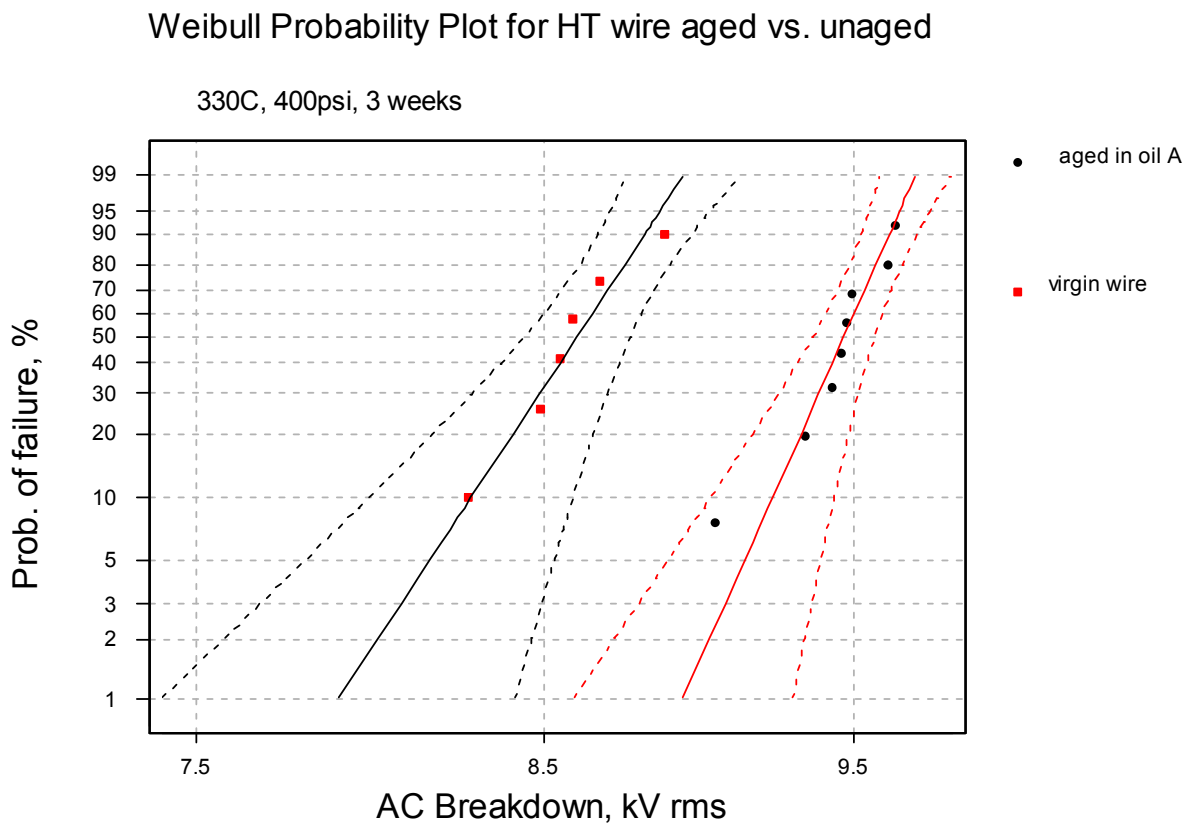

Figure 5.45 - AC breakdown comparison of HT wire before and after thermal aging at 330°C, 400 psi in oil (A) for three weeks

In subsequent tests, the composite ground insulation system was tested at elevated temperatures and pressures using the autoclave for one week. The ground wall insulation was sandwiched between electrodes and immersed in coolant oil. Current (A) was monitored as a function of Voltage (V) and at different times as shown in Figure 5.46. Each symbol corresponds to a different time of measurement; the measurements were performed every day with increasing voltage level. Although there are slight differences, they are due to temperature values at each measurement; the autoclave temperature was not constant in each measurement. When the slopes of the curves in Figure 5.47 (resistance) are plotted against the temperature, there is a clear linear dependence of the resistances as a function of temperature.

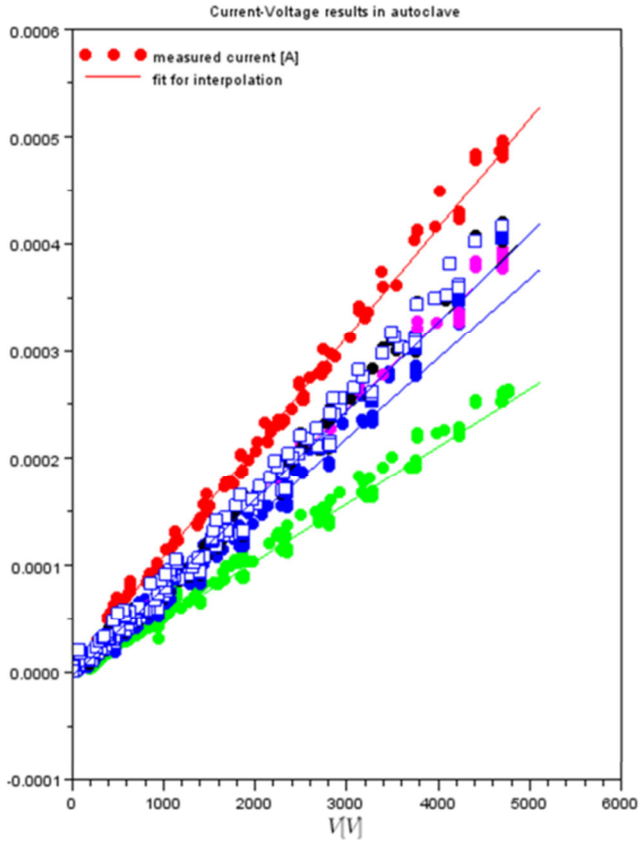

Figure 5.46 – Current (A) vs. Voltage (V)

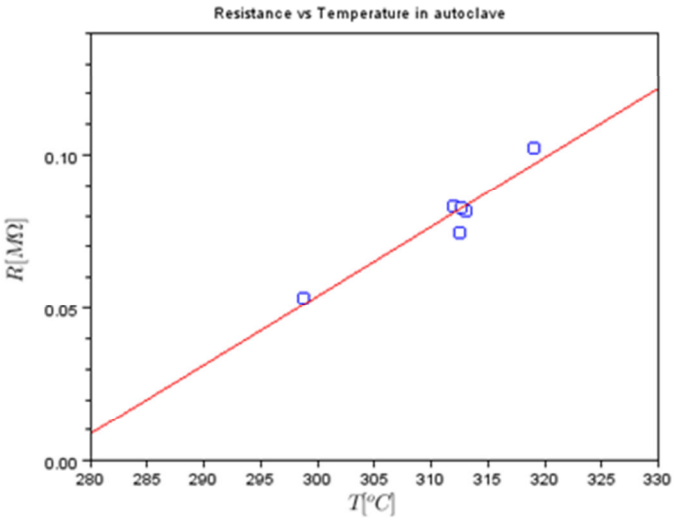

Figure 5.47 – Resistance (MOhm) vs. Temperature (°C)

5.2.4.5 Motor Back EMF Test and Inductance Measurements

Back EMF (No Load Voltage) via Flux Linkage Measurements

It is convenient to compare measured no-load flux linkages with corresponding simulation data especially if the speed cannot be well controlled during the test, as the no-load flux linkage is independent of the speed.

The goal here is to verify that the flux linkages of the three phases are nominally balanced and have comparable peak values and waveforms as predicted by simulation. This is to confirm that the armature winding was correctly wound and the strength of the permanent magnets matches what was assumed during the machine design.

Figure 5.48 shows the measured flux linkages of the scaled prototype motor. All three waveforms are well balanced with practically the same peak of 122 mWb-turns/phase. Figure 5.49 shows the simulated three-phase flux linkages with a peak of 115.7 mWb-turns/phase, which is within 5 percent of the measurement. The measured flux linkage waveforms are sinusoidal as predicted by simulation.

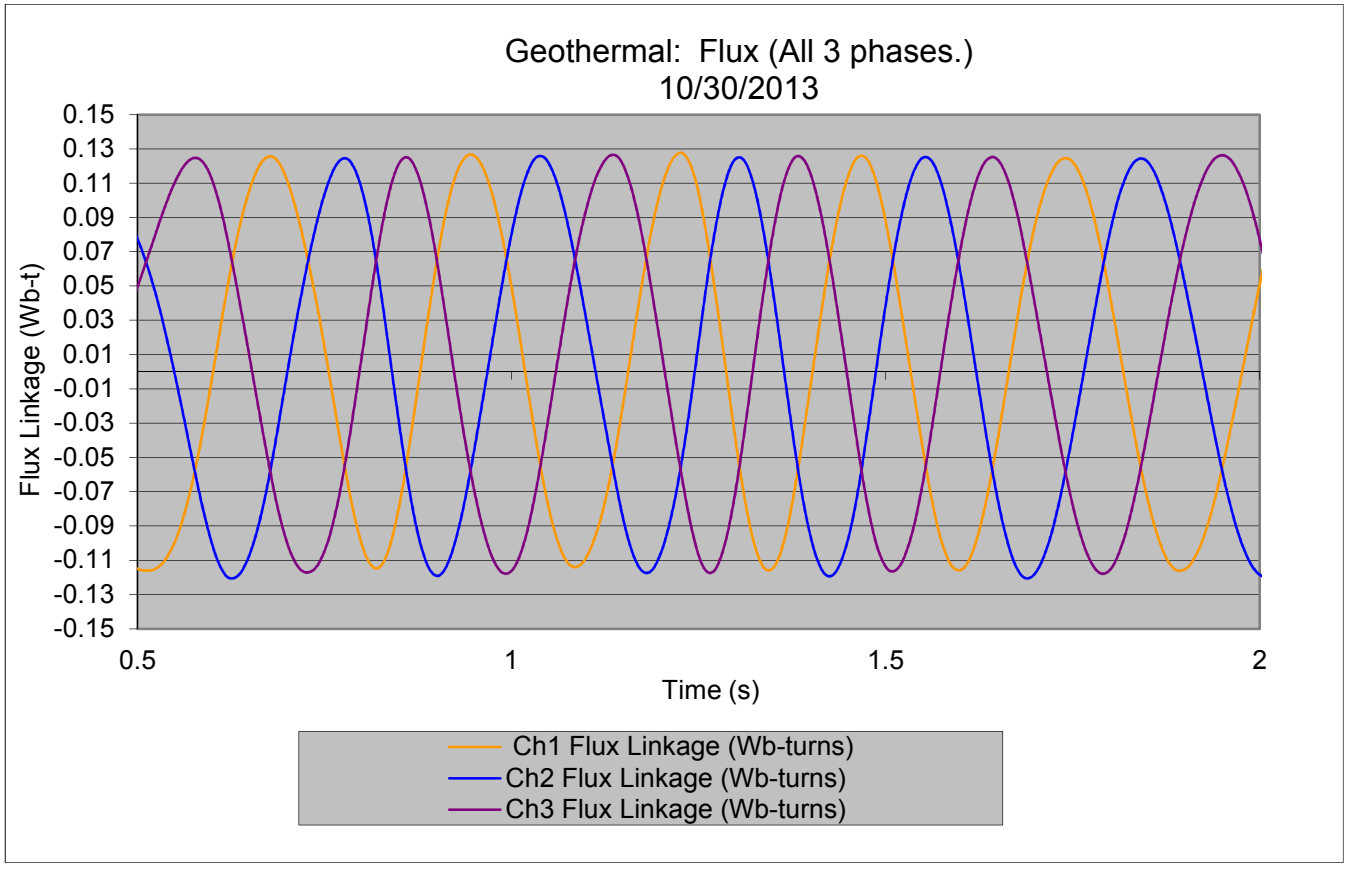

Figure 5.48- Measured Flux Linkages

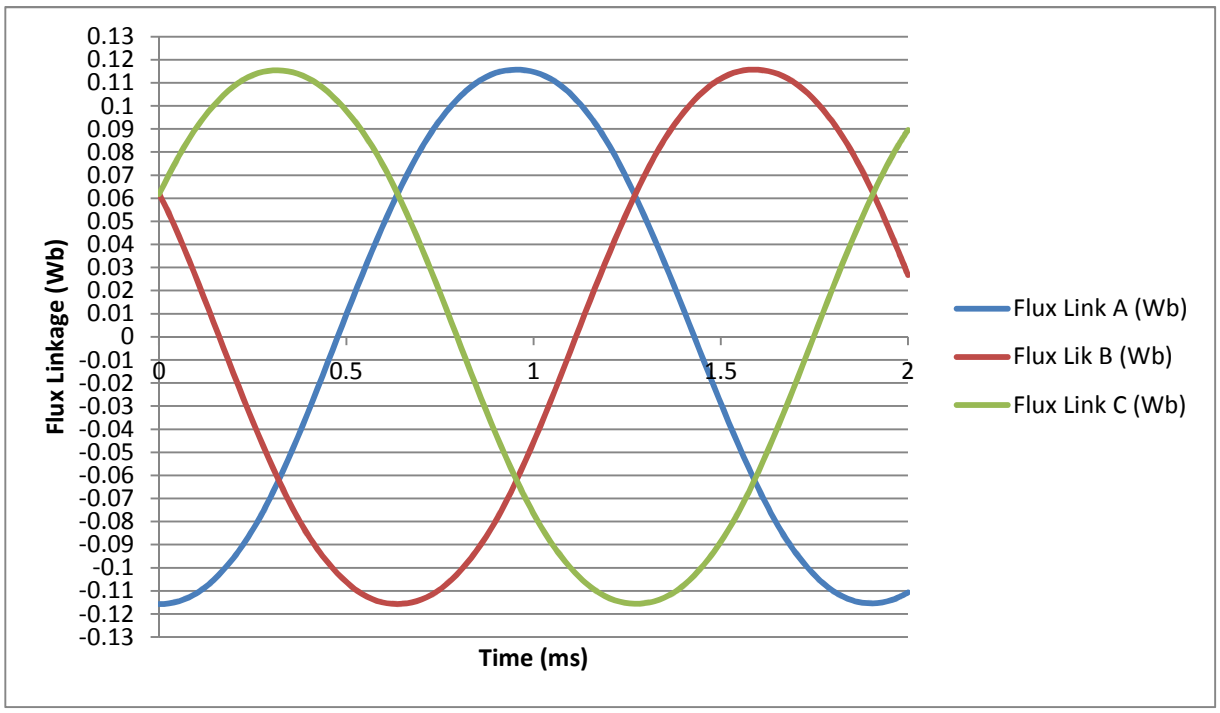

Figure 5.49: Phase flux linkages from simulation

Phase inductance measurements

The phase inductance was measured with two phases of the machine connected to a single phase variac with the third phase open. The rotor was stationary while voltage across the two energized motor phases and the current were measured. The overall resistance and inductance of the two phases in series are calculated by decomposing the voltage into two components: the component in-phase with the current is the resistive voltage drop, and the component in-quadrature with the current is the inductive voltage drop. The test was performed at 60 Hz. The phase resistance and inductance are half of the overall resistance and overall inductance measured. The measured voltage and current during this test are shown in Figure 5.50. The averaged measured values are 80.5 mOhms for phase resistance and 0.319 mH for phase inductance.

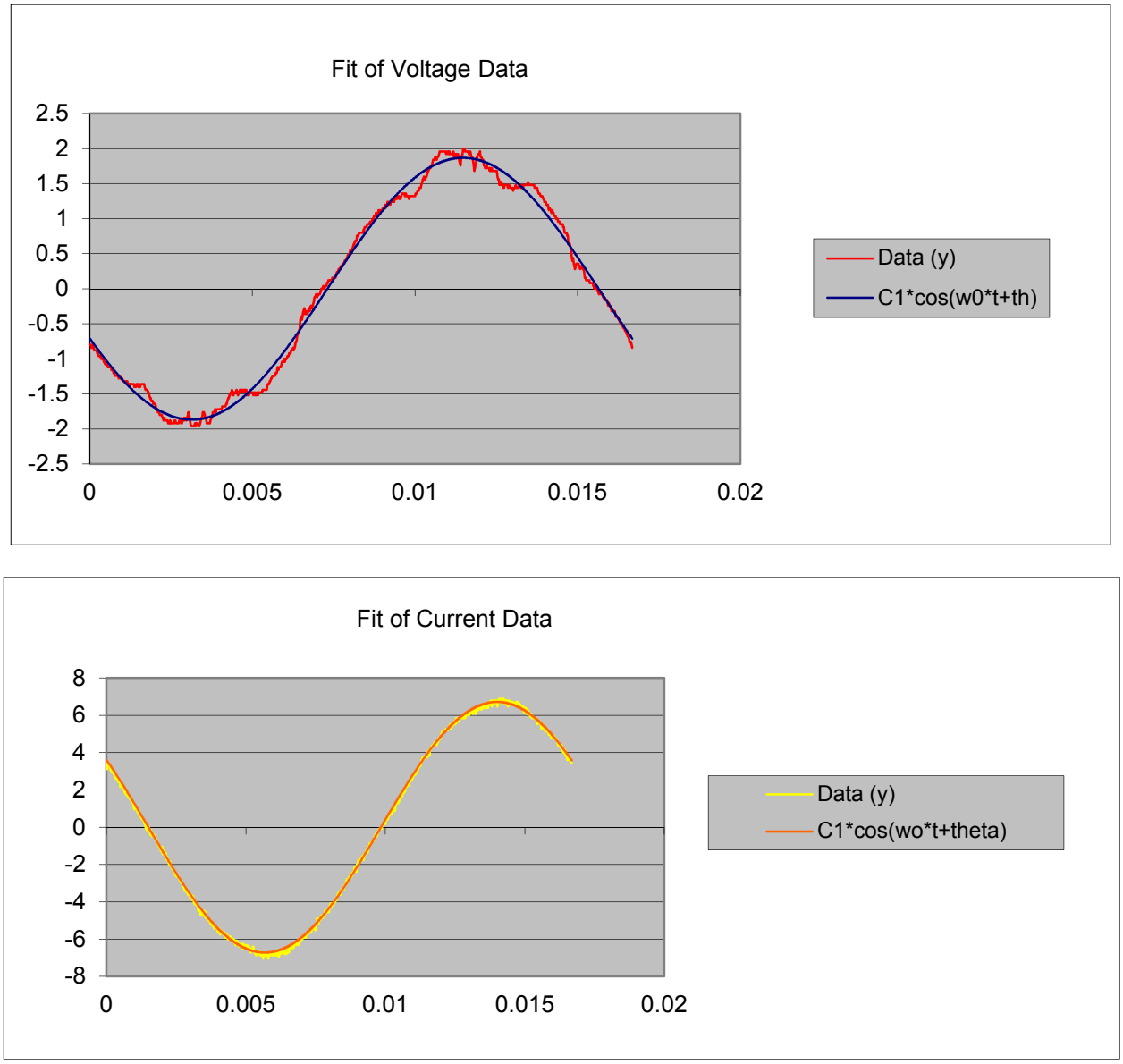

Figure 5.50: Measured Voltage (upper) and Current (Lower) during 60Hz inductance measurement test.

The test condition was replicated in a simulation to confirm the measured inductance. The same current level as in the test was used in the simulation to best replicate magnetic saturation. The simulated voltage and current waveforms are shown in Figure 5.51. The overall impedance is given by Z=V_peak/I_peak.

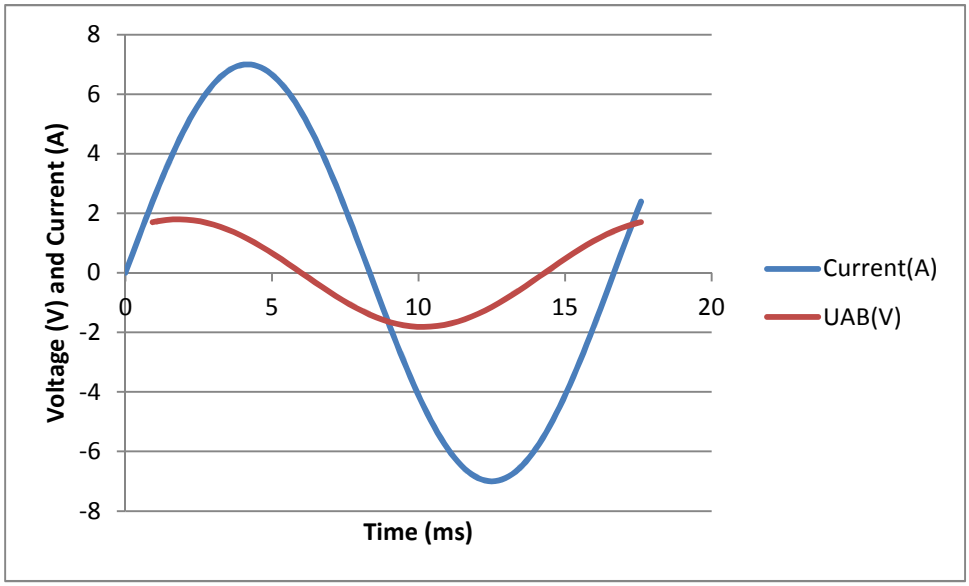

Figure 5.51: Simulated Current and Voltage waveforms

In order to separate the resistance, the active power (resistive loss) is calculated by P = average [u_ab(t)*i(t)] over an electrical cycle. The overall resistance is then deduced by R=P/Irms^2. Once the resistance is known, the overall (two-phase) reactance is calculated by X=√(Z^2-R^2). The phase inductance is easily deduced from the reactance by Lph = 0.5*X/(2*pi*frequency). It should be noted that the measured phase resistance was used to adjust the finite element model so as to better reflect the actual machine.

The "two-dimensional" phase inductance calculated by simulation for different rotor positions over a pole pitch averages out to be about 0.240 mH, ranging from 0.212 mH to 0.268 mH while the two measurements average out to be 0.319 mH. The magnetic saliency creates this position-dependent variation while the contributions of the end turns add to the "2D" value along with some contribution from the connecting cables. From similar machines built in the past, it can be broadly stated that the end turns can contribute 30% of the "2D" inductance. Presuming this to be applicable to the present machine, 0.240*1.3 = 0.312 mH can be considered to be the simulated value and it compares extremely well with the measured value of 0.319 mH. This gives confidence as to the design and performance prediction of this unique motor.

6. Test Facilities Design, Fabrication, and Installation

6.1 HIGH-TEMPERATURE HIGH-PRESSURE FLOW LOOP

The test program was modified from the original plan. It was decided that motor temperature capability would be demonstrated in a separate test of the motor alone. The flow loop test, using water as the working medium, would demonstrate the operation of the flow-through-the-bore motor driving a modified TJ12000 pump, at limited temperatures. This change in the test plan was made to minimize overall program risk while focusing on the key technical challenge, which is the motor temperature capability. As of this writing, all testing has been postponed indefinitely due to resources being applied to overcome unforeseen technical hurdles with the motor fabrication. All equipment and facilities are being held in their finished state in anticipation of conducting a full test program at a later date.

6.1.1 Design and Assembly

A high-temperature high-pressure flow loop facility, in which the lab-scale demonstrator will be operated, has been designed for the simulated conditions. It aims to demonstrate the technologies developed and prove the system can work properly under EGS conditions. The basic parameters of the flow loop are shown in Table 6.1 below.

Table 6.1 – Flow loop specifications

Parameter	Value			
	SI Unit		English Unit	
Suction Pressure	86	bar	1250	psi
Max. Suction Pressure	100	bar	1450	psi
DP	12	bar	174	psi
Max. Pressure	112	bar	1624	psi
Temperature	300	°C	572	°F
Max. Temperature	315	°C	600	°F
Mass Flow Rate	20	kg/s	44	lb/s
Volumetric Flow Rate	0.029	m^3/s	460	gpm
Motor Power	60	kW	80	hp
Motor Voltage	480	V	-	-

The piping and instrumentation diagram (P&ID) of the flow loop is shown as Fig. 6.1. The flow loop primarily consists of a pump/motor test section, an accumulator, a backpressure valve, a water chiller, and the piping and sensors between them. The pump/motor test section is in a horizontal alignment, with the motor driving the pump. Both pump and motor are submerged in up to 300˚C high-pressure water, simulating the geothermal downhole environment. The

accumulator, rated to 1500 psi at 650˚F, is fixed above the highest point of the entire flow loop to ensure that the entire flow loop is full of water at all times. The chiller is used to remove extra heat which comes from the pump/motor test section when the water temperature exceeds 300˚C. The pipes are 4" A53 Schedule 120 seamless carbon steel with a maximum allowed pressure of 2582 psi at 650˚F. A back pressure valve downstream of the test pump provides flow restriction to build up the pressure and maintain the water as liquid. Two pressure relief valves are located at both the high-pressure section and low-pressure section of the piping. The high-pressure relief valve will dump the water or steam to a dump tank when the pressure is above a 2050 psi set point, while the low-pressure relief valve will be set at 1500 psi to protect the Coriolis flow meter. In addition, all the pipe surface temperatures must be maintained below 140°F, thus the thickness of the Enerwrap80 thermal insulation is 4".

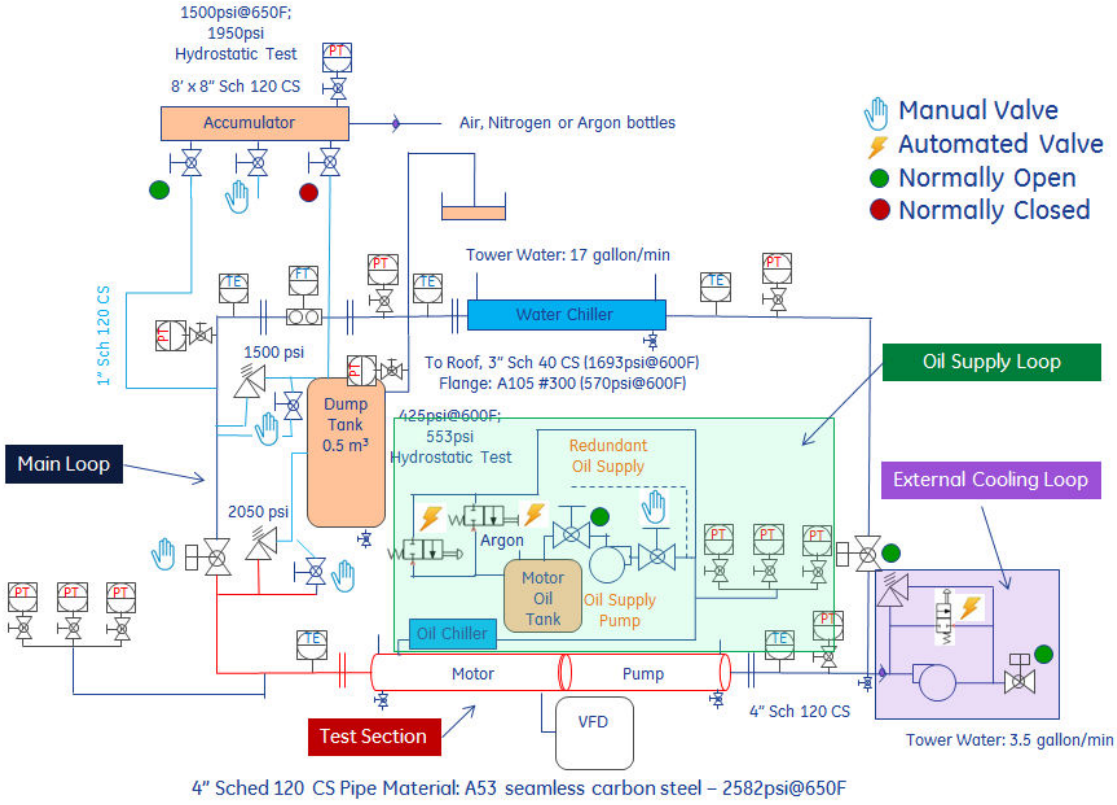

Figure 6.1 – P&ID of the flow loop

An emergency cooling loop has been added to the flow loop in case of emergency shutdown. During the emergency shutdown process, the motor/pump will have stopped running and thus no fluid will be circulated through the water chiller. In addition, the thermal insulation wrapped around the pipes prevents convection to the ambient. Therefore, an external cold water source is desired to bring down the water temperature faster. The emergency cooling loop is inactive during the normal operation. It consists of a reciprocating pump, a high temperature check valve, a control valve and a pressure relief valve, shown as Fig. 6.2.

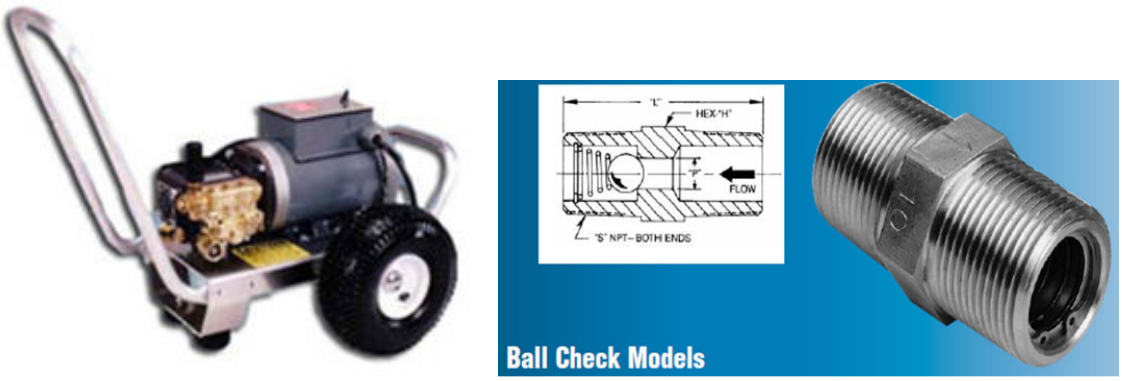

Figure 6.2 – External cooling pump and check valve

The flow loop has been designed, manufactured, delivered, and installed at GE Global Research. The overall dimensions for this test rig are 20' (L) ×8' (W) ×8' (H). The final configuration and the actual hardware including the main loop and the test section are shown as Figs. 6.3 – 6.4. Figure 6.5 displays the main loop that is in the final location with the test section being installed. The pump/motor test section, compared with the full-scale geothermal lifting system, keeps the same dimensions of full-scale wellbore and fluid temperature but scales down the flow rate and DP for lab testing. Thus, a single stage motor, and pump with reduced number of stages can be tested. The goal of such an experiment is to prove that the designed lifting system can operate reliably at the high temperature expected for EGS wells (300°C).

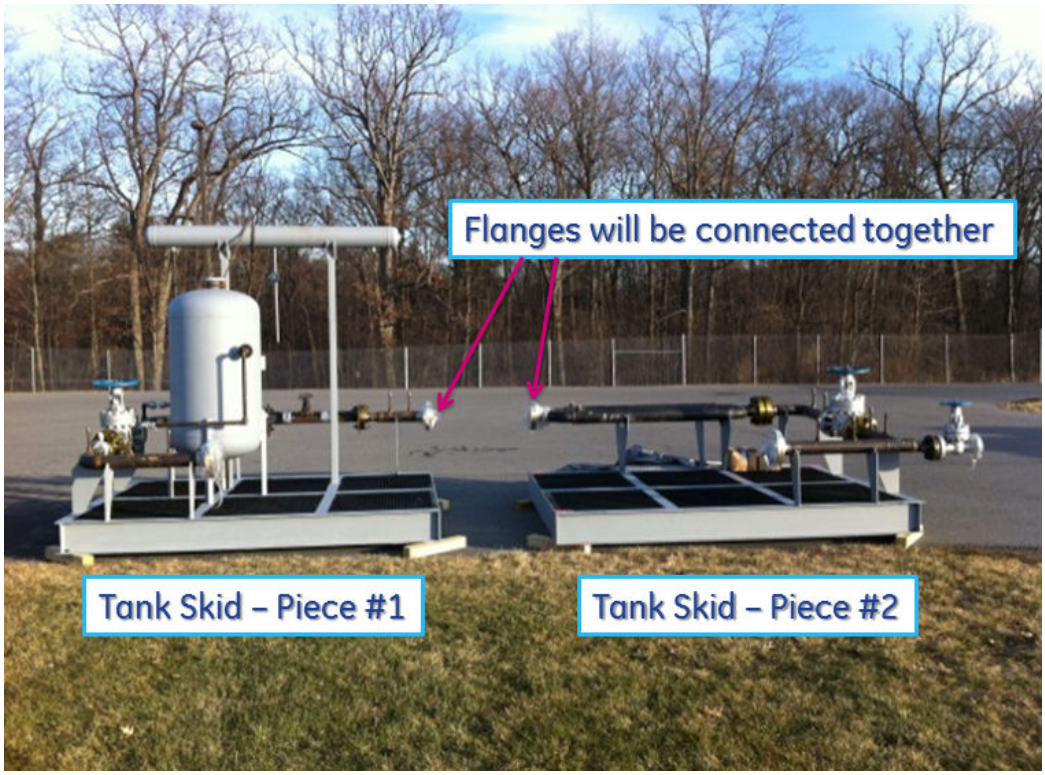

Figure 6.3 – View of the flow loop

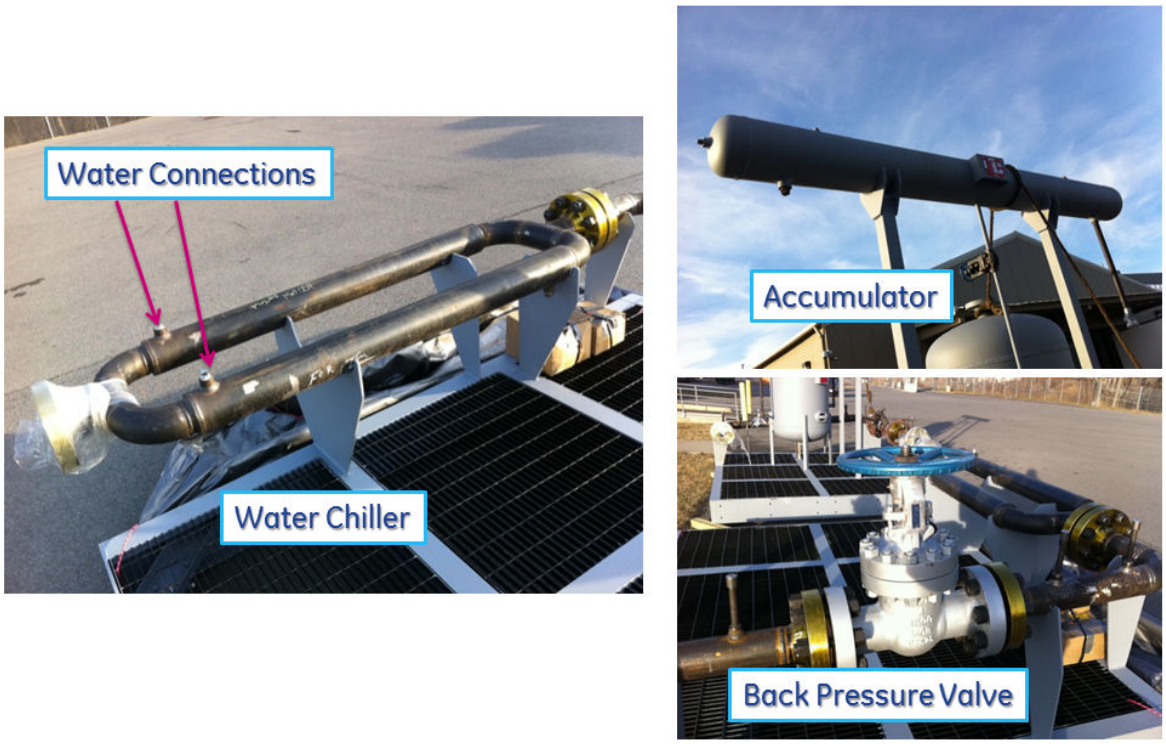

Figure 6.4 –Flow loop components

Figure 6.5 – Flow loop configuration

Instead of using a complicated protector, the flow loop uses full-size mechanical seals together with an external oil supply loop (as shown in P&ID of Fig. 6.1), including an oil tank, an oil pump, a pressure sensing system, an automated control valve (D1FP proportional valve). The purpose of this external motor oil loop is to supply the dielectric oil to the motor and provide extra space to compensate for oil thermal expansion. The automated control valve receives signals from the pressure transmitters and ensures that the motor's internal pressure is higher than the external water pressure. Due to the importance of the oil supply, redundancy has been considered in the loop design, including a redundant oil supply pump, a redundant D1FP valve and two redundant pressure transmitters. The configuration of the oil supply loop is shown as Fig. 6.6. The overall dimension is 5' (L) ×3' (W) ×4' (H). A control panel is assembled on the skid so that operators can easily program and control the pressure output.

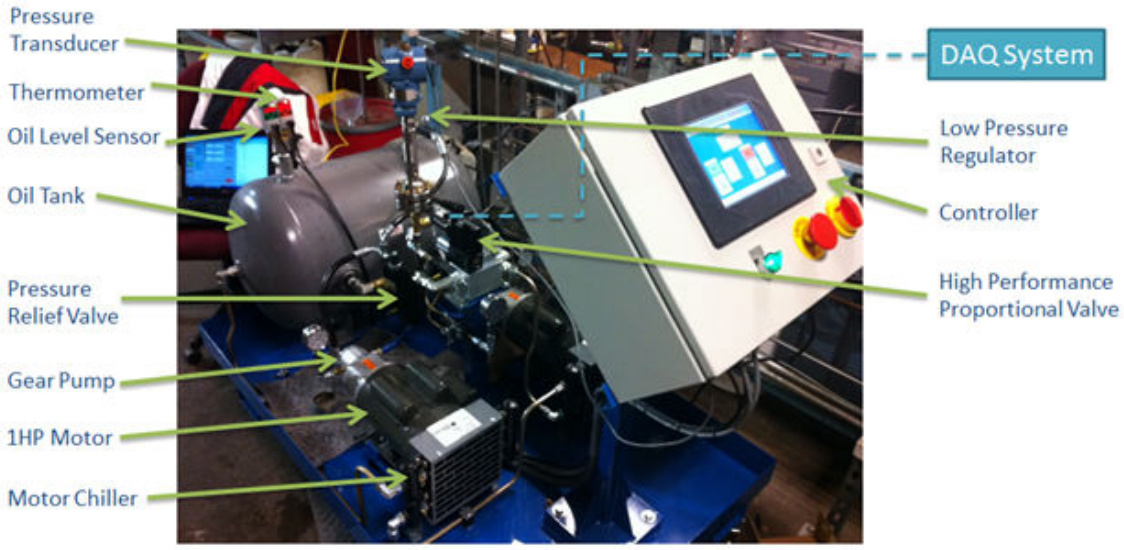

Figure 6.6 – Oil supply loop configuration

The oil supply loop validation has been completed. The tests performed include Minimum Pressure Test, Pressure Regulation Test, Fixed Pressure Test and Half Hour Degradation Test. These tests, described below, demonstrated that the oil skid will serve the needs of the motor thermal test. The generated pressure can be accurately regulated within the 15-50 psig desired range. The skid rapidly responds to a preset pressure and is capable of running at a fixed pressure. The half-hour degradation test shows a slight pressure drop as oil temperature increases, but this can be adjusted by the low pressure regulator. A PID controller will be added to the controller after the thermal test so that the oil skid can automatically follow the process water pressure source and generate pressure accordingly. Detailed test data can be found in sections below.

Minimum Pressure Test

This test is to determine the lowest gauge pressure that the oil skid can generate when it is running.

Conditions:
Preset Pressure: 29 psig (2bar)
Oil Temperature: 65°F
Sampling Rate: 1 record/second

Operation: Slowly tune the low pressure regulator to the fully open position.

Conclusion: The oil skid will generate at least 16.2psig (1.1 bar) when it is running, which is sufficient for the motor thermal test.

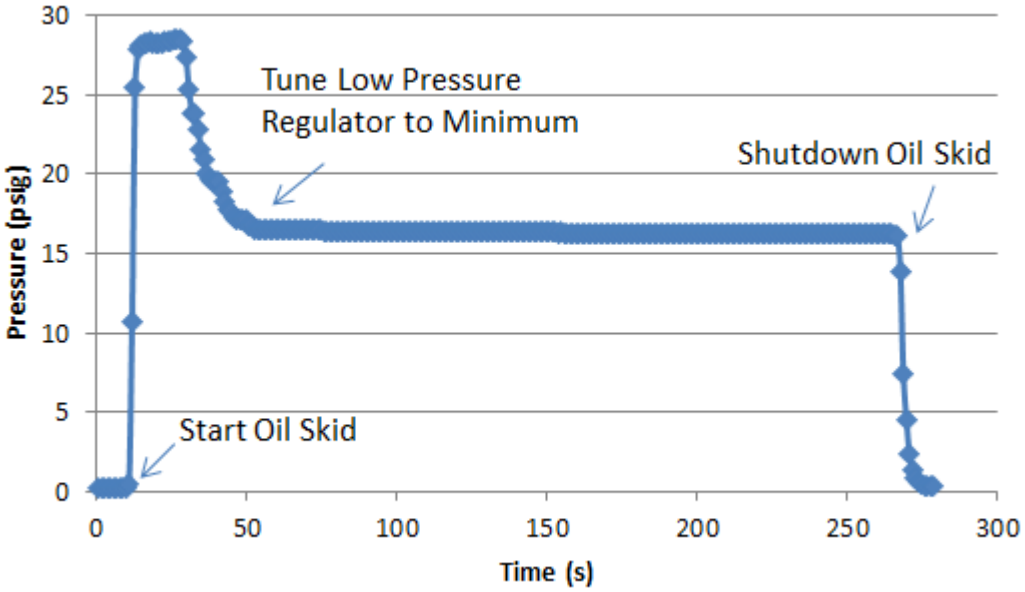

Figure 6.7 – Minimum pressure test

Pressure Regulation Test

This test is to check if the generated pressure can be tuned within 15-50 psi, which will be the operating pressure for the motor thermal test.

Conditions:
Preset Pressure: 43.5 psig (3bar)
Oil Temperature: 66°F
Sampling Rate: 1 record/second

Operation: Slowly tune the low pressure regulator up and down between the fully open position and the position where shows 50 psig reading.

Conclusion: The discharge pressure can be regulated within the desired range (15-50 psi).

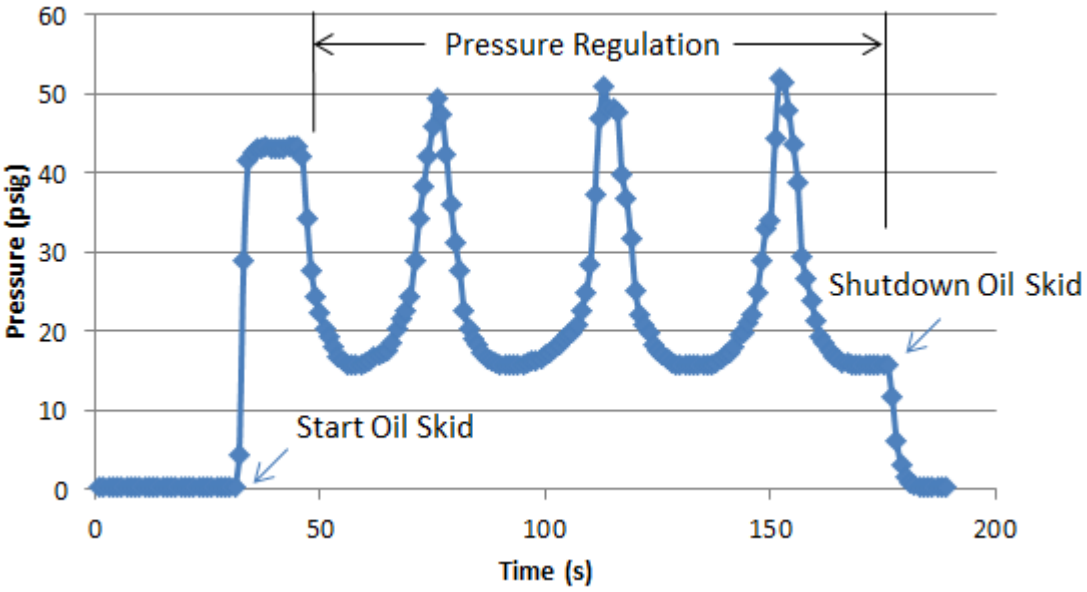

Figure 6.8 – Pressure regulation test

Fixed Pressure Tests

These tests aim to check the response time of the oil skid to a preset pressure, and confirm the oil skid can run at a fixed pressure.

Conditions:
Preset Pressure: 16.2 psig (1.1bar); 29 psig (2bar); 43.5 psig (3bar)
Oil Temperature: 66°F
Sampling Rate: 1 record/second

Operation: Preset the pressure and start the oil skid.

Conclusion: The pressure can be built up within 5 seconds, and then the oil skid will run at a fixed pressure.

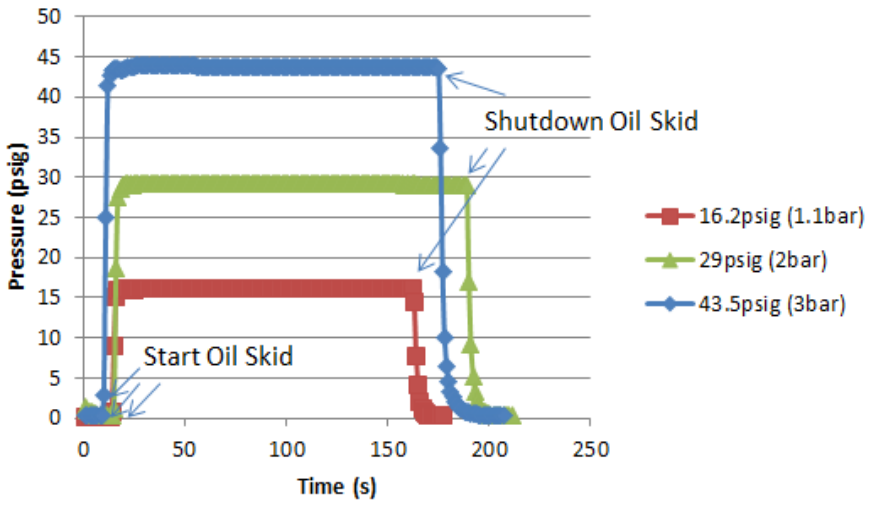

Figure 6.9 – Fixed pressure test

Half-Hour Degradation Test

When the oil skid is running, the oil temperature will gradually increase due to the heat generation from the gear pump. Eventually, the oil will reach thermal equilibrium at a certain temperature. As the oil temperature increases, the oil density and viscosity decrease resulting in slight drop of the discharge pressure. This test is to check the temperature effect and have a general idea of how pressure changes with time.

Conditions:
Preset Pressure: 30 psig (~2 bar)
Test Duration: 30 minutes
Oil Temperature at the Beginning: 66°F
Sampling Rate: 1 record/second

Operation: Preset the pressure and start the oil skid.

Conclusion: The oil temperature increases from 66°F to 68°F in 30 minutes. Discharge pressure drops from 30.4 psig to 28.3 psig, but the rate of pressure change decreases as the system approaches thermal equilibrium. Since the motor thermal test will take several hours, it is suggested an operator monitor the oil pressure at least one time per hour. If the pressure becomes too low (not likely to happen), then the low pressure regulator will be tuned to increase the pressure.

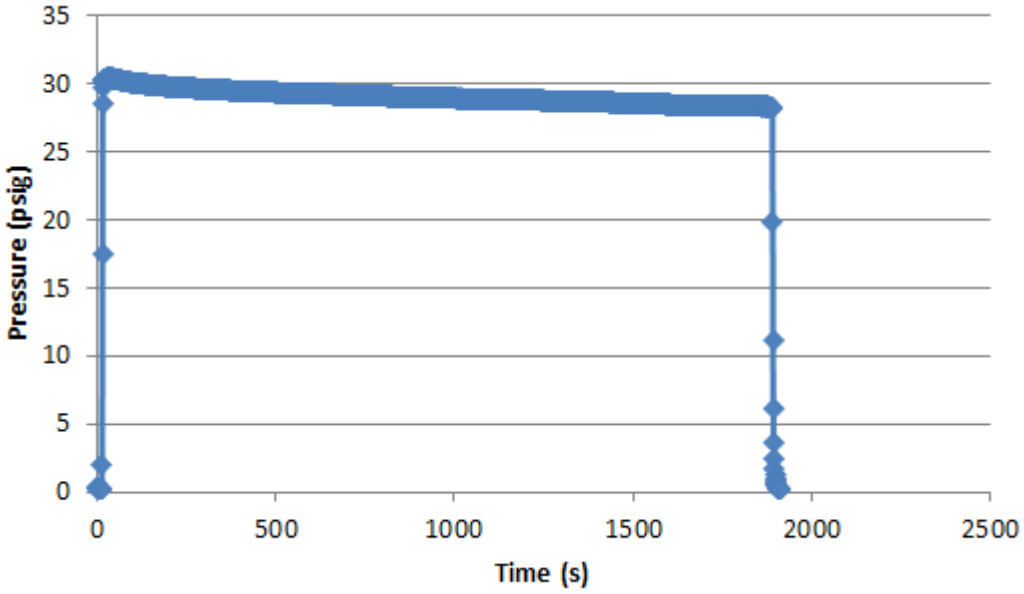

Figure 6.10 – Half -hour degradation test

The overall assembly for the geothermal pump-motor system is shown in Fig. 6.11. Special attention was given to the design of the conduits to extract power and instrumentation leads from the motor. There are a total of seven conduits, each of which is welded to the outer-most flange as indicated in the figure. The welded connection will provide an adequate seal for the high temperature water exiting the motor which will fill the conduit cavity.

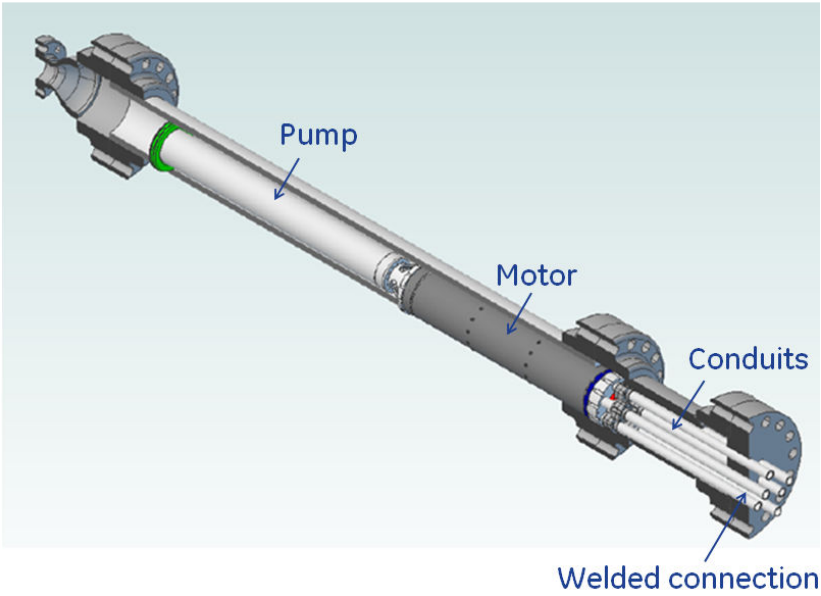

Figure 6.11: Schematic of geothermal pump and motor assembly

6.1.2 Instrumentation

Fig. 6.12 displays examples of a thermocouple (left) and pressure transmitter (right) that are installed in the test loop. The pressure transmitters have been calibrated from 0-4000 psi. The 316L flanges ensure the operating pressure up to 2500 psi. With the addition of a remote diaphragm seal, process temperatures of up to 315°C are acceptable at atmospheric pressure. The temperature can go higher when under pressure. The thermocouple is K-type with 12" long grounded probe. It is specially designed with Nickel-Chrome based sheathing for high temperature applications. The thermocouple is rated for measuring up to 1335°C.

Figure 6.12 –Thermocouple (left) and pressure transmitter (right)

Figure 6.13 below shows a schematic of the instrumentation used on the geothermal motor. There are a total of 12 thermocouples to measure temperature at various critical motor locations. Six thermocouples are used for monitoring winding temperatures: two on the cool oil inlet side, two on the oil outlet side, and two near the center of the stator. Similarly, four thermocouples are used to monitor the oil temperature at the seals as well as the start and end of the ventilation circuit. Finally, one thermocouple is placed on each journal bearing. Motor housing vibrations are monitored using single-axis accelerometers.

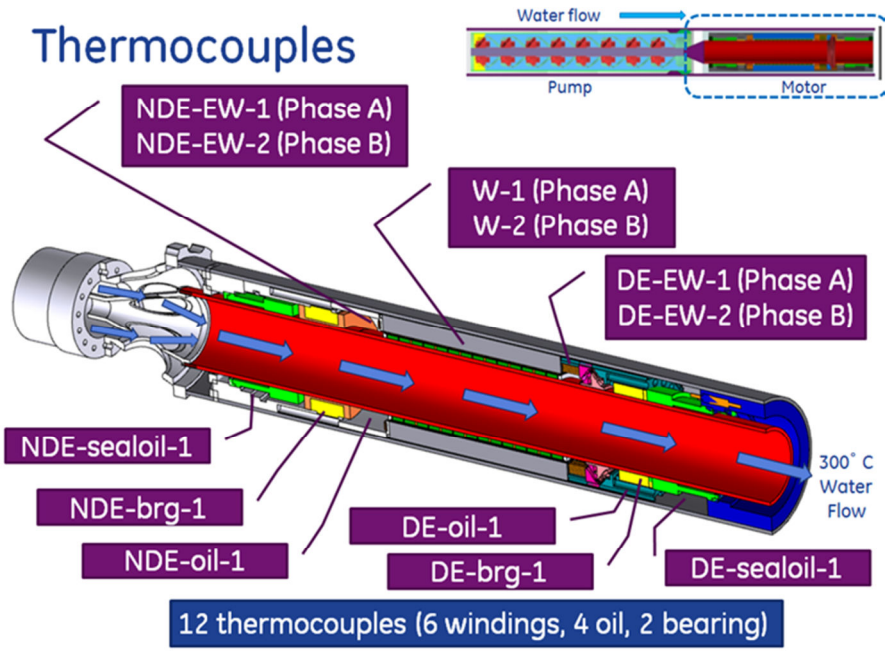

Figure 6.13: Isometric view of geothermal motor showing thermocouple locations

6.1.3 Experimental Procedure

Under normal operating conditions, the control logic of the flow loop is given in the table below:

Table 6.2 – Flow loop test procedure

Steps	Action	Input	Output
1	Feed oil into the motor	Open the valves in the oil supply loop	Motor internal pressure sensor
2	Fill water into the loop	Open 1" valve, back pressure valve and main valve	Water level
3	Pressurize the loop	Open air compressor or air bottle	Pressure sensors
4	Fully turn on the chiller	Adjust flow rate of cooling water	Thermocouples
5	Start the motor	Start VFD and adjust the speed	Motor speed
6	Adjust flow	Adjust back	Flow meter

	speed	pressure valve	
7	Adjust chiller	Adjust flow rate of cooling water to gradually increase temperature	Thermocouples
8	Data acquisition	Operation on data acquisition system	Data file storage
9	Fully turn on the chiller	Maximize the cooling water through chiller	Thermocouples
10	Shut down the motor	Shut down the motor via VFD	Motor speed
11	Release pressure	Open the bypass valve of the pressure relief valve	Pressure sensors
12	Drain water	Open the drains on test section, chiller and damp tank	NA
13	Shut down the oil supply loop	Close the automated valve in the oil supply loop	Motor internal pressure sensor

However, certain emergency circumstances during operation must be taken into account for safety reasons and for protecting the equipment. For example, a broken seal could be one of the most serious failure modes which results in a large amount of oil leaking into the hot water. Sudden loss of power is another example in which an operator has to take actions to cool and depressurize the system immediately. Figure 6.14 lists the step-by-step operation flow chart including the abovementioned emergency cases.

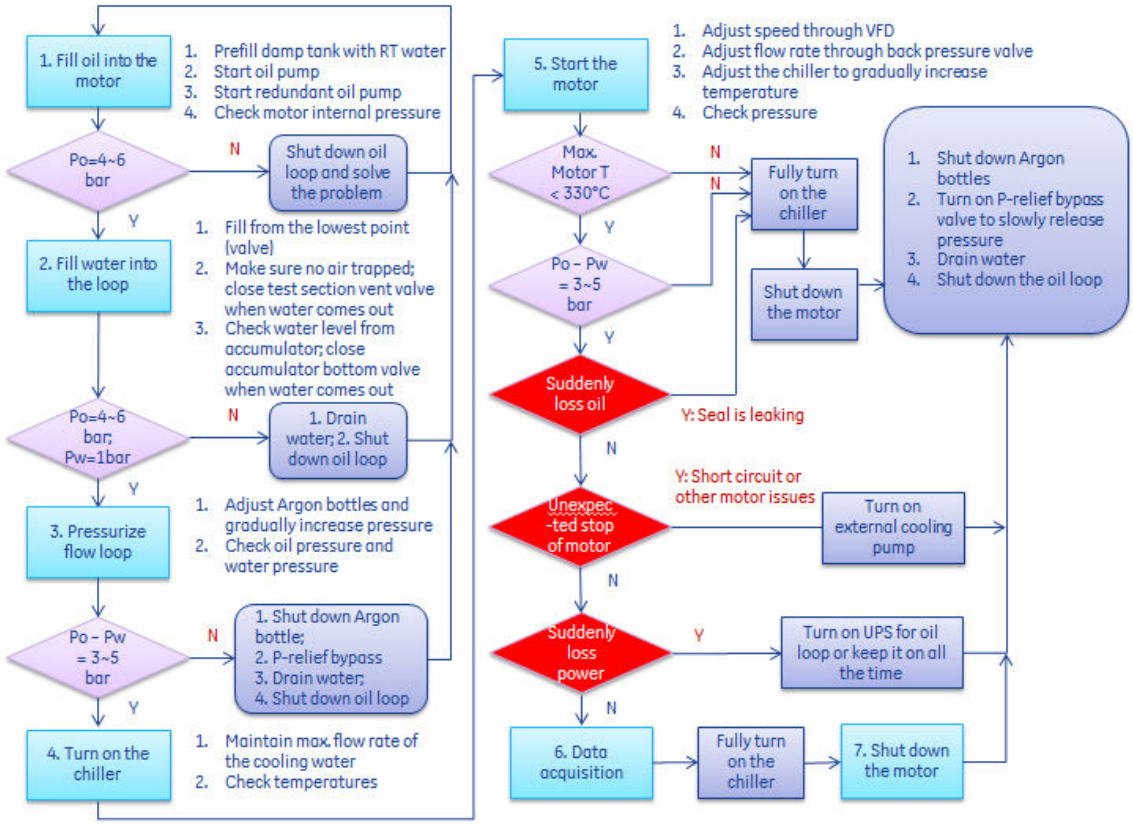

Figure 6.14 – Detailed operation flow chart

6.2 AIR COOLING THERMAL TEST RIG

6.2.1 Design and Assembly

The electric motor has been identified as having the highest risk of any system component in an EGS environment. Therefore, a thermal test on the motor was proposed to be performed independently before assembling it to the pump and the flow loop. The test is intended to demonstrate that the motor itself can work properly and operate reliably at 300°C.

The electric motor has been specifically designed to meet the test loop requirements of 58 kW. The motor cross-section is kept the same as the full size motor; it is reduced in core length to 14.577" with an electromagnetically effective length of 12.5". The stator winding turns-per-coil value is adjusted for this reduced length motor so that a Yaskawa 460-volt Variable Frequency Drive (VFD) for PM motors can be readily employed. The test consists of the motor standing alone on a test setup, filled with the appropriate high temperature dielectric oil, and building up the temperature while it is running. The hollow shaft and the outer surface of the motor are cooled by air pumped through an air blower. A system of ductwork around the motor guides the air flow. The oil supply loop is then connected to the motor to pressurize the oil and compensate for oil

thermal expansion. The temperatures inside and outside the motor, as well as the air temperature at the inlet and outlet of the ductwork, are measured. The configuration of the motor test is shown as Fig. 6.15.

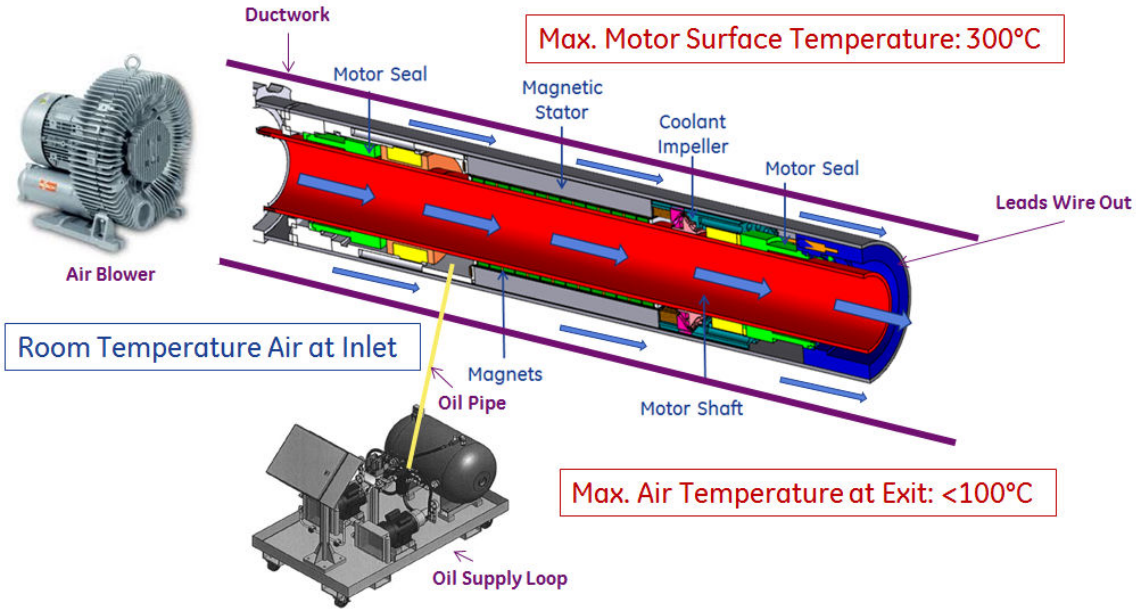

Figure 6.15 – Motor thermal test setup

Motor No-Load Thermal Test Analysis

As described above, to progressively evaluate the performance of the motor, one strategy is for the motor to be tested first outside of the flow loop under no load conditions. Such a test aims at establishing the motor's build integrity and temperature capability. The motor cavity is filled with dielectric oil. The oil impeller drives the internal oil circulation. Motor speed and input power are controlled by a Variable Frequency Drive (VFD). VFD-controlled electrical power input compensates for windage loss, oil impeller power consumption, and the motor power consumption under no load conditions. The mechanical loss under no load conditions is mainly influenced by motor shaft speed and oil temperature, determined by detailed CFD simulations. At the rated speed of 3150 RPM, the mechanical losses at 100°C and 300°C, and the electrical losses under no load and full load conditions are listed in Table 6.3.

	EM Loss [kW]	Mechanical Los [kW]	Total [kW]
No Load Oil Filled 100C	1.13	7.8	8.93
No Load Oil Filled 300C	1.13	5.1	6.23
Full Load Oil Filled 100C	7.79	7.8	15.59
Full Load Oil Filled 300C	7.79	5.1	12.89

Table 6.3 – Prototype motor losses at 3150 RPM under no load and full load conditions

Unlike within the flow loop when the motor is operated with full output power and where the motor is cooled by high-pressure high-temperature water, for the no-load test conditions the motor is cooled by ambient air driven by an external air blower. As schematically shown in Figure 6.16, air flows through an open loop, partly through the inner bore of the hollow rotor shaft and partly through the air space between the casing and motor outer diameter, to cool the motor through parallel paths. To enhance the cooling effectiveness, radial fins at the motor stator outer diameter serve to increase the surface area for air cooling. The motor casing is also moved outward to boost the air flow area around the stator outer diameter. During the no load tests, motor speed is increased progressively while motor temperature is monitored from the built-in thermocouples. The air blower is sized to meet the cooling needs at the highest speed of 3150 RPM for continuous operation.

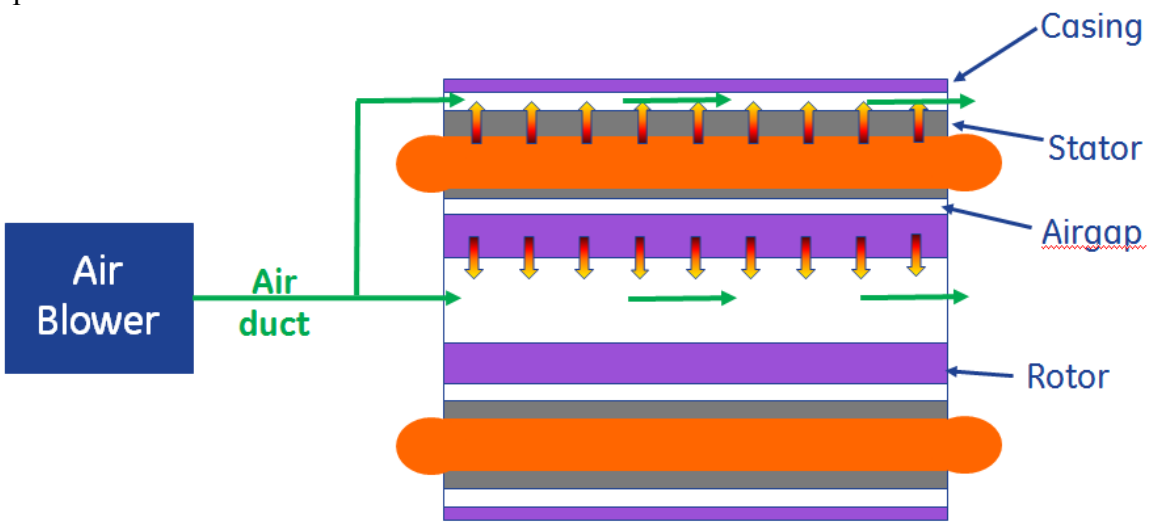

Figure 6.16 - Schematic of motor cooling with air for no load thermal test

To better establish the appropriate procedures for the no load test, the transient thermal response of the motor was evaluated at 3150 RPM. Without air or water cooling, the natural heat dissipation to ambient by the motor itself is negligible. Instead, heat generated from motor operation is absorbed by the thermal mass of the motor and that of the oil. With the motor temperature limit at 330°C and ambient at 30°C, without cooling, the motor can be operated with an allowable temperature rise of ~300°C. Using the lumped-capacitance method as a 1st order estimation, Figure 6.17 shows the transient temperature response of the motor without cooling. Under no load conditions, the motor can be operated continuously for approximately 20-30 minutes to achieve a ~300°C internal temperature rise.

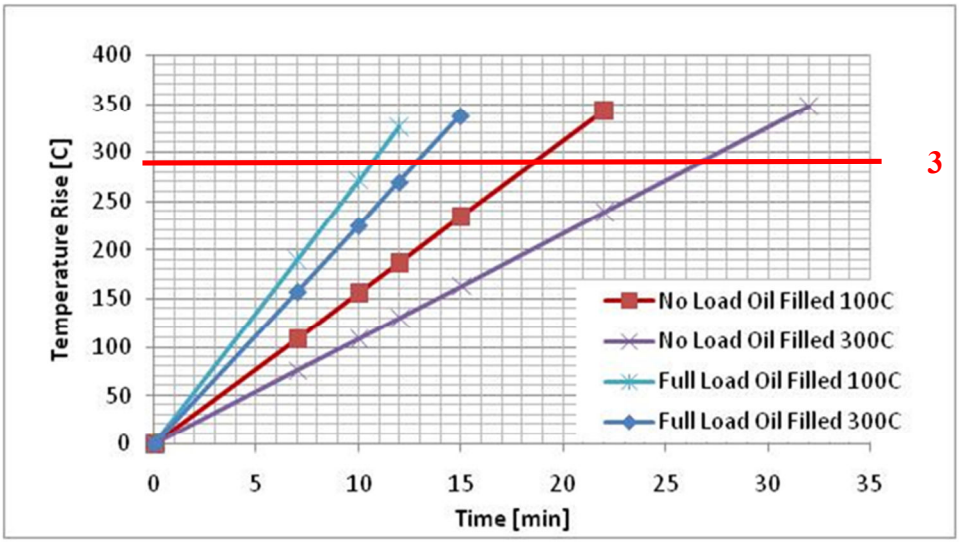

Figure 6.17 - Motor transient temperature response

Under no-load conditions with air cooling, motor temperature can be estimated by:

$$T_{\max} = T_{Air} + \Delta T_{Air} + \Delta T_{Conv} + \Delta T_{Cond}$$

where:

- T_{Air} represents the air temperature at motor inlet;
- ΔT_{Air} represents the air temperature rise from motor inlet to exit;
- ΔT_{Conv} represents the convection temperature rise on cooling surface;
- ΔT_{Cond} represents the conduction temperature rise from cooling surface to motor hotspot.

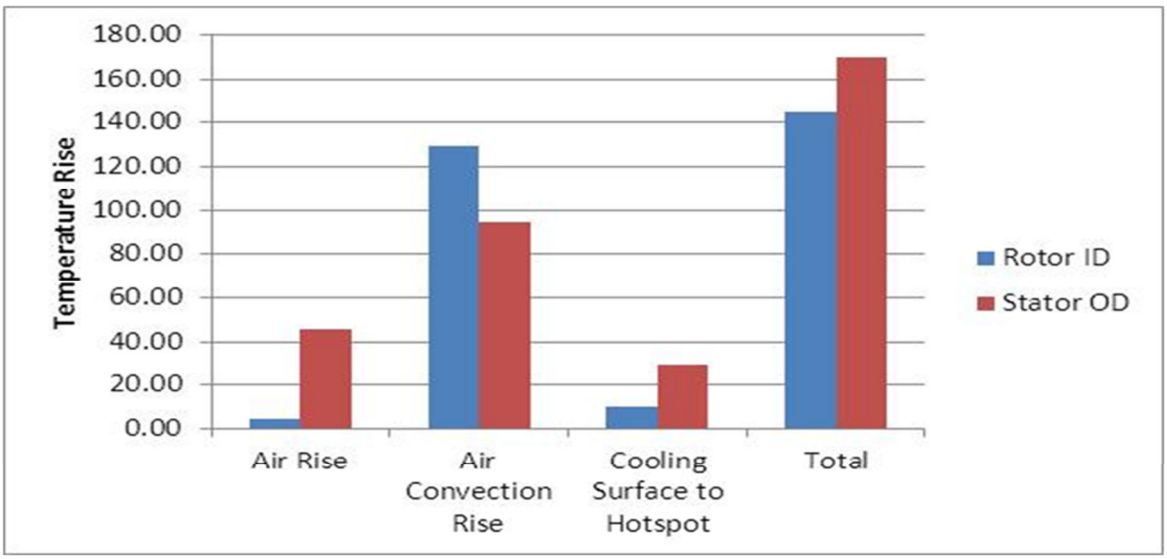

Figure 6.18 - Motor no-load continuous operation temperature response.

Based on the preliminary no-load test stand concept and an exemplary air blower, the no load continuous temperature response of the motor is shown in Figure 6.18. This estimation is based on the no-load losses at 3150 PRM and 300°C. The total temperature rise is ~170°C. The same estimation based on the no load losses at 3150 RPM and 100°C yields a total temperature rise of ~240°C. With ambient air at the blower inlet, the motor hotspot temperature is expected to be well below the 330°C limit. These results, together with the transient response in Figure 6.17, suggest that air cooling is sufficient in managing the temperature of the motor for the no-load test. To achieve the goals of verifying motor build integrity and temperature capability, motor speed should be stepped up gradually while the cooling flow will be adjusted to manage all motor internal temperatures. All motor and oil temperatures can be maintained to <330°C as indicated by temperature readings of key thermocouples built into the motor.

6.2.2 Experimental Procedure

A detailed test procedure for the motor validation has been established. It ensures sufficient data to demonstrate the motor's operability and performance at temperatures up to 300°C. The test is intended to demonstrate the overall motor design, cooling system effectiveness and motor material temperature capability. The step-by-step test procedure is listed in this section as below.

Bake Oil and Motor under Vacuum

This step prepares the dielectric oil and motor simultaneously by removing oxygen and moisture from the system. This procedure is to be followed as part of the motor oil fill process, to be carried out immediately prior to any test program. As the test program for the prototype motor has been postponed indefinitely, the oil fill has not been carried out as of this writing, to avoid any possible contamination of the oil due to oxygen exposure during the oil fill process or during motor storage.

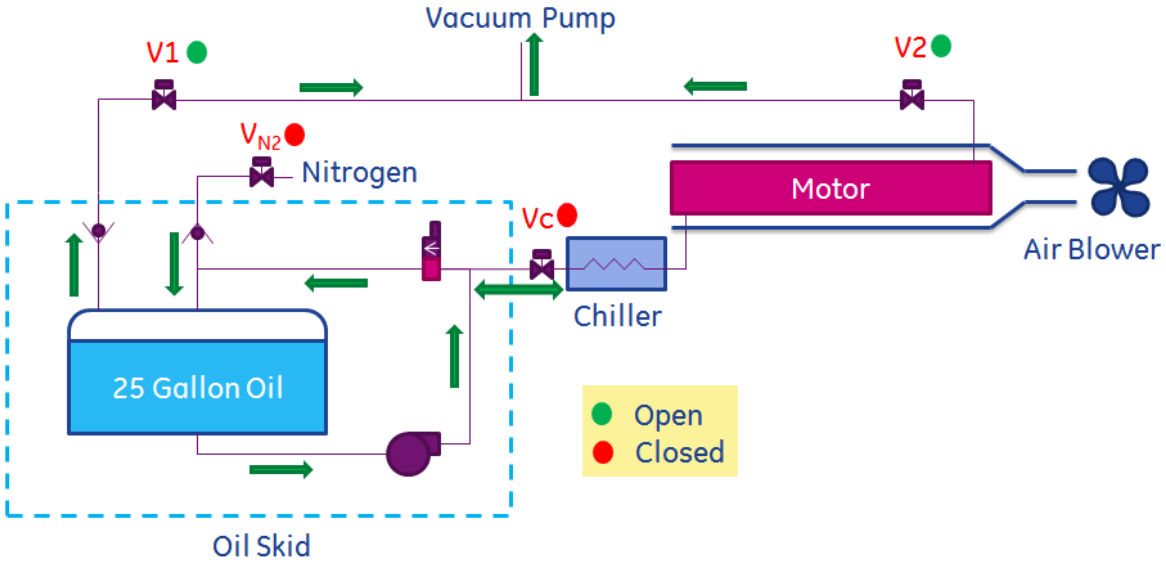

Figure 6.19 – Bake oil under vacuum

Operations:

1) Close the vacuum rated ball valves on the top and the bottom of the oil tank (isolate the oil tank from the rest of the oil skid).
2) Open valve V1 and V2, close Vc and V_{N2}.
3) Heat 25 gallons of oil to 80°C (176°F) and maintain the temperature.
4) In the meanwhile, heat the motor to 120°C (248°F) and maintain the temperature.
5) Start vacuum pump to -23in Hg.
6) Keep vacuum pump running for 24 hours.
7) Shutdown vacuum pump.
8) Shutdown the oil heater.
9) Shutdown the motor heater.

Fill with Nitrogen

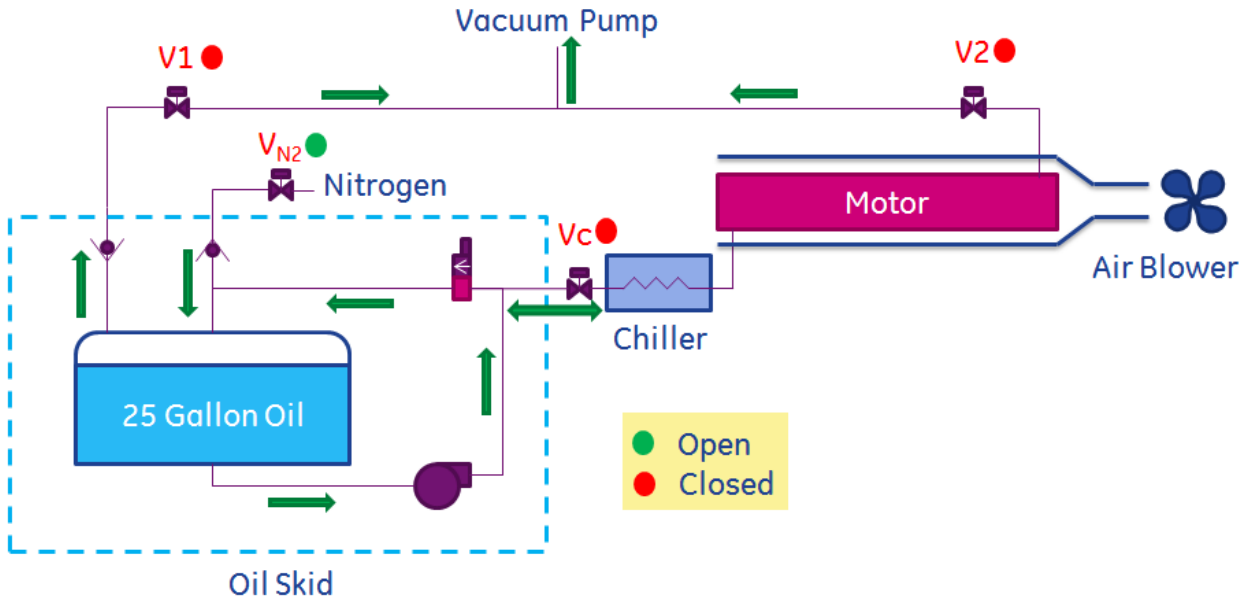

Figure 6.20 – Fill with nitrogen

Operations:

1) Keep Vc closed.
2) Close V1 and V2.
3) Open V_{N2}.
4) Slowly open Nitrogen regulator to fill Nitrogen into the tank.
5) Keep internal pressure of the oil tank to slightly higher than 1 bar. Note there is a recently-added 100 psi pressure relief valve on the oil tank.
6) Keep the vacuum rated ball valve on the top of the tank closed.
7) Disconnect the needle valve from the tank and put it in a bottle lower than the bottom of the tank.
8) Open the vacuum rated ball valves (upstream of the pump) on the bottom of the oil tank.
9) The residual oil inside the pipes drains out under the pressure of Nitrogen.
10) Wait until ~1 liter of oil has been collected.
11) Connect the needle valve back to the tank.

Now the oil in the tank is fully prepared. The untreated residual oil in the pipe line has been pushed out of the oil skid.

Fill Motor with Oil

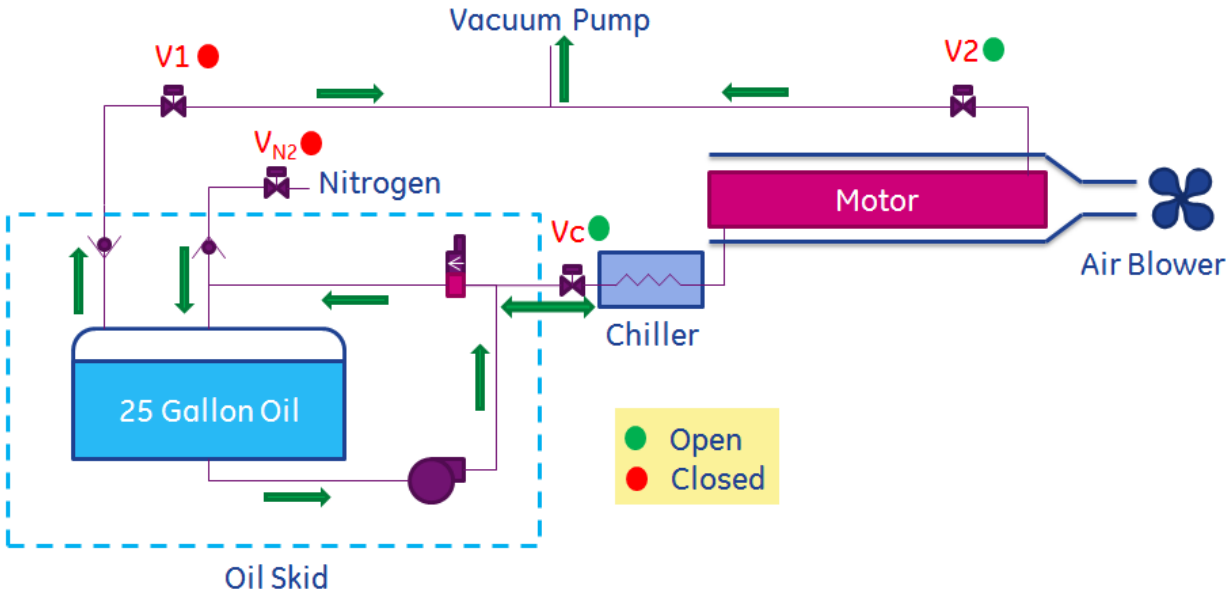

Figure 6.21 – Fill motor with oil

Operations:

1) Keep V1 closed.
2) Open V2.
3) Keep the vacuum pump running.
4) Start oil skid.
5) Close V_{N2}.
6) Slowly open Vc to fill the motor from the bottom.
7) If it is difficult to pump oil into the motor, quickly open and close V_{N2} to release some nitrogen into the oil tank.
8) Stop the vacuum pump until oil flows out of the motor into the transparent pipe.
9) Close V2 before oil flows into the vacuum pump to prevent pump damage.
10) Slowly regulate the needle valve on the oil skid until discharge pressure (motor's internal pressure) is within 20-40 psi range (30 psi is recommended).

Preheat Motor

Operations:
1) Wrap heating elements around the motor.
2) Preheat motor to 100°C to reduce oil viscosity.

Low-Speed Thermal Test

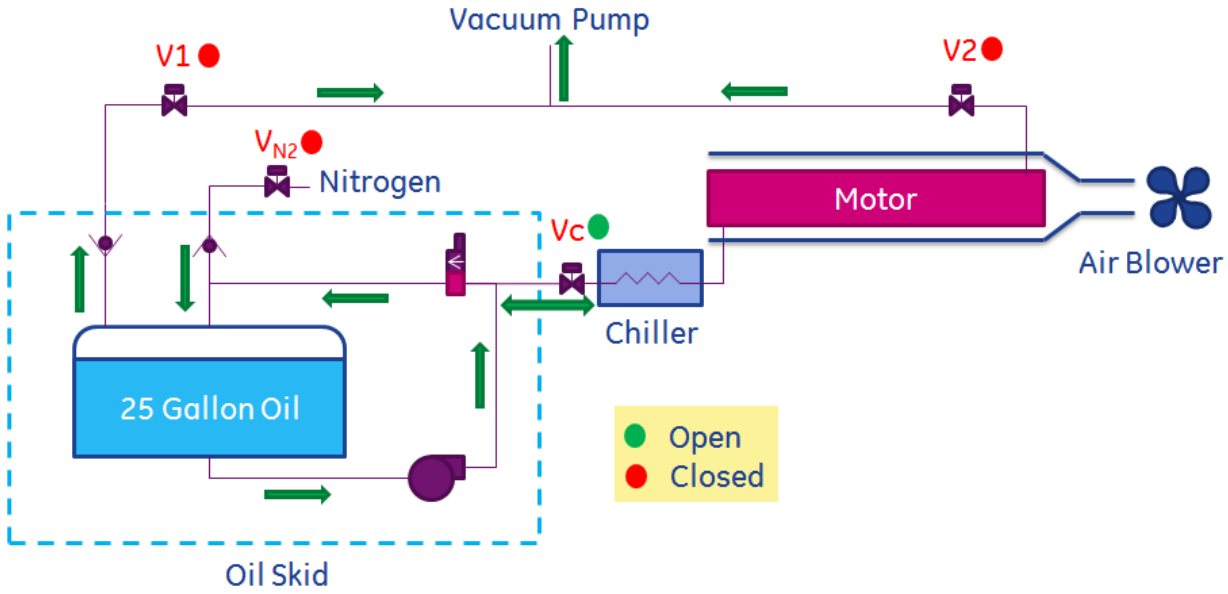

Figure 6.22 – Low-speed thermal test

Operations:
1) Start air blower to full speed.
2) Start motor through VFD at the lowest speed that motor can run steadily.
3) Monitor all instrumentation for any unexpected readings.
4) Increase speed slowly to 1000 rpm.
5) Regulate air blow to maintain 150°C internal temperature.
6) Monitor oil level sensor for possible leakage.
7) Monitor oil temperature both inside the motor and inside the oil tank.
8) Monitor motor's internal pressure.
9) Monitor rotor's vibration.
10) Record data through DAQ.
11) Measure current leakage as necessary.
12) Increase speed to 1500 rpm.
13) Regulate air blower to maintain 200°C and record data.

High-Speed High-Temperature Thermal Test

Operations:

1) Gradually increase speed to 2000 rpm and 2500 rpm.
2) Regulate air blower to maintain 250°C and record data.
3) Refer the chart below for oil flow rate and motor power consumption.
4) Increase speed to 3150 rpm.
5) Regulate air blower to maintain 250°C and record data.
6) Regulate air blower to gradually increase temperature to 275°C and then 300°C.
7) Record data.
8) Maintain temperature within 275°C to 300°C range for up to 120 hours (5 days).

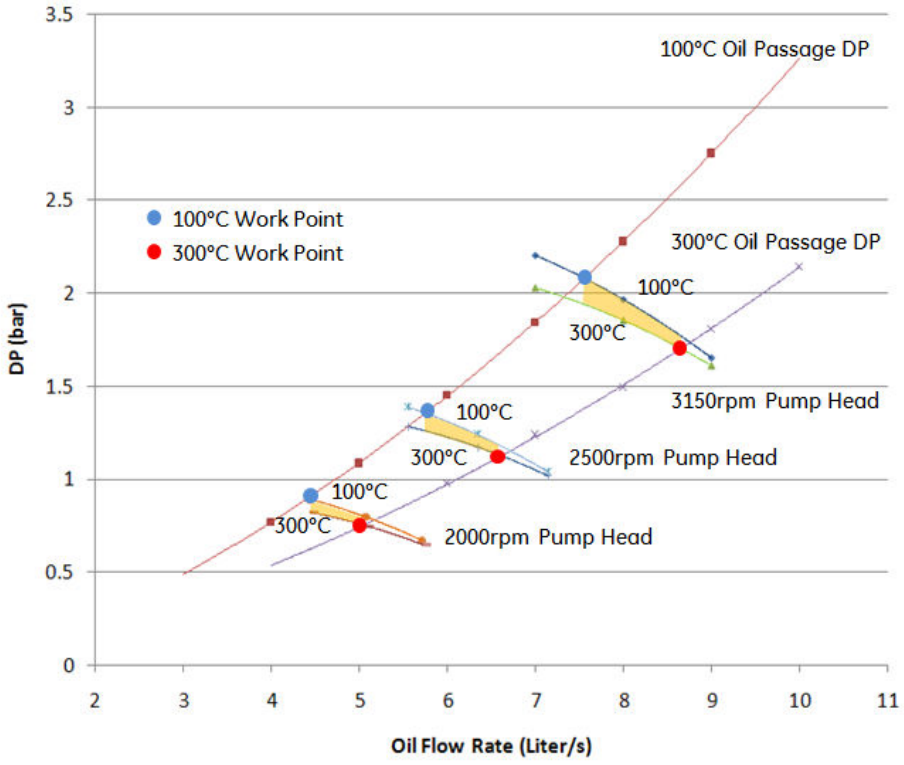

Flow Rate (liter/s)		
RPM	100°C	300°C
3150	7.5	8.8
2500	5.7	6.6
2000	4.4	5.0

Power (kW) Windage + Impeller Consumption		
RPM	100°C	300°C
3150	7.8	5.1
2500	4.5	2.8
2000	2.6	1.6

Figure 6.23 – High-speed high-temperature thermal test

Shutdown Process

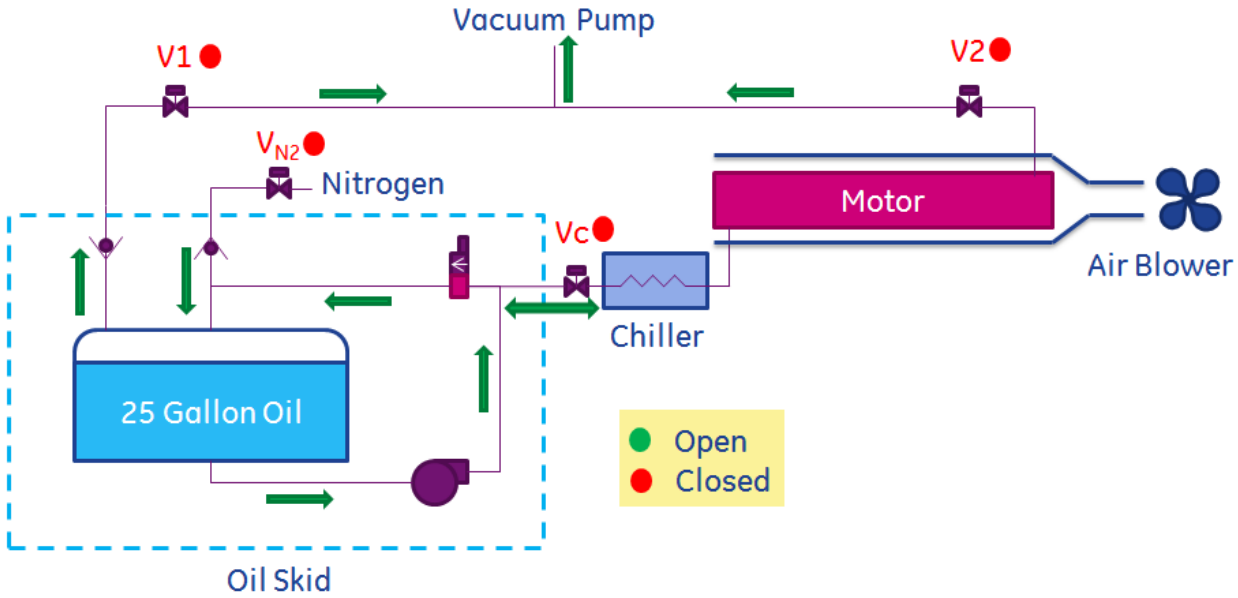

Figure 6.24 – Shutdown process

Operations:

1) Shutdown motor using the VFD.
2) Close Vc to isolate motor from oil skid in order to maintain oil inside the motor.
3) Shutdown oil skid.
4) Turn off DAQ.

7. Conclusions & Recommendations

The first phase of the program was dedicated to establishing the technical requirements for the EGS lifting system and evaluating the various lifting methodologies that might be developed to meet those requirements. The conclusion of this work is that a system based on an electric submersible pump (ESP) is the preferred method, and the one with the shortest technical path to meeting the demands of EGS. Challenges included increasing the temperature capability of the ESP from the advertised 220°C to 300°C, and the overall power from ~1.5 MW to 4-5 MW. Meeting those challenges is a formidable task as it requires a modular approach in which multiple motor sections, each with a maximum power rating of approximately 300 kW, are coupled together to drive a series of mixed flow pump stages. Lesser numbers of motor modules and pump stages can be used for applications with lower flow rates and/or pressure requirements.

The conventional ESP arrangement in which motor diameter is minimized is flow-limiting; a better approach is to maximize power density by pushing the motor diameter to nearly fill the well diameter, and allow the majority of process water to flow through the motor bore. Another advantage of this "flow-through-the-bore" arrangement is that it allows heat transfer to the process water to take place both at the motor outer diameter and at the inner diameter, helping to limit the peak motor internal temperature. Placing the motor downstream of the pump allows a portion of the well bore to be used for cabling without having to pass the electrical cables around the pump, further limiting flow area; the disadvantages of this arrangement are the need for an additional motor seal and the need for "gentle" motor starts in which pressure spikes at the motor inlet seal are minimized. These are relatively minor challenges; the additional seal at the upstream end of the motor is simply a replication of the downstream seal, and the "base load" nature of an EGS plant means that starts/stops will be extremely infrequent and manageable. In addition to these fundamental changes in ESP architecture, the use of a permanent magnet (PM) motor instead of the more traditional induction motor further increases the power density of the system, helping to limit the number of motor modules and overall system axial length.

The challenge of meeting the high temperature requirement of up to 300°C is met by combining two approaches. First, the arrangement of motor internals is selected to allow circulation of the dielectric oil through cooling passages in the stator as well as the rotor/stator gap. The motor speed of 3150 RPM is selected to balance the need for pumping efficiency with the need to minimize motor temperature rise. Thus, the motor is designed to keep the internal temperature rise to an established minimum value. Secondly, any non-metallic motor materials are selected to perform under elevated temperatures of up to 330°C. These include the stator wire, wire insulation, and dielectric oil. Similarly the permanent magnets used for the rotor are rated for temperatures far above the expected maximum motor internal temperature of 330°C.

Several ESP system elements required component-level development and/or testing. These include the motor face seals (to minimize leakage of the dielectric oil to the process water), non-metallic pump seals, motor and pump bearings, and pump interstage thrust washers, as well as the motor dielectric oil and stator insulation for both the windings and slot liners.

System components that need to be developed in a follow-on effort include the cabling and cable connections required to deliver up to 4MW of power to the ESP motor, as well as the "protector", the self-contained source of make-up oil that maintains the oil supply to the motor at a pressure slightly above the external well water pressure to ensure motor cooling and lubrication of motor bearings and seals. The subscale prototype fabricated in this program uses cabling that is based on the stator wire design, and an external oil supply eliminates the need for a proper "protector" module.

In parallel with the design and development of the full scale and prototype ESP systems, a flow loop test facility was designed, fabricated, and installed at GE Global Research. This test facility was designed to accommodate a flow rate of up to 20 kg/s (1/4 of the maximum expected flow rate of an EGS well) of 300°C water at up to 112 bar of pressure. The flow loop is designed to accommodate the prototype ESP system developed and fabricated during the program, and the expectation is that it will be used upon the successful completion of a separate motor thermal test to demonstrate that the motor can successfully operate at temperatures up to 300°C.

Lastly, the fabrication of the prototype ESP motor uncovered a number of technical hurdles such as packaging the stator end turns in a very limited axial space, ensuring that no insulation was damaged during the assembly process, accounting for the relative difference in thermal expansion between adjacent materials, and the controlled insertion of the PM rotor into the stator without damaging either component. While each of these challenges was overcome and a finished motor was delivered, the time and budget allocated to meet these challenges left insufficient resources to complete a thorough test of the motor or ESP system. While it would have been possible to complete the motor oil fill and conduct a very limited thermal test of the motor in the time remaining, the possibility of contaminating the oil over an extended period of time could jeopardize a more thorough test in the future. As a result, it was decided that the most prudent course of action, and the one that minimized the risk to the prototype hardware, was to complete fabrication of the prototype ESP motor and leave it oil-free until a separate program can be established to execute a complete test program. Thus, the following "next steps" are recommended as part of a subsequent, independent program:

- Complete the oil fill of the prototype EGS motor at a time as close to the start of testing as possible, to minimize the possibility of contaminating the oil.
- Complete a motor-only thermal test to demonstrate motor operability up to 300°C in an ambient air environment with forced convection to control the motor temperature. (Note that if the thermal test uncovers issues with excessive motor internal temperatures, limited motor rework and additional thermal testing may be necessary to further refine the design before proceeding to flow loop testing.)
- At the conclusion of a successful thermal test, complete the assembly of the motor and pump into the flow loop for flow testing.
- Complete flow testing in a water medium at elevated temperature (300°C) and pressure (100 bar) to evaluate the performance of the system and the thermal management capability of the "flow-through-the-bore" motor in a water environment.
- Upon successful demonstration of the prototype system in the flow loop, identify design improvements to be implemented as part of a scaled-up design to be tested in

an actual downhole environment. This “mid-scale” prototype could be of an intermediate power rating (such as 500-1000 kW) and could be installed in an existing geothermal well to demonstrate the ability of the technology to transition from the lab to the field.

8. Acknowledgements

This material is based upon work supported by the U.S. Department of Energy under Award Number DE-EE0002752. In addition to the Geothermal Technologies Program office, the authors would like to acknowledge the following colleagues in the associated business units of GE for their help and for sharing valuable information:

- Juan Albeniz (Business Program Manager - GE O&G, GE Global Research)
- Vishal Gahlot (Engineering Manager, GE O&G)
- Rene Garcia (Engineering Manager, GE O&G)
- Michael Hughes (Chief Consulting Engineer/Technologist, GE O&G)

Lastly, the authors would also like to thank Altarock Energy Inc. for their key support of this project.

9. References

1. World Energy Outlook 2010, International Energy Agency, (2010)
2. http://altarockenergy.com/media/AltaRock_Stimulation_Release_Final_1_21_13.pdf